Ústav organické chemie a biochemie
Akademie věd České republiky
a
Matematicko-fyzikální fakulta Univerzity Karlovy v Praze

Modelování struktury a dynamiky kapalných klastrů a povrchů

Disertační práce

Mgr. Martin Mucha

Školitel: Doc. Mgr. Pavel Jungwirth, CSc.
F-4 Biofyzika, chemická a makromolekulární fyzika

Praha 2006

Institute of Organic Chemistry and Biochemistry
Academy of Sciences of the Czech Republic
and
Faculty of Mathematics and Physics, Charles University, Prague

Modeling of Structure and Dynamics of Liquid Clusters and Surfaces

Doctoral Thesis

Martin Mucha

Advisor: Doc. Mgr. Pavel Jungwirth, CSc.
F-4 Biophysics, chemical and macromolecular physics

Prague 2006

Contents

1 Introduction

The current thesis consists of seven publications[1, 2, 3, 4, 5, 6, 7] in peer-reviewed journals with an extended introduction and detailed description of these papers. The common denominator of the presented work is the study of the structure and dynamics of aqueous interfaces using computer simulations of the classical molecular dynamics (MD) type. More specifically, our interest was directed towards the following overlapping issues:

- *Propensity of atomic and molecular inorganic ions for the air/water interface*
  This topic is covered by the first five papers and by the chapters 2-5 of the present text. Chapter 2 provides a motivation behind our interest in inorganic ions at the air/water interface and puts the present works into a broader context involving atmospherically relevant heterogeneous chemical reactions. Chapter 3 summarizes the methodology used for performing MD simulations. We discuss the approach of modelling extended vacuum/liquid interfaces and comment on the inclusion of molecular polarizability in the forcefield. Chapter 4 introduces the standard model of ion-free air/water interfaces and shows how it reconciles with our results. Chapter 5 provides a description of the the five papers relevant to the topic.

- *Dicarboxylate dianions in water clusters and at the air/water interfaces*
  This topic is covered by the last two papers and by the chapter 6 of the present text, where we give the description of the papers.

Several of the papers represent a collaborative effort with experimental laboratories, however the experimental part is not the concern of the present thesis.

2 Relevance of Ions at the Air/Water Interface

Let us start with motivation that arised from atmospheric chemistry. Ions at aqueous interfaces began to draw attention of the atmospheric community in the 1990s. The interest was fostered by detection of unusually high concentrations of gaseous molecular chlorine in coastal air.[8] It was believed that chlorine originates from sea salt aerosols – micron-sized liquid particles that are formed by the breaking of waves. The phenomenon was then reproduced in an atmospheric chamber.[9] The microdroplets of concentrated aqueous NaCl were suspended in air at room temperature with increased concentration of ozone and irradiated by UV light with a wavelength of 254 nm. The amount of Cl_2 produced could not be explained by the aqueous bulk reactions only. As a matter of fact, it has been inferred that reactions at the air/water interface are dominant. A necessary condition for the interfacial reactions is the presence of the reactants, i.e., chloride ions. However, the idea of any simple inorganic ions being present at the air/water interface was against the conventional wisdom, as explained in Chapter 3. In short, when the ions at the air/water interface are modelled as point charges, and water as a dielectric continuum, a net electrostatic force acts on the ions in the direction towards the bulk liquid away from the interface. This is due to the fact that the dielectric constant pertinent to water is 80 times larger than that of air. Second, as increasing the salt concentration increases the surface tension of the solution, therefore, by thermodynamic argument known as Gibbs adsorption isotherm[10], there should be a negative surface excess of the solute at the interface. This served as a basis from which it used to be inferred that the concentration of ions monotonously decreases when approaching the interface. However, these notions had to be reassessed following the early molecular dynamics simulation by Dang[11, 12, 13], Berkowitz[14, 15] and Jungwirth and Tobias[16], which showed that Cl^- was readily available at the interface. The distinguishing feature of this work was the use of polarizable forcefield, i.e., a non-zero point polarizability was ascribed to the atoms and ions.

As other examples of the importance of inorganic ions at the air/water interface let us mention the following:

1. Bubble coalescence – a process in which two or more air bubbles in water (or other liquid) merge during contact to form a single daughter bubble. Many salts inhibit bubble coalescence[17] which for example contributes to higher foaminess of seawater in ocean relative to freshwater lakes.

2. Brine rejection – a process occurring at the sea water/ice interface in which salt is rejected into the unfrozen sea has profound climatic effects in polar regions.[18]

3. Thundercloud electrification – salt ions from cloud condensation nuclei can play a role in electrification of thunderclouds.[19]

3 Molecular Dynamics: a Molecular Level Probe to Interfacial Layer

In the present section we describe the methodology used for molecular dynamics simulations. More details are included than those in the attached papers. Especially, we concentrate on the following issues:

1. Description of the basic methodology for simulating extended interfaces – the so called slab geometry.
2. The treatment of polarizability, and the reasons that make us to argue that it's effect is important.
3. The phenomenon of polarization catastrophe, and the scheme we employed to prevent it.

3.1 Molecular Dynamics Simulations in a Slab Geometry

3.1.1 Basic Definition of the Slab Geometry

The usual manner to simulate a condensed phase in MD simulations is to employ periodic boundary condition, in which a unit cell with finite number of particles (molecules) is replicated along all three dimensions. In contrast, when studying an interface, the problem is no longer isotropic, and the arrangement has to be modified accordingly. Throughout our simulations we use a slab geometry which is a particular arrangement in which the molecules of a liquid are distributed in a simulation box, see Figure 1A. The molecules occupy only a portion of the box along the z-axis leaving the rest empty. Along the other two axes, by contrast, the molecules fill up the simulation cell completely. Replicating the cell infinitely perpendicular to the z-axis thus creates an extended liquid slab 1B. The space above and below[1] the slab is actually not empty, but in thermodynamic equilibrium it contains the vapor of the liquid. The vapor-liquid interface, i.e. the region where the density changes continuously from the vapor to the liquid value, is central to our interest. In our arrangement we have two such interfaces – the upper and the lower one.

As a matter of practice, the simulation cell is often replicated also along the z-axis, i.e., we employ 3-dimensional (3D) periodic boundary condition instead of two-dimensional (2D). That results in a situation outlined by Figure 1B. Instead of a single slab we have an infinite number of its replicas, that are shifted by the length of the simulation box in the z-direction, separated by vapor regions. The reasons for this are purely practical. First, when a hot molecule evaporated from the slab leaves the upper side of the cell, it

[1]Of course, the term above and below are completely arbitrary, since we do not consider gravity. "Above" means simply in the direction of the z-axis as defined in the Figure 1

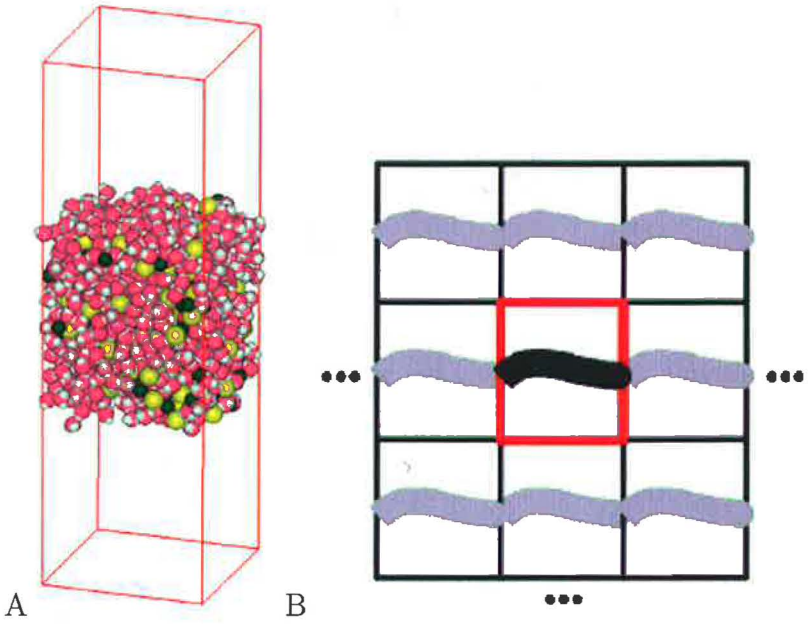

Figure 1: Slab geometry

reappears from the bottom and the number of particles is preserved. Second, the algorithm for treatment of long range coulombic interactions – Ewald summation – is efficient only to the 3D case. However, only long range interactions between molecules within the same slab are desired, the interactions between distinct images of the slab are an unwelcome artifact. Next subsection is devoted to these considerations.

3.1.2 Periodic Boundary Conditions in a Slab Geometry

In bulk systems, the standard and commonly used treatment of long range coulombic interactions is the method of Ewald summation[20]. One of the reason of it's widespread popularity is the existence of fast algorithms that implement the method. Two most prominent examples are the Particle Mesh Ewald (PME) method of Tom Darden[21, 22], and Particle-Particle Particle-Mesh (PPPM) method of Hockney and Eastwood[23, 24]. The Ewald summation is by design a method for three-dimensionally periodic systems. A two-dimensional Ewald summation is possible, but computationally very expensive[25]. In the slab geometry, however, another approach is possible: we extend the cell in the z direction, so that the neighboring replicas of the slab are separated by a sufficiently wide region of empty space. The wider is the empty space, the smaller are the intermolecular interactions between the periodic images in the z direction. The shortcoming of this approach is that elongating the cell increases also the computational cost of the Ewald method. Therefore, a reasonable tradeoff has to be found. A step further is to use the Berkowitz' correction term[26] in the Ewald sum. It applies to the slab geometry with a net neutral unit cell. The extra term introduces forces that act against the formation of a non-

zero z-component of the total electric dipole of the unit cell. In our simulations, we have used an elongated cell with PME algorithm as implemented in the Amber package[27]. We have also modified the Amber package in order to implemented the Berkowitz correction, but the results with the correction did not differ from the pure PME. Therefore, in most of our simulations we did not use the correction.

3.2 Forcefield and the Treatment of Polarizability

We use the term polarizability of a molecule throughout this thesis in the meaning of the ability to undergo "electronic polarization", i.e., the displacement of electronic cloud with respect to the molecular nuclei in response to an electric field. Within the simplest model the charge distribution of an atom is represented by a point charge and a point dipole that exhibits a linear response to the electric field, i.e., a dipole $\vec{p}$ is induced proportionally to the electric field, $\vec{E}$, with the constant of proportionality called atomic or molecular polarizability, α:

$$\vec{p} = \alpha \vec{E}. \tag{1}$$

Implementation of this model in MD simulations rests on attributing a point polarizability to each atomic site, i.

$$\boldsymbol{p}_i = \alpha_i \boldsymbol{E}_i. \tag{2}$$

The total electric field at an atomic site depends on all charges and induced dipoles in the system. It can be written as

$$\boldsymbol{E}_i = \boldsymbol{E}_i^{\mathrm{Q}} + \sum_{j \neq i} \boldsymbol{T}_{ij} \boldsymbol{p}_j, \tag{3}$$

where $\boldsymbol{E}_i^{\mathrm{Q}}$ is electric field due to charges in the system and where

$$\boldsymbol{T}_{ij} = \frac{3\boldsymbol{R}_{ij}\boldsymbol{R}_{ij}}{R_{ij}^5} - \frac{\boldsymbol{I}}{R_{ij}^3} \tag{4}$$

is the dipole-dipole interaction tensor, $\boldsymbol{R}_{ij}$ is the vector connecting atomic sites i and j and $\boldsymbol{I}$ is the unit tensor. Substituting (3) into (2) and adopting matrix notation we can write for the following linear system for the collection of induced dipoles, $\boldsymbol{p}$:

$$(\boldsymbol{I} - \boldsymbol{\alpha T})\boldsymbol{p} = \boldsymbol{\alpha E}^{\mathrm{Q}}. \tag{5}$$

Solving of this large dense linear system of equations is usually done iteratively, taking advantage of the known dipoles from the previous simulation step, assuming that $\boldsymbol{T}$ and $\boldsymbol{E}^{\mathrm{Q}}$ changed only little.

The importance of polarization in simulating ion-water interactions was first acknowledged in the early MD studies of Cl^-, Br^- and I^- solvation in small water clusters by Dang[11, 12, 13] and Berkowitz[14, 15]. The authors showed that the effect of atomic polarizability has to be taken into account in order to reproduce the experimentally determined asymmetric solvation, i.e., structures where halide anion is exposed at the surface

of the cluster. That contrasted with the weakly polarizable sodium cation, which solvates in the center of the cluster. Later Jungwirth and Tobias[16] showed that the effect persists when going from clusters to planar surfaces provided a polarizable forcefield is used. They predicted that chloride anions move all the way to the interface with heavier and more polarizable bromide and iodide actually exhibiting concentration enhancement at certain regions of then interface, while the weakly polarizable fluoride anion and sodium cation were repelled from the interface. The lesson learned is that polarization is important especially when simulating non-centrosymmetric environments with a non-vanishing average electric field, such as surfaces of clusters or interfaces. In such cases, no pair-wise additive potential can properly describe the intermolecular interactions.

In our work we have focused especially on highly polarizable species, such as azide[1] and thiocyanate[2]. Increased polarizability means increased surface effects but also possible computational difficulties. The major problem appears to be the so called polarization catastrophe. The essence of the problem is that when two polarizable sites get closer to each other than a certain critical distance, the matrix on the r.h.s. of equation 5 becomes indefinite and the solution to the linear system exhibits infinite negative energy – the induced dipoles diverge. The larger the polarizability, the longer the critical distance and the more probable is the occurrence of the polarization catastrophe.

We have developed a simple scheme to prevent the polarization catastrophe, that was successfully applied to the simulation of aqueous NaSCN solution.[2] Instead of a linear dependence of the induced dipole on the applied field (Equation 1) we use a more elaborate functional form, that is linear only for small fields. Above a certain field strength the functional dependence monotonously levels off, so that the induced dipole cannot overcome a specified maximal value, see Figure 2. This approached can be justified by realizing that in all our simulations the polarization catastrophes were relatively rare events and, therefore, it was possible to choose the parameters of the functional form such that most of the time the system stayed in the linear regime.

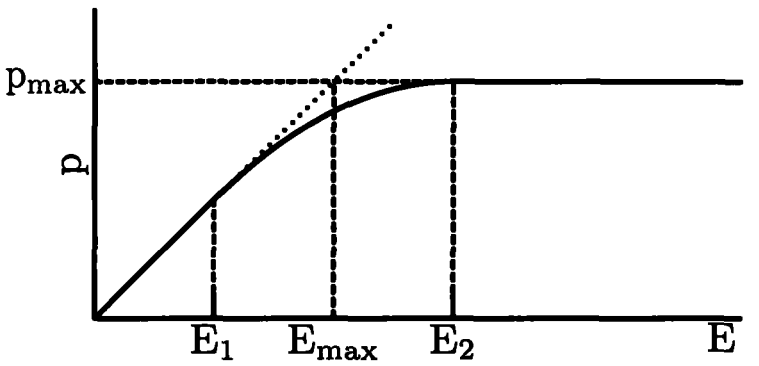

Figure 2: Dependence of induced dipole, p, on the electric field strength, E, implemented in the cut-off scheme for prevention of polarization catastrophe. The dependence is linear for $E < E_1$ quadratic for $E_1 \leq E < E_2$ and constant for $E > E_2$. The induced dipole has an upper bound, $p_{\max}$.

4 Standard Model of the Air/Solution Interface of Aqueous Electrolytes

The basis of what we call the standard model of the air/water interface of simple electrolytes has been laid down first by C. Wagner[28] in 1924 and later elaborated by Lars Onsager and Nicholas N. T. Samaras in 1930's in their study on surface tension of electrolytes[29]. Within their model the ion is represented by a point charge and the water is treated as a ideally soft dielectric continuum fully characterized by its dielectric constant. The air is approximated by a vacuum with dielectric constant of a free space. The two media are separated by a geometric infinitely sharp planar interface. In spite of obvious shortcomings, such as the neglect of molecular structure or the lack of discrimination between cations and anions, the model possesses a favorable quality. It entails orientational polarization of water in an averaged way. Figure 3 captures a situation when a positive charge (ion) of magnitude q is placed into the dielectric medium (water) close to the planar interface with a free space (air) on the left hand side. In an ideally soft dielectric polarization is induced in the medium that has the same direction as the intensity of the electric field generated by the charge. As a result, a surface charge density of like sign emerges on the dividing boundary, as shown schematically in the Figure. The charge q is then repelled by this surface charge density away from the interface towards the bulk liquid.

The problem of finding this repulsive force is often formulated in terms of an *electrostatic image force*, i.e. a force due to a fictious image charge. The idea is that the effect of the surface charge density induced by the "ion" can be substituted by the effect of a single point charge q', placed as a mirror image of the "ion" with respect to the plane of the interface. It can be shown that this fictious charge has a magnitude

$$q' = \frac{\epsilon_r - 1}{\epsilon_r + 1} q. \tag{6}$$

For a full derivation see textbooks on classical electrodynamics, e.g., [30].

The next common argument in favor of ion free interfaces is thermodynamic in nature and is not concerned with the underlying microscopic picture. It rests on a thermodynamic theory of interfaces due to Gibbs.[10] From the Gibbs-Duhem equation for the surface one can derive the Gibbs adsorption relation

$$\Gamma = \frac{-1}{RT} \left(\frac{\partial \gamma}{\partial \ln a} \right)_T. \tag{7}$$

Here, Γ is the surface excess of the solute, γ is the surface tension, a is activity of the solute, T is temperature and R is gas constant. Since for dilute solutions activity increases with concentration, the Gibbs adsorption relation leads to the conclusion that solutes that increase the surface tension tend to exhibit negative surface excess, i.e. a net depletion of the solute in the surface layer. Since simple inorganic salts increase the surface tension of water, the ions should be repelled from the surface layer in average. The thermodynamic

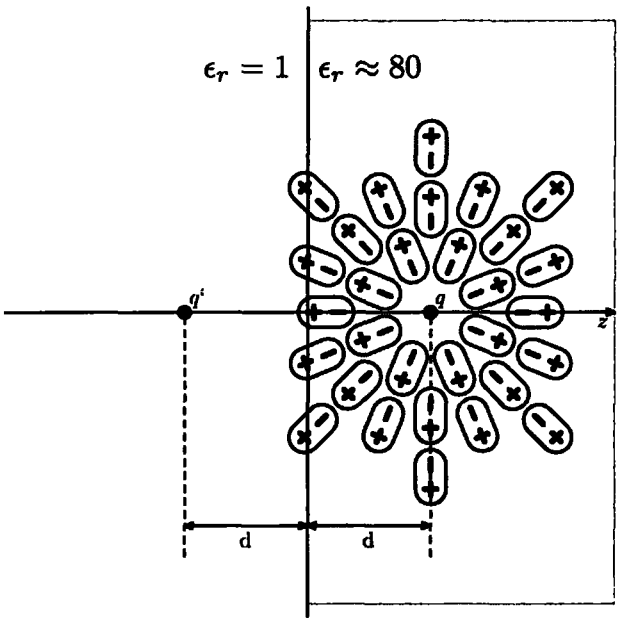

Figure 3: A point charge q (ion) placed into the region of relative dielectric constant $\epsilon_r \approx 80$ (water) induces polarization in the medium. Since the charge is placed close to the dividing plane that separates the dielectric on the right from the free space (air) on the left, a surface charge density of like sign is created on the boundary. The net result is that the point charge q is repelled away from the boundary into the interior. The magnitude of this force is the same as if it was generated by a fictious coulomb charge, $q' = \frac{\epsilon_r - 1}{\epsilon_r + 1} q$, placed at the point of a mirror image of q.

theory, however, does not address the functional form of the concentration profile close to the interface. The concentration profile does not need to be monotonous, as shown in top panel of Figure 4. The bottom panel illustrates that negative surface excess can be the result of surface peak more than compensated by the subsurface depletion. As an example of the latter behavior in the actual density profiles obtained from our MD simulations we offer the plot in Figure 5 panel c, which relates to the simulation of 3.5 M aqueous solution of NaSCN[2].

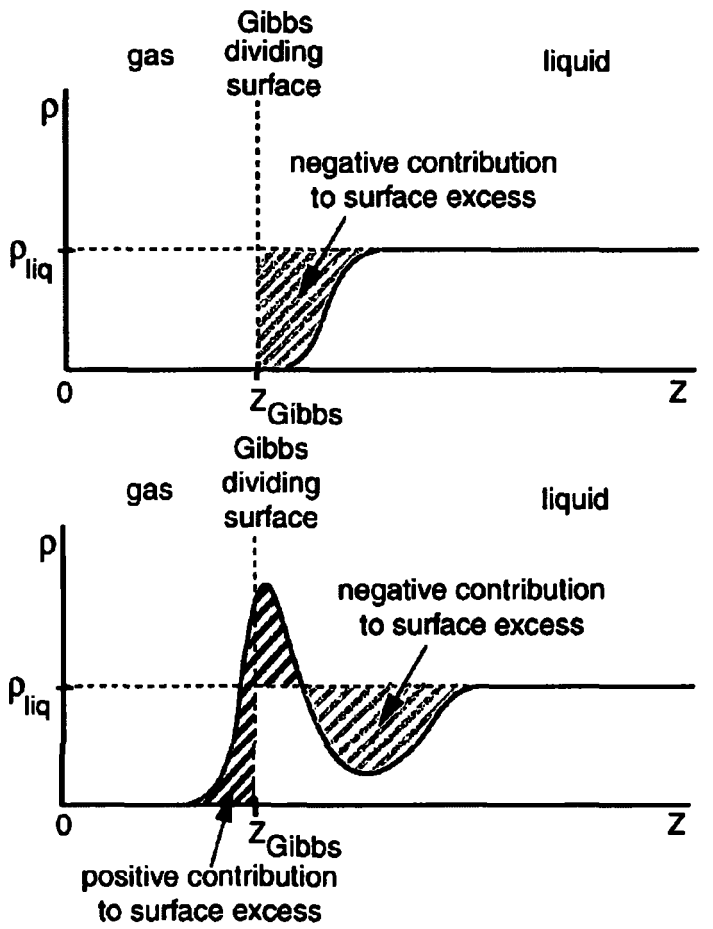

Figure 4: Ion density profiles giving rise to negative surface excess. The top panel shows the case with ions repelled from the surface, the bottom panel shows the case with surface peak followed by subsurface depletion.

5 Inorganic Ions at the Air/Water Interface

This chapter provides description of the papers that are concerned with studying the propensity of inorganic ions for the air/water interface.

5.1 Solvation of the Azide Anion (N_3^-) in Water Clusters and Aqueous Interfaces: A Combined Investigation by Photoelectron Spectroscopy, Density Functional Calculations, and Molecular Dynamics Simulations[1]

The following paper is a study on the solvation of N_3^- in water. It combines experiment - photoelectron spectroscopy (PES) - with theoretical approaches - density functional theory (DFT) calculations, and molecular dynamics (MD) simulations. The PES and DFT work has been done by the group of Lai-Sheng Wang at Pacific Northwest National Laboratory. The objective of the work was to study the solvation state of the azide anion from microsolvation in small water clusters up to the limiting case of bulk solvation. The primary result from PES are the adiabatic and vertical detachment energies of $N_3^-(H_2O)_n$ clusters where n=0–16. Increase of the detachment energies with the number of water molecules in the cluster is readily explained by the fact that the interactions of the polar water molecules with the charged anion are stronger than with the neutral N_3. Interesting is, however, that the first four water molecules stabilize the electron notably more than the following water molecules. This observation suggests that only four waters form a first solvation shell, whereas the weakening of the solute-solvent interaction starting from the fifth water molecule, as manifested by the relatively small stabilization to the electron binding energy, is the evidence of the onset of the second solvation shell. Considering the size of the azide we argue that by spatial considerations only it would easily accommodate more solvent molecules in its first solvation shell. That this is not the case indicates that the second solvation shell is formed asymmetrically along one side of the anion and leads to surface solvated N_3^-. However, the PES is not a structural tool and in order to confirm the solvation structure, the DFT and MD are beneficial. DFT can predict the structures of small clusters, whereas for larger clusters, DFT calculations were beyond computational resources and the structural information needs to be taken from MD simulations. We have used two distinct model forcefields. Model 1 uses the full polarizability of 1.95 Å^3, whereas the model 2 pertains to the reduced polarizability of 1.2 Å^3. The purpose was the possibility of comparison between the cluster simulation and the slab simulation discussed later in text. In the slab simulation the use of full polarizability leads to polarization catastrophe, hence we artificially reduced the polarizability down to a value, at which the catastrophe stopped to occur. Certain reduction can be substantiated by the solvent effects, and for this reason it is common in simulations to reduce the gas phase value by about 5-20 %. For the prevention of polarization catastrophe, however, the reduction had to be larger.

Figure 4 depicts a typical snapshot of a cluster with 16 water molecules. The azide clearly prefers the surface solvation. This surface preference is quantified in Figure 5 which shows statistical distributions of the distance from the center of mass of the water cluster for both a water molecule and the azide anion. Comparison of the water distribution (solid line) with azide distribution (dashed line) shows that the azide signal peaks at the outer shell of water molecules and leads to a conclusion that N_3^- prefers surface solvation. The results for both models are similar, only the surface solvation is more pronounced for the case with full polarizability. Another piece of evidence comes from the statistical distribution of angles formed by the line connecting azide with the center of water cluster and by the azide's axis of symmetry, shown in Figure 6. A uniform distribution would correspond to the interior solvation, while the actual distribution peaks at 90 degrees with minimum at 0 degrees. In other words the azide lies flat on the surface of the cluster. Differences between the two models are negligible. However, when the polarizability is switched off altogether[2], the azide solvates symmetrically in the center of the water cluster, in disagreement with the experimental PES spectra. This argument also refutes a possible assertion that the surface effect of the azide can perhaps be attributed to its size only. Although the experiment dealt only with clusters, and the experimental setup did not allow for studying of azide anion at extended water/vacuum interfaces, the question whether the surface propensity of the azide persists upon moving from clusters to aqueous surface is interesting and was addressed by MD simulations. In analogy to cluster study we collected statistically averaged distribution of distances of azide molecule from the center of the slab (Figure 7) and statistical distribution of angles formed by the azide's principal axis of symmetry and by the normal to the surface (Figure 8). As the figures indicate, both the surface propensity of the azide and its orientation being parallel to the surface are preserved also at the extended interface. It has to be stressed that the results were obtained with the forcefield corresponding to the model 2 in cluster study, i.e., with reduced polarizability in order to prevent polarization catastrophe. Use of the true, higher polarizability, would increase the effect even more. In short, the out cluster study on azide solvation in small water cluster supplement the experimental results and support the evidence in favor of asymmetrical – surface solvation of the anion. The slab simulations go beyond the potential of the given experimental setup and predict that the azide extends the family of small inorganic anions with surface propensity at the extended aqueous interfaces.

[2]the results for the non-polarizable simulation were not shown in the paper

5.2 Enhanced concentration of polarizable anions at the liquid water surface: SHG spectroscopy and MD simulations of sodium thiocyanide[2]

The paper presents a joined experimental and computational study examining the proposition that highly polarizable inorganic ions can exhibit enhanced concentration at air/solution interface. The particular anion studied was SCN^-[3] in a NaSCN aqueous solution. Thiocyanate anion represents a convenient candidate for examining the proposition for several reasons. First, it possesses high molecular polarizability, which amounts to almost 12 $Å^3$ along the molecular symmetry axis. Next, thiocyanate dissolved in water is spectroscopically accessible due to it's strong charge-transfer-to-solvent (CTTS) transition in the UV. Last but not least, the CTTS transition of SCN^- inhere a large nonlinear response, which enabled probing selectively the anions located at the surface via second harmonic generation (SHG) spectroscopy. The surface specificity of SHG stems from the fact that it is a second-order nonlinear process, which is, within the dipole approximation, forbidden in bulk centrosymmetric media. As a result, the SHG signal averages to zero from the whole volume of the sample except for a thin interfacial region, where the central symmetry is broken. In this way the intensity of the outcoming SHG signal is directly related to the concentration of the thiocyanate anions at the surface.

In the experiment, the SHG intensity, and thus the surface concentration of the anions was measured as a function of the bulk NaSCN concentration, which was then fitted to the Langmuir adsorption isotherm. From the fitted Langmuir constant,a Gibbs free energy of adsorption for thiocyanate of -1.80 $\pm$ 0.03 kcal/mol is extracted.

In order to complement the experiment, we performed a series of simulations of aqueous NaSCN solution in a liquid slab at three distinct concentrations, 0.6, 1.2 and 3.5 molar. From the simulations we obtained 2 ns long trajectories that were statistically processed and expressed in the form of density profiles for water, sodium and for each atomic type of thiocyanate separately, see Figure 5. Main observations are that

1. the SCN^- ions exhibit surface enhancement. The peak is highest for the most dilute solution reaching more than 50% above the bulk concentration. This surface enhancement is consistent with the negative value of Gibbs adsorption energy determined in the experiment.

2. the surface enhancement of SCN^- decreases with increasing bulk concentration, suggesting the beginning of surface saturation in accord with the experimental findings and is consistent with the use of Langmuir adsorption isotherm model.

3. the surface peak of SCN^- is accompanied by subsurface depletion

[3]this anion is referred to in the title as thiocyanide, which is an inaccurate use of nomenclature. The correct name, used in the present text, is thiocyanate

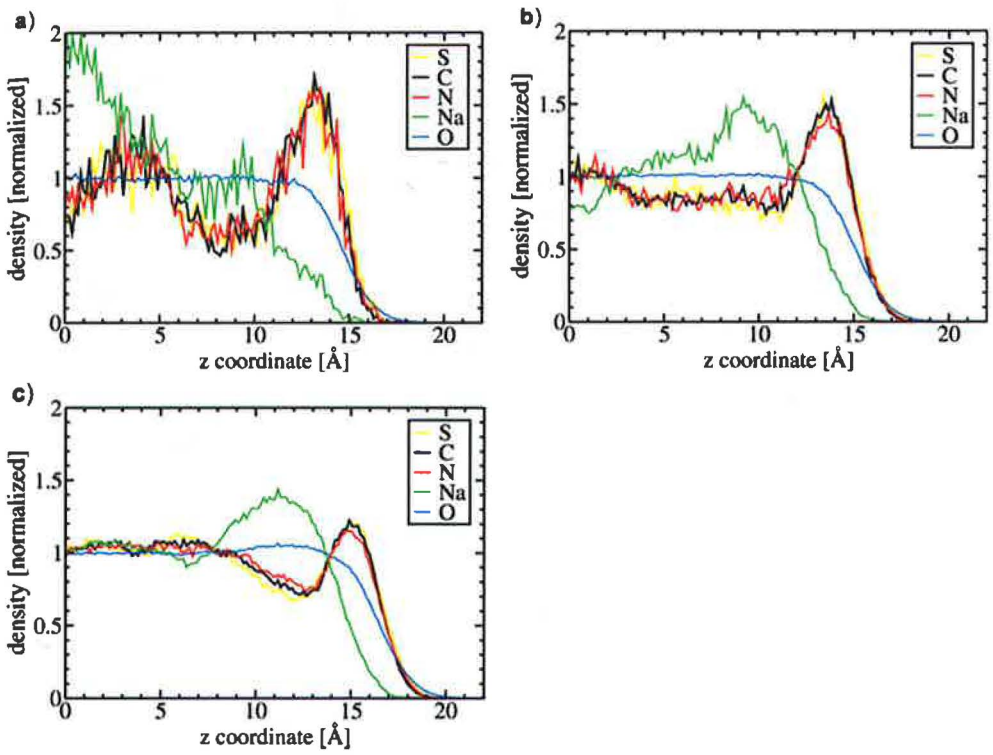

Figure 5: Statistically average density profiles from 2 ns long simulation of air/solution interface of the (a) 0.6, (b) 1.2, and (c) 3.5 molar aqueous NaSCN solution. The water oxygen density (blue curve) defines the interface. The green curve corresponds to the Na^+. The yellow, red and black curves correspond to the S,C, and N atoms of SCN^-. The densities are normalized so that the area under them is equal and the bulk water density is one.

4. small non-polarizable sodium cation is repelled from the surface, while the situation in the subsurface is reversed – the SCN^- is depleted and Na^+ exhibits a peak, except for the most dilute system, where the statistics are worse due to the small number of ions.

In conclusion, the paper contributes to the ever more detailed description of inorganic ions in the interfacial region of the air/solution interface. The following consistent picture emerges – small non-polarizable (hard) ions, like sodium, are repelled from the aqueous surface pursuant to the standard model described in section 4. In contrast, soft polarizable anions exhibit a nonmonotonic interfacial distribution, being enhanced at the outermost surface layer, but depleted in the subsurface. From that follows that the ions can play an active role in heterogeneous chemical reactions occuring at surfaces of aqueous electrolytes.

5.3 Unified molecular picture of the surfaces of aqueous acid, base, and salt solutions[3]

In this feature article we propose, based on MD simulations, a unified picture of air/solution interfaces of simple aqueous acids, bases and salts. Within this picture (see Figure 6), in salt solutions and bases the positively charged ions, such as alkali cations, are repelled from the interface, whereas the anions, such as halides or hydroxide, exhibit a varying surface propensity, correlated primarily with the ion polarizability and size. The behavior of acids is different due to a significant propensity of the hydronium cations for the air/water interface. Therefore, both cations and anions exhibit enhanced concentrations at the surface and, consequently, these acids (unlike bases and salts) reduce the surface tension of water.

The conceptual change in perception of the surface of electrolytes described in the paper has already been recognized in studies of chemistry of aqueous sea-salt aerosols[9], whereas for acids we provide a new insight. Hydronium cation behaves differently than other atomic cations such as alkali ions primarily due to the "hydrophobic" character of its oxygen. Although the three hydrogens of H_3O^+ are good hydrogen bond donors, the oxygen is, due to significantly reduced negative charge a relatively poor hydrogen bond acceptor. As a result hydronium can be stabilized at the air/solution interface with its H atoms hydrogen bonded to surrounding water molecules, while its oxygen atom remains unbound and pointing into the gas phase. This view is supported by the experiment reported in the same paper by our experimental collaborators. Their vibrational sum frequency generation data reveal that a protonated water exists in the interfacial region.

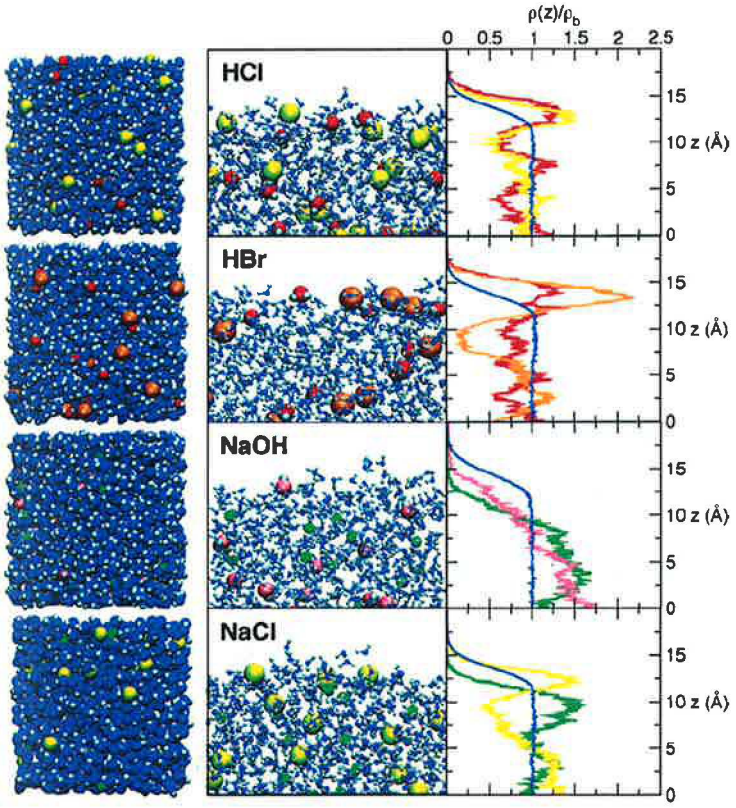

Figure 6: Snapshots from MD simulations (side and top views of the slabs) and density profiles (i.e., histogrammed densities of the electrolyte ions and water molecules in layers parallel to the surface, from the center of the slab across the interface into the gas phase) for 1.2 M aqueous HCl, HBr, NaOH, and NaCl. Color coding: water oxygen - blue; hydronium oxygen - red; hydroxide oxygen - pink; hydrogen - gray; sodium ions - green; chloride ions - yellow; bromide ions - orange.

5.4 Propensity of soft ions for the air/water interface[4]

This paper reviews results from previous MD studies on ions at the air/water interface, but also provides new insight. First, we commented on the reconciliation of results from MD simulations (soft polarizable ions exhibit surface enhancement) with the conventional wisdom (ion-free interfaces), along the lines of section 4. Special attention is paid to the electronic polarization and to the way how it gives rise to surface propensity of polarizable anions. It is argued that two opposing forces are at play: On one hand, interaction of the ionic charge with polar solvent favors hydration and, consequently, solvation in the bulk, where the water can fill the whole solvation shell around the ion. On the other hand, for ion at the interface the waters are present only on one side of the ion. Consequently, there is significant electric field resulting from the sum of water dipoles polarizing the soft anion. This leads to an additional stabilization at the interface, which can, depending on the value of ionic polarizability, overcome the bulk-driving hydration. Among other examples, we mention a counter-example, where even substantial polarizability does not lead to surface propensity. We refer to MD simulations of sulfate, SO_4^{2-}, which is repelled from the surface. Here, it is the multiple charge that which shifts the balance towards the bulk-driving hydration, in spite of its large polarizability in water equal to 7 $Å^3$.

We also reported on previously unpublished investigation into the effect of polarizable forcefield, or the lack of it, on density surface propensity. We performed four analogical simulations of a benchmark system – aqueous NaI solution – in a slab geometry: (1) with non-polarizable forcefield, (2) with non-polarizable ions and polarizable water, (3) with polarizable ions and non-polarizable water and, finally, (4) with polarizability on both ions and water. The main finding is that the water polarizability comes into play too. Not only the water polarizes the anion as explained above, but also the ion polarizes the water in a complex, non-additive fashion. The polarizability on water only (case 2) suffices to cause a sizeable surface peak and subsurface depletion in the iodide density profile, not found in the non-polarizable case 1. The effect is slightly stronger with case 3, while fully polarizable case 4 leads to the larger surface enhancement stronger by 50%, see Figure 7.

The final section of the paper summarized up-to-date experimental observation that are consistent with the presence of soft polarizable ions at the air/water interface. First, it is shown that the surface tension measurement of simple inorganic salts do not contradict this picture, as originally thought, see section 4. Next, two spectroscopic experiment are discussed: (a) the X-ray reflectometry which probed electron density distributions in the direction normal to the surface of aqueous alkali halide solutions and (b) vibrational sum frequency generation spectroscopy of the same system.

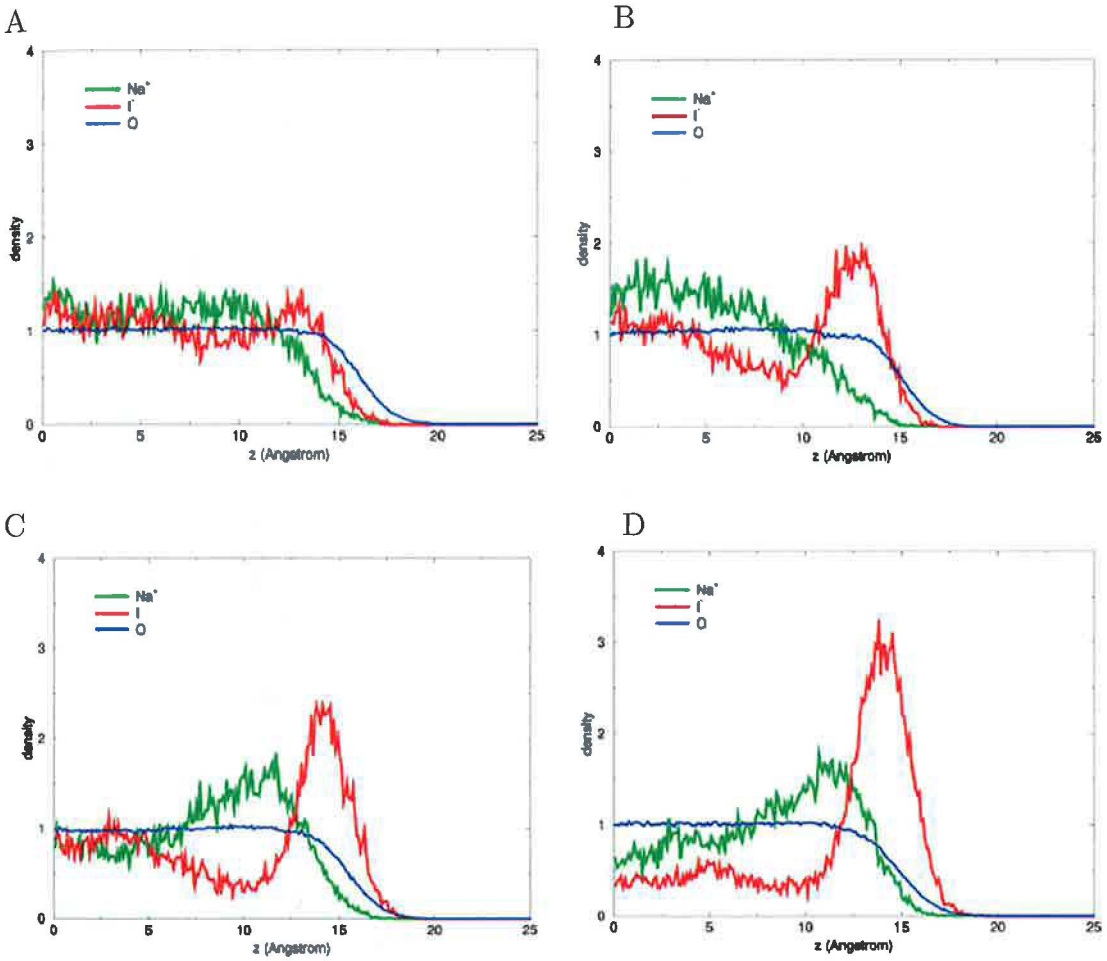

Figure 7: Comparison of density profiles of water oxygen (blue), sodium (green), and iodide (red) from the center to the surface of a 1.2 M aqueous NaI slab obtained from MD simulation using forcefields with polarizability incorporated at various levels: (A) non-polarizable force field, (B) non-polarizable ions and polarizable water, (C) polarizable ions and non-polarizable water, and (D) fully polarizable force field.

5.5 Structure and vibrational spectroscopy of salt water/air interfaces: Predictions from classical molecular dynamics simulations[5]

The aim of this paper was to calculate the vibrational sum frequency generation (SFG) spectra of aqueous sodium iodide interface. Previous MD simulations of Jungwirth and Tobias[31] challenged the standard model of air/solution interface that assumes ion free surface. Their results suggest that the interface can be rich in heavier halides. Another indirect evidence came from kinetic studies mentioned in section 2. The amount of molecular chlorine produced from sea salt aerosols under specific condition in an atmospheric chamber could not be explained by bulk reactions only. The match between kinetic modelling and experiment was achieved only when heterogeneous reactions involving reactant chloride taking place at the surface of aqueous sea salt particles were taken into account.

However, a spectroscopic attempt to address the question was still missing. Obviously, the proper spectroscopic tool should be surface specific,i.e., able to suppress the contributions from the bulk of the sample. This condition is fulfilled by the various non-linear spectroscopies which involve a second-order optical process that is electric-dipole forbidden in centrosymmetric media but allowed at the interface where the inversion symmetry is broken. An example represents the vibrational sum frequency generation (SFG) spectroscopy that has been used to study the air/liquid interface of pure water by Du et al.[32] and of aqueous solution of NaF, NaCl, NaBr and NaI by Raymond and Richmond[33] and by Liu et al.[34]. The vibrational SFG involves two incident beams with frequencies, ω_1 and ω_2, typically in the infrared and visible region respectively. In the sample, an output beam of $\omega_{SFG} = \omega_1 + \omega_2$ is generated and resonantly enhanced provided the incident infrared radiation coincides with the transition in the medium. In the above mentioned experiments the spectra are measured over a range of frequencies spanning water OH vibrations. The ionic species are thus not probed directly. However, the OH stretching frequency is sensitive to the hydrogen bonding environment that is altered by the presence of the ions. The interpretation of the spectra therefore involves the comparison of the pure water interface with the salt solution interface.

The interpretation is often ambiguous and it lacks the kind of molecular detail available from MD simulations. Our paper aims to bridge this gap.

Earlier MD simulations of aqueous NaI solution in a slab geometry[31] employed a rigid water model that did not allow for the OH water vibrations that give rise to the vibrational SFG spectra. Therefore we recalculated these simulations with a flexible SPC/E-like water model with an anharmonic term in the OH vibration[35]. Based on a series of 15 ps long trajectories we calculated the SFG spectra using methodology developed by Morita and Hynes[36]. This approach is time-dependent – the resonant term of the nonlinear susceptibility that contributes to the SFG intensity is expressed in terms of a time correlation function of the system polarizability and the dipole moment. The polarizabilities and dipole moments of individual molecules at each time step are determined from ab initio

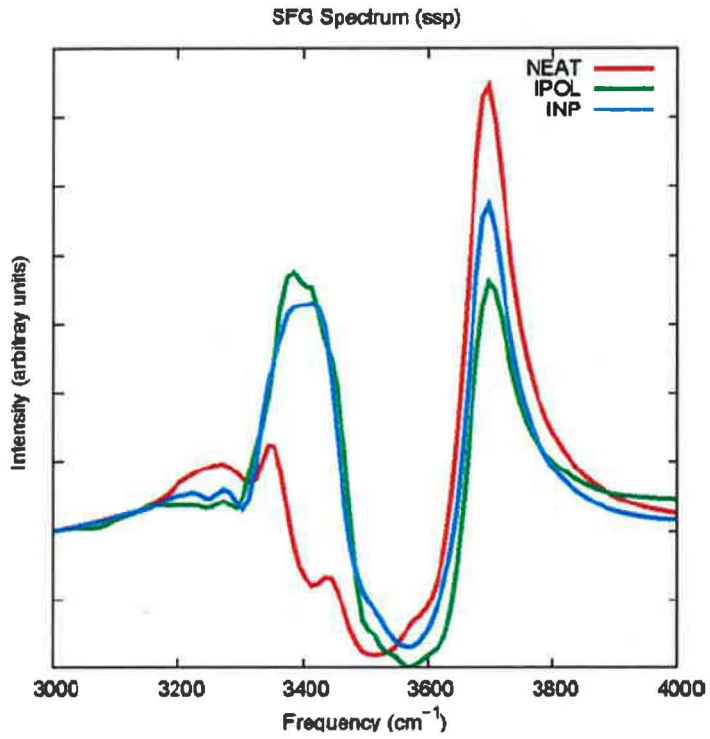

Figure 8: Calculated vibrational SFG spectra of neat water interface (red curve), NaI solution with polarizable forcefield (green) and NaI solution with non-polarizable forcefield (blue).

data.

For calculation of SFG spectra we actually considered three systems: (1) the 1.2M aqueous NaI solution with polarizable ions, (2) the same solution but with non-polarizable forcefield and, finally, (3) neat water interface. The calculated spectra are shown in Figure 8 The computed SFG spectra of the three systems exhibit similar features, also found in the experimental spectra[34]: a broad band around 3400 cm^{-1} corresponding to the stretching of hydrogen-bonded waters and a sharp peak at 3750 cm^{-1} corresponding to the free OH stretch, often attributed to the dangling OH bonds protruding from the surface of the liquid. The major difference in the spectra of neat water versus salt water is that in the salt water system there is a considerable increase in intensity in the region around 3400 cm^{-1} with respect to the free OH region – in agreement with experiment.[34] We attempted to attribute these differences in the spectra to the differences in the structure of the waters in the interfacial region. For this purpose we analyzed the MD trajectories using depth-resolved orientational distribution function of the water dipole moments. At the Gibbs dividing surface, where the dangling OH bonds are most populous, the differences in water ordering between the different systems are tiny. However, in the subsurface, for the systems containing ions, there is a significant ordering of waters corresponding to an

angle of 0° between the water dipole moments and the surface-normal vector. We attribute this water ordering be the ion double layer formed by the iodines in the surface layer and the sodiums in the subsurface. We also suggest that this ordering of the water molecules is the reason behind the increase in the SFG intensity in the 3400 cm^{-1} region.

6 Dicarboxylate Dianions in Water Clusters and in Bulk Water

This part of our work is focused on dicarboxylate dianions, $^{-}O_2C(CH_2)_nCO_2^{-}$, which are organic ions composed of an aliphatic chain of varying lengths terminated on both ends by a negatively charged carboxylate group. Our findings are reported in two papers, one dealing with dianions in the water clusters[6] and the other focusing on their bulk versus interfacial aqueous solvation.[7]. Both reports were prepared in collaboration with experimental laboratory. In the first paper the cooperation is direct, the results from computer simulations help to explain the molecular level mechanism behind the observed experimental photoelectron spectra. In the second paper experiment and simulations complement each other in a different way – experiment focuses on dianions in water clusters only while our MD simulations are concerned with dianions at the extended air/water interface.

6.1 Solvent-mediated folding of a doubly charged anion[6]

In this paper our objective was to elucidate the ion-water interactions that manifest themselves in the photoelectron spectra measured by our experimental collaborators. The specific dicarboxylate dianion under investigation was suberate, $^{-}O_2C(CH_2)_6CO_2^{-}$. In the experiment, clusters containing one suberate dianion and wide range of water molecules were created using electrospray ionization technique and subsequently intercepted by a probe laser beam of a photon energy above the electron binding energy. Form the kinetic energy of emitted photoelectrons the vertical and adiabatic detachment energies were obtained. The most interesting phenomenon observed is the following (see Figure 9 panel A): When increasing the number of water molecules in the cluster, the electron binding energy increases, because the interactions of the each additional water molecule with the extra charge on the carboxylate group stabilizes the doubly charged anion with respect to the mono-anion. However the experimental spectra show a sudden drop in the electron binding energy when adding the 16th water molecule to the cluster.

With the aid of our MD simulations we were able to gain a molecular insight into this phenomenon. We performed a series of simulations at the microsecond timescale of a cluster containing a single dianion and 15, 18, 21 and 24 water molecules respectively and in order to assess the effect of temperature we repeated the simulations at 230K and at 150K. We observed that above a temperature dependent number of solvent water molecules sharply increases the probability that suberate undergoes a solvent mediated folding. For a small number of water molecules the two carboxylate groups are solvated independently and they repel each other coulombically which gives rise to the linear structure of the aliphatic chain. When the number of water molecules is large enough, the two separate water clusters around the respective carboxylate groups merge together to form a single hydrogen-bonded network that pushes the two end-groups together overcoming their coulombic repulsion and distorting the dihedrals of the connecting aliphatic chain (See Figure 9 panels B and

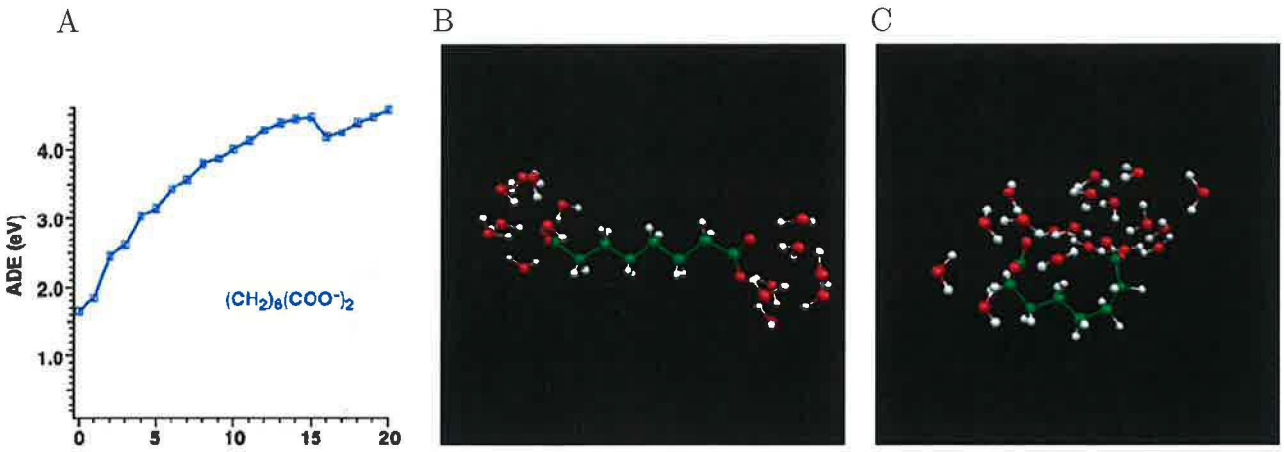

Figure 9: **(A)** Adiabatic electron detachement energies of $^{-}O_2C(CH_2)_6CO_2^{-}(H_2O)_n$ (n = 0-20). **(B)** Snapshots from simulations of the suberate dianion solvated in 15 waters – a linear structure and **(C)** a cluster containing 18 waters – a folded structure

C). This extra coulomb repulsion causes the observed drop in the adiabatic detachment energy. The folding is quantitativelly captured in Figure 4 in the paper, that pertains to the simulations at 230K. We were monitoring the time-dependent distance between the terminal carboxylate groups which we then expressed in terms of a time-averaged probability density. For the clusters with 15 and 18 waters (panels a and b) the most probable conformation corresponds to a linear suberate with the end-to-end distance of 9 Å. For the clusters with 21 and 24 water molecules (panels c and d) the broad peak around 5.5 Åsignifies a high probability to find the cluster in a folded state. Thus the transition occurs between 18 and 21 waters in the simulation, whereas between 15 and 16 waters in the experiment. This discrepancy might be caused by imperfections of the simulation forcefield but we have found that the temperature might play a role as well. First, the temperature in the experiment is not precisely defined, but is assumed to be significantly below room temperature due to evaporative cooling. Second, simulations at 150K indicate that the effect of decreasing the temperature is non-negligible, shifting the critical cluster size for folding to smaller values. However, the smaller temperature means also higher non-ergodicity of the simulation and we were not able to obtained fully thermodynamically converged results.

In conclusion, the PES spectra of suberate dianion sequentially solvated by water molecules exhibit an unexpected drop in adiabatic detachment energy when adding the 16th water to the cluster, from which a solvent mediated folding of the aliphatic chain of the suberate is inferred. However, PES is not a structural tool and therefore, computer simulations of classical MD type were used to complement the experiment to obtain the molecular level description of the phenomenon.

6.2 Bulk versus interfacial aqueous solvation of dicarboxylate dianions[7]

In our previous paper on suberate dianion hydrated in small water clusters we established a quantitative agreement between computer simulations and results from photoelectron spectroscopy. Building on this success, in this paper on a series of dicarboxylate dianions with varying aliphatic chain lengths, the experiment and computer simulations are used in a complementary way – experimental part is concerned with the structures of dicarboxylate dianions in and on small- and medium-sized water clusters, while the computational part is aiming to elucidate directly the thermodynamically averaged structures of these dianions in the aqueous bulk or at the extended vapor/water interface.

We performed a series of MD simulations of a liquid water slab, as described in section 3, each simulation cell in addition containing a single dianion and two sodium counter-cations to keep the overall system electrically neutral. We repeated the simulations with the following dianions: oxalate, $C_2O_4^{2-}$, adipate, $^-O_2C(CH_2)_4CO_2^-$, suberate, $^-O_2C(CH_2)_6CO_2^-$. MD trajectories were statistically processed and the results expressed in the form of density profiles along the dimension normal to the slab surface (Figure 10). The results can be summarized as follows: Oxalate, the smallest dicarboxylate dianion, lacking the the hydrophobic CH_2 group present in longer dicarboxylates, was found to solvate deeply in the aqueous bulk, avoiding the surface altogether. Due to its multiple charge it is found to be repelled from the surface even more strongly than the sodium counter-cation. Adipate, a dicarboxylate dianion with the aliphatic chain of 4 hydrophobic CH_2 groups, still solvates in the bulk. The hydrophilic forces of the charged end-groups win over the hydrophobic forces of the aliphatic chain, that favor the surface solvation. Upon moving from adipate to suberate, i.e. adding two more CH_2 groups, a transition from bulk to surface solvation occurs. Analogously to our previous cluster studies, the aliphatic chain of the suberate appears to be somewhat bent, which manifest itself in the fact that the density profile of the carbons from the aliphatic chain peaks closer to the vapor phase, while the signal from the oxygens of the end-groups is slightly shifted closer to the bulk. The effect is even more apparent in the case of the tetradecandioic dianion, the longest of the studied dicarboxylates, having the aliphatic chain length of 12 CH_2 groups. Again, the dianion solvates at the interface, the aliphatic chain bends and sticks out into vapor phase while the CO_2^- groups point into the bulk. The bulk versus surface solvation of dicarboxylate dianions also has an effect on the structure of aqueous solvation shells. From the carboxylate oxygen-water oxygen radial distribution functions obtained from the MD trajectories we learned that there are roughly seven water molecules in the first solvation shell of the bulk solvated adipate while this number drops to five in the case of the longer dicarboxylates. The five waters in the solvation shell of surface solvated suberate agrees with the experimental results from cluster studies. These show a negligible even-odd effect in the adiabatic detachment energies above ten water molecules, i.e., once each end-group is solvated by five waters, since additional water do not interact directly with the negative charges but are added to the second solvation shell.

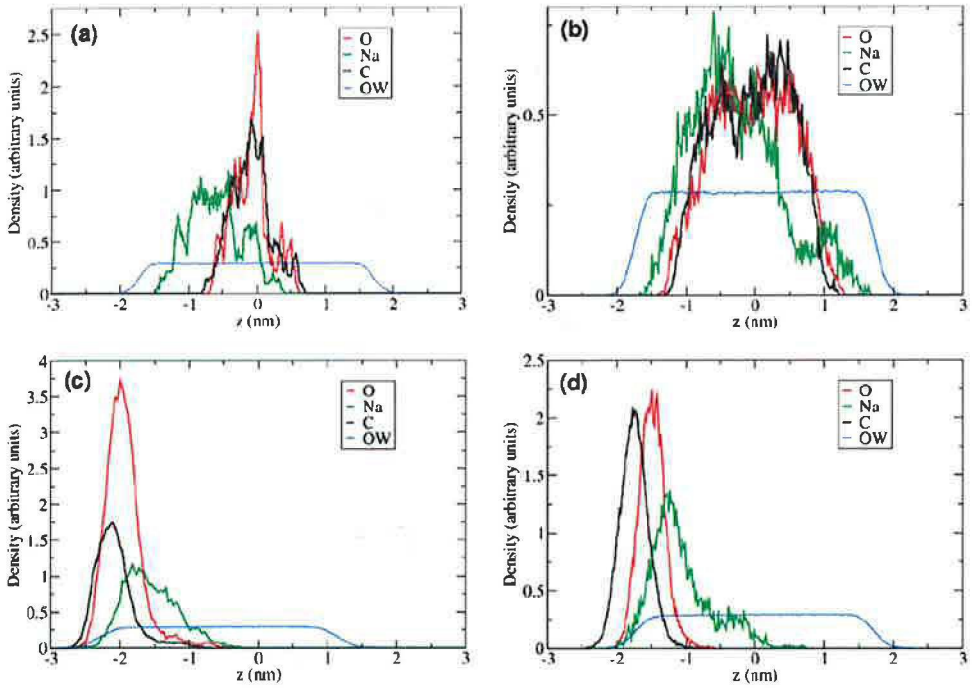

Figure 10: Density profiles of dicarboxylate dianions in an aqueous slab. Color coding: red - carboxylate oxygen, black - carbon, green - sodium countercations, blue - water oxygen. (a) Oxalate (bulk solvation), (b) adipate (bulk solvation), (c) suberate (surface solvation), (d) tetradecandioic dianion (surface solvation)

In conclusion, in the described paper we report MD simulations of dicarboxylate dianions with varying length of the aliphatic chain solvated in and on a extended liquid water slab. Thereby we complement the experimental results that are available only for the clusters. We observed a competition between hydrophobic forces due to the aliphatic chain that favor the surface solvation with the hydrophilic effect of the negative charge on the terminal carboxylate groups. It leads to a transition from aqueous bulk solvation of shorter dicarboxylate to interfacial solvation of the longer ones. Whereas oxalate and adipate solvate in the inner parts of the aqueous slab, suberate and longer dicarboxylate dianions exhibit a strong propensity for the surface. We have learned that this transition has also effect on the folding of the flexible aliphatic chain and on the structure of the first solvation shell around the charged carboxylate groups.

7 Conclusions

In the seven papers that constitute the present thesis we have investigated various ionic species at aqueous surfaces, both on the surface of water clusters and at the extended air/water interface. In papers [1], [2], [3], [4] and [5] we have focused on simple inorganic ions which, within the standard textbook description, were thought to be repelled from the air/water interface of aqueous electrolytes. This turns out to be true for small hard non-polarizable ions such as fluoride and alkali cations. However, thanks to specific ionic effects, the most prominent being electronic polarization, large soft polarizable anions such as azide, thiocyanate, and heavier halides exhibit surface enhancement at the aqueous surfaces. Similar behavior, although for a different reason, can be attributed to the hydronium cation. Surface propensity of this species derives from its specific hydrogen bonding favoring surface sites. Predictions from MD simulations are supported by a mounting experimental evidence. Several of the papers represent a collaboration with experimental laboratories. The experimental techniques that point to the presence of soft anions at surfaces of water clusters or water interfaces are photoelectron spectroscopy[1] and electronic[5, 3] and vibrational[2] nonlinear surface selective spectroscopies.

The presence of inorganic ions at liquid aqueous surfaces has important possible consequences for atmospherically relevant heterogeneous chemical reactions as well as for biological and technological processes. Let us mention just a few examples – molecular chlorine production from sea-salt aerosols[9], bubble coalescence[37], or thundercloud electrification[19].

The second part of the thesis is based on papers [6] and [7]. Here we focused not only on the static picture of statistically averaged densities of ions at aqueous surfaces, but also on the solvent mediated dynamics of structurally more complicated ionic species – the dicarboxylate dianions. First study focused on the microsolvation of suberate dianion in small water clusters. Our MD simulations helped to elucidate experimentally observed unexpected decrease in electron binding energy for a suberate solvated by 16 water molecules relative to that for the 15-water solvated suberate. The shift was attributed to the folding of the long aliphatic chain of suberate that links two negatively charged carboxylate groups. The folding takes places once there is enough solvent water molecules to screen the negative charges and pull them closer together through a hydrogen bonded water bridge overcoming their Coulomb repulsion. In the second study we have taken into consideration not only suberate but also other dicarboxylate dianions with longer and shorter aliphatic chains and investigated their bulk versus interfacial solvation at aqueous interfaces. The study revealed a competition between hydrophilic interactions of the charged carboxylate groups and the hydrophobic interactions of the aliphatic chain. This competition leads to transition from bulk solvation of small dicarboxylates to solvation at the air/water interface of the larger ones, in accord with the solubility data of the corresponding acids. For the surface active species, similar solvent mediated folding was observed as in the cluster study.

References

[1] X. Yang, B. Kiran, X. B. Wang, L. S. Wang, M. Mucha, and P. Jungwirth. Solvation of the azide anion (N_3^-) in water clusters and aqueous interfaces: A combined investigation by photoelectron spectroscopy, density functional calculations, and molecular dynamics simulations. *JOURNAL OF PHYSICAL CHEMISTRY A*, 108(39):7820 – 7826, 2004.

[2] P. B. Petersen, R. J. Saykally, M. Mucha, and P. Jungwirth. Enhanced concentration of polarizable anions at the liquid water surface: SHG spectroscopy and MD simulations of sodium thiocyanide. *JOURNAL OF PHYSICAL CHEMISTRY B*, 109(21):10915 – 10921, 2005.

[3] M. Mucha, T. Frigato, L. M. Levering, H. C. Allen, D. J. Tobias, L. X. Dang, and P. Jungwirth. Unified molecular picture of the surfaces of aqueous acid, base, and salt solutions. *JOURNAL OF PHYSICAL CHEMISTRY B*, 109(16):7617 – 7623, 2005.

[4] L. Vrbka, M. Mucha, B. Minofar, P. Jungwirth, E. C. Brown, and D. J. Tobias. Propensity of soft ions for the air/water interface. *CURRENT OPINION IN COLLOID & INTERFACE SCIENCE*, 9(1-2):67 – 73, 2004.

[5] E. C. Brown, M. Mucha, P. Jungwirth, and D. J. Tobias. Structure and vibrational spectroscopy of salt water/air interfaces: Predictions from classical molecular dynamics simulations. *JOURNAL OF PHYSICAL CHEMISTRY B*, 109(16):7934 – 7940, 2005.

[6] X. Yang, Y. J. Fu, X. B. Wang, P. Slavicek, M. Mucha, P. Jungwirth, and L. S. Wang. Solvent-mediated folding of a doubly charged anion. *JOURNAL OF THE AMERICAN CHEMICAL SOCIETY*, 126(3):876 – 883, 2004.

[7] B. Minofar, M. Mucha, P. Jungwirth, X. Yang, Y. J. Fu, X. B. Wang, and L. S. Wang. Bulk versus interfacial aqueous solvation of dicarboxylate dianions. *JOURNAL OF THE AMERICAN CHEMICAL SOCIETY*, 126(37):11691 – 11698, 2004.

[8] C.W. Spicer, E.G. Chapman, B.J. Finlayson-Pitts, R.A. Plastridge, J.M. Hubbe, J.D. Fast, and C.M. Berkowitz. Unexpectedly high concentrations of molecular chlorine in coastal air. *NATURE*, 394(6691):353 – 356, 1998.

[9] E.M. Knipping, M.J. Lakin, K.L. Foster, P. Jungwirth, D.J. Tobias, R.B. Gerber, D. Dabdub, and B.J. Finlayson-Pitts. Experiments and simulations of ion-enhanced interfacial chemistry on aqueous nacl aerosols. *SCIENCE*, 288(5464):301 – 306, 2000.

[10] J.W. Gibbs. *The collected works*. Longmans: New York, 1928.

[11] L.X. Dang, J.E. Rice, J. Caldwell, and P.A. Kollman. Ion solvation in polarizable water - molecular-dynamics simulations. *JOURNAL OF THE AMERICAN CHEMICAL SOCIETY*, 113(7):2481 – 2486, 1991.

[12] L.X. Dang and D.E. Smith. Molecular-dynamics simulations of aqueous ionic clusters using polarizable water. *JOURNAL OF CHEMICAL PHYSICS*, 99(9):6950 – 6956, 1993.

[13] L.X. Dang and B.C. Garrett. Photoelectron-spectra of the hydrated iodine anion from molecular-dynamics simulations. *JOURNAL OF CHEMICAL PHYSICS*, 99(4):2972 – 2977, 1993.

[14] L. Perera and M.L. Berkowitz. Structure and dynamics of cl-(h2o)20 clusters - the effect of the polarizability and the charge of the ion. *JOURNAL OF CHEMICAL PHYSICS*, 96(11):8288 – 8294, 1992.

[15] L. Perera and M.L. Berkowitz. Ion solvation in water clusters. *ZEITSCHRIFT FUR PHYSIK D-ATOMS MOLECULES AND CLUSTERS*, 26(1-4):166 – 168, 1993.

[16] P. Jungwirth and D.J. Tobias. Surface effects on aqueous ionic solvation: A molecular dynamics simulation study of nacl at the air/water interface from infinite dilution to saturation. *JOURNAL OF PHYSICAL CHEMISTRY B*, 104(32):7702 – 7706, 2000.

[17] V.S.J. Craig, B.W. Ninham, and R.M. Pashley. Effect of electrolytes on bubble coalescence. 364(6435):317 – 319, 1993.

[18] L. Vrbka and P. Jungwirth. Brine rejection from freezing salt solutions: A molecular dynamics study. *PHYSICAL REVIEW LETTERS*, 95(14):148501, 2005.

[19] P. Jungwirth, D. Rosenfeld, and V. Buch. A possible new molecular mechanism of thundercloud electrification. *ATMOSPHERIC RESEARCH*, 76(1-4):190 – 205, 2005.

[20] M.P. Allen and D.J. Tildesley. *Computer Simulations of Liquids.* Oxford University, New York, 1987.

[21] T. Darden, D. York, and Pedersen L. Particle mesh ewald: An n-log(n) method for ewald sums in large systems. *JOURNAL OF CHEMICAL PHYSICS*, 98(7):10089 – 10092, 1993.

[22] U. Essmann, L. Perera, M.L. Berkowitz, T. Darden, H. Lee, and L.G. Pedersen. A smooth particle mesh ewald method. *JOURNAL OF CHEMICAL PHYSICS*, 103(19):8577 – 8593, 1995.

[23] R.W. Hockney and J.W. Easrwood. *Computer Simulation Using Particles.* McGraw-Hill, New York, 1981.

[24] B.A. Luty, I.G. Tironi, and W.F. Vangunsteren. Lattice-sum methods for calculating electrostatic interactions in molecular simulations. *JOURNAL OF CHEMICAL PHYSICS*, 103(8):3014 – 3021, 1995.

[25] E. Spohr. Effect of electrostatic boundary conditions and system size on the interfacial properties of water and aqueous solutions. *JOURNAL OF CHEMICAL PHYSICS*, 107(16):6342 – 6348, 1997.

[26] I.C. Yeh and M.L. Berkowitz. Ewald summation for systems with slab geometry. *JOURNAL OF CHEMICAL PHYSICS*, 111(7):3155 – 3162, 1999.

[27] D.A. Pearlman, D.A. Case, J.W. Caldwell, W.S. Ross, T.E. Cheatham, S. Debolt, D. Ferguson, G. Seibel, and P. Kollman. Amber, a package of computer-programs for applying molecular mechanics, normal-mode analysis, molecular-dynamics and free-energy calculations to simulate the structural and energetic properties of molecules. *COMPUTER PHYSICS COMMUNICATIONS*, 91(1-3):1 – 41, 1995.

[28] C. Wagner. The surface tension of dilute solutions of electrolytes. *Physikalische Zeitschrift*, 25:474–477, 1924.

[29] L. Onsager and N.T. Samaras. The surface tension of debye-hückel electrolytes. *JOURNAL OF CHEMICAL PHYSICS*, 2:528 – 536, 1934.

[30] J.D. Jackson. *Klassische Elektrodynamik*. Gruyter, 2002.

[31] P. Jungwirth and D.J. Tobias. Molecular structure of salt solutions: A new view of the interface with implications for heterogeneous atmospheric chemistry. *JOURNAL OF PHYSICAL CHEMISTRY B*, 105(43):10468 – 10472, 2001.

[32] Q. Du, R. Superfine, E. Freysz, and Y.R. Shen. Vibrational spectroscopy of water at the vapor water interface. *PHYSICAL REVIEW LETTERS*, 70(15):2313 – 2316, 1993.

[33] E.A. Raymond and G.L. Richmond. Probing the molecular structure and bonding of the surface of aqueous salt solutions. *JOURNAL OF PHYSICAL CHEMISTRY B*, 108(16):5051 – 5059, 2004.

[34] D.F. Liu, G. Ma, L.M. Levering, and H.C. Allen. Vibrational spectroscopy of aqueous sodium halide solutions and air-liquid interfaces: Observation of increased interfacial depth. *JOURNAL OF PHYSICAL CHEMISTRY B*, 108(7):2252 – 2260, 2004.

[35] D.M. Ferguson. Parameterization and evaluation of a flexible water model. *JOURNAL OF COMPUTATIONAL CHEMISTRY*, 16(4):501 – 511, 1995.

[36] A. Morita and J.T. Hynes. A theoretical analysis of the sum frequency generation spectrum of the water surface. ii. time-dependent approach. *JOURNAL OF PHYSICAL CHEMISTRY B*, 106(3):673 – 685, 2002.

[37] V.S.J. Craig. Bubble coalescence and specific-ion effects. *CURRENT OPINION IN COLLOID & INTERFACE SCIENCE*, 9(1-2):178 – 184, 2004.

A Attached Publications

Solvation of the Azide Anion (N_3^-) in Water Clusters and Aqueous Interfaces: A Combined Investigation by Photoelectron Spectroscopy, Density Functional Calculations, and Molecular Dynamics Simulations†

Xin Yang, Boggavarapu Kiran, Xue-Bin Wang, and Lai-Sheng Wang*

Department of Physics, Washington State University, 2710 University Drive, Richland, Washington 99352, and W. R. Wiley Environmental Molecular Sciences Laboratory, Pacific Northwest National Laboratory, MS K8-88, P.O. Box, Richland, Washington 99352

Martin Mucha and Pavel Jungwirth

Institute of Organic Chemistry and Biochemistry, Academy of Sciences of the Czech Republic and Center for Complex Molecular Systems and Biomolecules, Flemingovo nam. 2, 16610 Prague 6, Czech Republic

Received: January 26, 2004; In Final Form: March 29, 2004

We report a photoelectron spectroscopy and computational study of hydrated N_3^- anion clusters, $N_3^-(H_2O)_n$ ($n = 0-16$), in the gas phase. Photoelectron spectra of the solvated azide anions were observed to consist of a single peak, similar to that of the bare N_3^-, but the spectral width was observed to broaden as a function of cluster size due to solvent relaxation upon electron detachment. The adiabatic and vertical electron detachment energies were measured as a function of solvent number. The measured electron binding energies indicate that the first four solvent molecules have much stronger interactions with the solute anion, forming the first solvation shell. The spectral width levels off at $n = 7$, suggesting that three waters in the second solvation shell are sufficient to capture the second shell effect in the solvent relaxation. Density functional calculations were carried out for N_3^- solvated by one to five waters and showed that the first four waters interact directly with N_3^- and form the first solvation shell on one side of the solute. The fifth water does not directly solvate N_3^- and begins the second solvation shell, consistent with the observed photoelectron data. Molecular dynamics simulations on both solvated clusters and bulk interface revealed that the asymmetric solvation state in small clusters persist for larger systems and that N_3^- prefers interfacial solvation on water clusters and at the extended vacuum/water interface.

Introduction

As a classical example of a strong nucleophile, the azide anion is of considerable importance in organic and inorganic chemistry.[1-3] The structure and properties of N_3^- have been well studied by various spectroscopic methods in the gas phase,[4-7] solution,[8-13] and crystal and solid matrixes.[14-16] Theoretical calculations have also been carried out on the electronic structure of the azide anion and its behavior in solution.[17-23] Despite all the experimental and theoretical investigations in bulk solution, little information has been obtained about the microsolvation of the azide anion in water clusters, which can provide molecular level understanding about the azide-water interactions. The large values of the quadruple moment and polarizability[22] make N_3^- a very special solute. One interesting issue is whether azide anion resides on the surface or in the center of a water cluster and how the solvation state evolves upon increasing the cluster size.

Gas-phase photoelectron spectroscopy (PES) is an important tool for studying the energetics and dynamics of solvated anions. It has been used to study the electronic structure of hydrated electron and halide anions.[24-28] Very recently, our group has investigated the solvation of complex anions, such as $^-O_2C-(CH_2)_n-CO_2^-$ ($n = 2-10$),[29,30] NO_3^-,[31] SO_4^{2-},[32-34] and $C_2O_4^{2-}$,[35] using a PES apparatus coupled to an electrospray ionization (ESI) source.[36] In the current work, we report a combined study on the solvation of N_3^- using PES, density functional theory (DFT) calculations, and molecular dynamics (MD) simulations. Hydrated clusters of the azide anion, $N_3^-(H_2O)_n$, were produced by an ESI source. We measured the PES spectra of the solvated species for $n = 0-16$ at 193 nm (6.424 eV) and obtained the adiabatic and vertical electron detachment energies. The stepwise increase in the electron detachment energies revealed that the first four water molecules have strong interactions with N_3^-. DFT calculations were carried out, focusing on how the first few waters solvate N_3^-. The solvation state of N_3^- in large water clusters and at the extended vacuum/water interface was investigated by MD simulations. Both the PES data and the theoretical studies suggest an asymmetric solvation state with a surface character of the azide anion on water clusters and at extended water/vacuum interfaces.

Experimental Method

The experiment was carried out using an apparatus equipped with a magnetic-bottle time-of-flight (TOF) photoelectron analyzer and an ESI source. Details of the experimental method have been reported elsewhere.[36] Only a brief description is given here. A 10^{-4} M sodium azide solution in a water/acetonitrile (20/80 volume ratio) mixed solvent was sprayed through a 0.01 mm diameter fused quartz syringe needle biased at −2.2 kV.

† Part of the special issue "Richard Bersohn Memorial Issue".

* To whom correspondence should be addressed. E-mail: ls.wang@pnl.gov.

10.1021/jp0496396 CCC: $27.50
Published on Web 05/08/2004

The resulting negatively charged droplets were fed into a desolvation capillary heated to ~70 °C. Anionic species emerging from the desolvation capillary were guided by a radio frequency quadruple system into a quadruple ion trap. The anions were accumulated in the ion trap for 0.1 s before being pushed into the extraction zone of a TOF mass spectrometer.

After mass selection and deceleration, the $N_3^-(H_2O)_n$ anion clusters of interest were intercepted by a 193 nm (6.424 eV) laser beam from an ArF excimer laser in the detachment zone of the magnetic-bottle photoelectron analyzer. Photoelectrons were collected at nearly 100% efficiency by the magnetic bottle and analyzed in a 4 m long TOF tube. The experiment was done at 20 Hz repetition rate with the ion beam off at alternating laser shots for background subtraction. The photoelectron TOF spectra were converted to kinetic energy spectra calibrated by the known spectra of I^- and O^-. The electron binding energy spectra presented were obtained by subtracting the kinetic energy spectra from the detachment photon energy. The energy resolution ($\Delta E/E$) was about 2%, i.e., ~10 meV for 0.5 eV electrons, as measured from the spectrum of I^- at 355 nm.

Theoretical Methods

We used DFT calculations to explore the structures of the small solvated clusters, $N_3^-(H_2O)_n$ (n = 0–5). The final geometries were optimized using the hybrid B3LYP functional and the 6-311++G** basis set. The selection of the functional was based on a recent study, which shows that this method provides reliable data concerning the geometry and energetics of hydrated species.[37] Several initial geometries were considered. All calculations were done without any symmetry constraints using a tight geometry convergence criterion. Vertical detachment energies (VDE) were also calculated as the difference in total energy between the optimized anions and the corresponding neutral clusters at the anionic geometries. The DFT calculations were performed using the NWChem program package.[38]

Molecular dynamics simulations were performed for two systems: (1) a cluster consisting of an azide anion and sixteen water molecules and (2) an extended aqueous system in a slab geometry containing a single N_3^- species in the unit cell. In the latter case, 556 water molecules and one azide anion were placed in a periodic box of dimensions 26.4 × 26.4 × 100 Å^3. The extension of one of the box dimensions leads to the slab arrangement of the system with two vacuum/water interfaces. For the calculations with periodic boundaries the nonbonded interactions were cut off at 12 Å and long-range electrostatic interactions were accounted for using the particle mesh Ewald procedure.[39] These simulations were performed at 300 K, whereas the cluster calculations were run at 250 K to prevent water evaporation. Both systems were first equilibrated for several hundreds of picoseconds with a subsequent 1 ns production run. The time step was set to 1 fs and all OH bonds were constrained using the standard SHAKE procedure.[40] All MD calculations were performed using the Amber 6 program package.[41]

A polarizable force field was employed in the MD simulations. For water, we used the POL3 model.[42] For N_3^- we evaluated its gas-phase polarizability at the MP2/aug-cc-pvtz level. The resulting mean value of 5.85 Å^3 was evenly distributed on the three nitrogen atoms of the anion. For the slab calculations, the use of this value of polarizability led to the so-called polarization catastrophe, which occurs in the case of proximal, strongly polarizable centers.[43] Therefore, we had to reduce the atomic polarizabilities on nitrogen atoms from 1.95 to 1.2 Å^3. At the same ab initio level we also evaluated the partial charges using the natural population analysis, yielding −0.62 |e| on the terminal nitrogens and +0.24 |e| on the central nitrogen atom. The van der Waals parameters of N_3^- were adopted from ref 44.

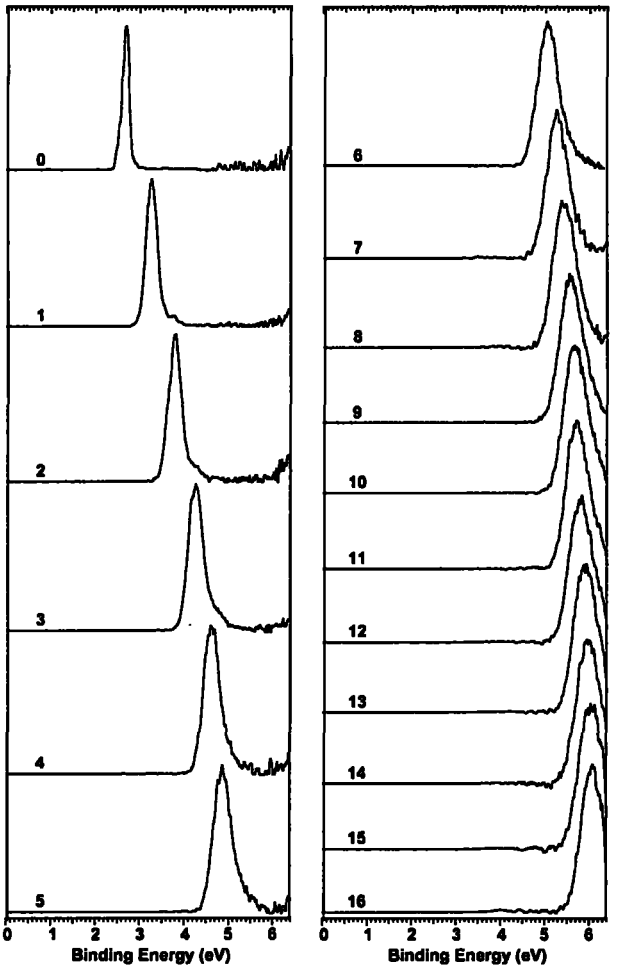

Figure 1. Photoelectron spectra of $N_3^-(H_2O)_n$ (n = 0–16) at 193 nm (6.424 eV).

Results and Discussion

Photoelectron Spectra. Figure 1 shows the PES spectra of $N_3^-(H_2O)_n$ (n = 0–16) at 193 nm. We also took the spectrum of the bare N_3^- at 355 nm with a higher energy resolution (not shown). The spectra of N_3^- at both wavelengths consist of a single sharp peak,[7] indicating that there is little geometry change between the ground states of the anion and the neutral species. This result is consistent with the calculated geometries of N_3 and N_3^-.[18] The spin–orbit splitting of N_3 is very small (9 meV), so the width of the peak in the 193 nm spectrum (Figure 1) is mostly due to the instrumental resolution for electrons at this kinetic energy.[7] The adiabatic electron detachment energy of N_3^- measured from the 355 nm spectrum was 2.68 ± 0.03 eV, in excellent agreement with previous studies on the azide anion.[5,7] The spectra for the solvated species also consist of a single feature and shift consistently to higher binding energies with increasing solvent number. The spectra became broadened and diffuse due to solvation and the spectral width seemed to increase with increasing solvent numbers.

Adiabatic and Vertical Detachment Energies and Evidence of the First Solvation Shell. The adiabatic (ADE) and

TABLE 1: Adiabatic (ADE) and Vertical (VDE) Electron Detachment Energies (eV) for $N_3^-(H_2O)_n$ (n = 0−16)[a]

n	ADE	ΔADE[b]	VDE	ΔVDE[c]	λ[e]
0	2.68(3)[d]		2.68(3)[d]		0
1	3.14(6)	0.46(6)	3.25(6)	0.57(6)	0.11
2	3.58(6)	0.44(6)	3.78(6)	0.53(6)	0.20
3	4.04(6)	0.46(6)	4.25(6)	0.47(6)	0.21
4	4.38(6)	0.34(6)	4.63(6)	0.38(6)	0.25
5	4.54(6)	0.16(6)	4.85(6)	0.22(6)	0.31
6	4.70(8)	0.16(8)	5.03(8)	0.18(8)	0.33
7	4.84(8)	0.14(8)	5.25(8)	0.22(8)	0.41
8	4.98(8)	0.14(8)	5.42(8)	0.17(8)	0.44
9	5.12(8)	0.14(8)	5.55(8)	0.13(8)	0.43
10	5.25(8)	0.13(8)	5.65(8)	0.10(8)	0.40
11	5.34(8)	0.09(8)	5.70(8)	0.05(8)	0.36
12	5.37(8)	0.03(8)	5.79(8)	0.09(8)	0.42
13	5.45(8)	0.08(8)	5.89(8)	0.10(8)	0.44
14	5.49(8)	0.04(8)	5.95(8)	0.06(8)	0.46
15	5.58(8)	0.09(8)	6.02(8)	0.07(8)	0.44
16	5.62(8)	0.04(8)	6.07(8)	0.05(8)	0.45

[a] The numbers in the parentheses represent the uncertainties in the last digit. [b] ADE(n) − ADE(n−1). [c] VDE(n) − VDE(n−1). [d] The EA of N_3 measured from the 355 nm spectrum. This value was measured to be 62.1 ± 2.8 kcal/mol (2.69 ± 0.12 eV) from ref 4 and 2.68 ± 0.01 eV from ref 7. [e] VDE − ADE.

vertical (VDE) electron detachment energies for $N_3^-(H_2O)_n$ (n = 0−16) are listed in Table 1. For N_3^-, the ADE and VDE are identical because the geometry change between the anion and neutral is negligibly small. For the solvated clusters, the spectra became broader due to solvent relaxation upon electron detachment. Because no vibrational features were resolved, the ADE was estimated by first drawing a straight line at the leading edge of the photodetachment feature. Then a constant was added to the intersection with the binding energy axis to take into account the instrumental resolution. The VDE was obtained from the peak maximum in each spectrum.

The ADE and VDE as a function of solvent number are plotted in Figure 2a. Both curves show a monotonic increase with a clear change of slope at n = 5. This turning point can be observed more clearly in the incremental increase in binding energies, as shown in Figure 2b. The quantity, ΔADE [ADE(n) − ADE(n−1)], represents the electron stabilization energy with the addition of one extra solvent molecule. The first four waters clearly have the strongest stabilizing effect with ΔADE ≥ 0.34 eV (Table 1). The ΔADE suddenly drops to 0.16 eV for n = 5 and steadily decreases for larger solvent numbers. The observation suggests that the first four water molecules interact strongly with N_3^-, evident of the first solvation shell, whereas the solute−solvent interactions become much weaker starting from the fifth water molecule, evident of the onset for the second solvation shell.

Spectral Width and Solvent Relaxation. The spectral width in the PES spectra represents the Franck−Condon envelope of the electronic transition between the anion and the relevant neutral state, i.e., the geometry changes between the anion ground state and the final state of the neutral species. As shown in Figure 1 and in previous studies,[7] the PES spectrum of N_3^- gave a single sharp peak, indicating that there is very little geometry change upon electron detachment. However, the spectra of the solvated species became broadened and the spectral width seemed to increase with the solvent number. A good measure of the spectral width can be obtained from the difference between the ADE and VDE. These are listed in Table 1 as λ. This value increases steadily from n = 0−7 and then levels off for n > 7, reaching a value of ~0.45 eV. Because there is little geometry change upon electron detachment for

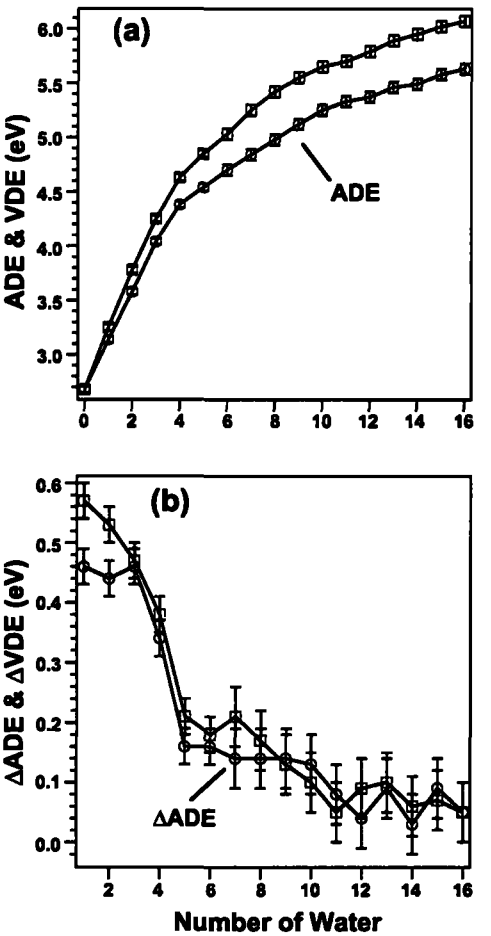

Figure 2. (a) Adiabatic (ADE) and vertical (VDE) detachment energies of $N_3^-(H_2O)_n$ (n = 0−16) as a function of solvent number (n). (b) Incremental increase of electron detachment energies, ΔADE = ADE(n) − ADE(n−1) and ΔVDE, as a function of solvent number (n).

N_3^- itself, the spectral width of the solvated clusters should be mainly due to the solvent relaxation around the solute upon electron detachment. It is interesting to note that the solvent relaxation levels off at seven water molecules, which is beyond the first solvation shell. This observation suggests that the second solvation shell is very important for the solvent relaxation. That the additional solvent beyond n = 7 does not significantly increase the relaxation energies indicates that three solvent molecules in the second solvation shell are sufficient to reproduce the effect of solvent reorganization.

DFT Calculations for Small Solvated Clusters, $N_3^-(H_2O)_n$ (n = 0−5). The calculated geometries of $N_3^-(H_2O)_n$ (n = 0−5) are presented in Figure 3 along with the solute charge distributions and key bond lengths. The calculated VDE for each structure is given in Table 2. The azide anion is linear with centrosymmetric charge distribution (Figure 3, **a**). Note that the terminal nitrogen atoms carry more than half of an electron charge. The first water forms a strong hydrogen bond with one terminal nitrogen and breaks the symmetry of the solute anion. The N···H H-bond length is extremely short (Figure 3, **b**) and the nitrogen atom that forms the H-bond carries more charge than the nitrogen at the free end. This polarization is accompanied by a small change in the N−N bond lengths (Figure 3, **b**). For n = 2, there are two energetically degenerate solvation structures: (1) with the two water molecules solvating the two terminal N symmetrically (Figure 3, **c1**) and (2) with both water

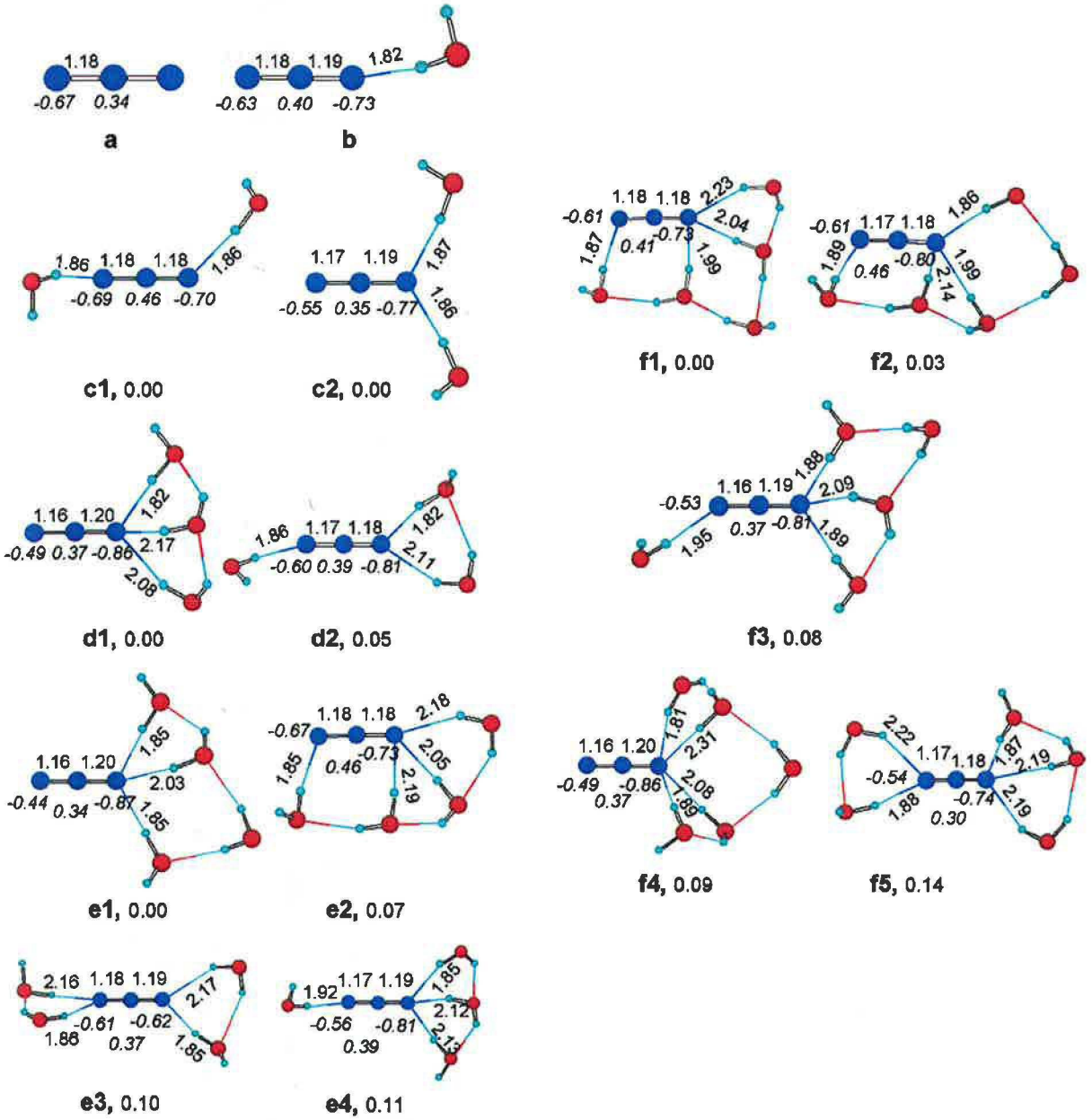

Figure 3. Optimized structures for the lowest energy isomers of $N_3^-(H_2O)_n$ ($n = 0-5$) at B3LYP/6-311++G**. Relative energies are given in electronvolts. Mulliken charges on the nitrogen atoms are also given, along with key bond lengths in angstrom.

molecules solvating only one terminal nitrogen (Figure 3, **c2**). In the latter case, the azide anion is further polarized. In both structures, the water−N H-bonds are strong with rather short N···H bond lengths. Interestingly, for $N_3^-(H_2O)_3$ the one-end solvation structure (Figure 3, **d1**) is slightly preferred because of the favorable water−water H-bonding.

For $N_3^-(H_2O)_4$, four low-energy structures (Figure 3, **e1**−**e4**) were obtained. The lowest energy one (**e1**) is similar to **d1** of $N_3^-(H_2O)_3$ with the fourth water forming only water−water hydrogen bonds. Thus, the maximum coordination number for one terminal nitrogen with water seems to be three, which is consistent with a previous MD simulation.[23] The second lowest energy solvation structure (**e2**) is very interesting. The four solvent molecules form a water chain along one side of the azide anion with three of them coordinating to one terminal nitrogen and the fourth water coordinating to the other terminal nitrogen. The other two structures for $N_3^-(H_2O)_4$ (**e3**, **e4**) both involve solvating the two terminal N separately and are energetically unfavorable, again showing the importance of the solvent−solvent H-bonding. The "side-chain" structures turned out to be the lowest energy conformations for $N_3^-(H_2O)_5$ (Figure 3, **f1**, **f2**), which both can be viewed as adding the fifth water to the second solvation shell of the "side-chain" structure of $N_3^-(H_2O)_4$ (**e2**). The other three conformations for $N_3^-(H_2O)_5$ (Figure 3, **f3**, **f4**, and **f5**) were all built from the low-lying isomers of $N_3^-(H_2O)_4$ and were slightly unfavored relative to **f1** and **f2**. However, as shown in Table 2 for the calculated VDEs, the lowest energy structure (**f1**) seems to be the most likely isomer responsible for the observed PES spectrum.

The calculated VDEs for all the low-lying isomers shown in Figure 3 for $N_3^-(H_2O)_n$ ($n = 0-5$) are given in Table 2. The calculated VDE for N_3^- is in excellent agreement with the

TABLE 2: Calculated Vertical Detachment Energies (VDE, eV) for $N_3^-(H_2O)_n$ ($n = 0-5$) Compared with the Experimental Value from Table 1[a]

n	isomers	VDE (theo)	VDE (exp)[b]
0	**a**	2.72	2.68 (3)
1	**b**	3.42	3.25 (3)
2	**c1**	4.04	3.78 (6)
	c2	4.05	
3	**d1**	4.49	4.25 (6)
	d2	4.52	
4	**e1**	4.87	4.63 (6)
	e2	4.82	
	e3	4.97	
	e4	4.96	
5	**f1**	4.96	4.85 (6)
	f2	5.17	
	f3	5.24	
	f4	5.36	
	f5	5.31	

[a] See Figure 3 for the Labels of the Isomers. [b] Reproduced from Table 1.

experimental measurement. However, the theoretical VDEs for the solvated species appear to be too large by between 0.17 and 0.26 eV for the low-lying isomers of $N_3^-(H_2O)_n$. For $n =$ 2 and 3, the two isomers are close in energy and they also have nearly identical theoretical VDEs, suggesting that they might both be populated and contribute to the PES spectra. For $N_3^-(H_2O)_4$, the two higher energy isomers (**e3**, **e4**) give VDEs that are higher than the experimental value by more than 0.3 eV and can be ruled out. It is interesting to observe that the "side-chain" structure (**e2**) gives the best VDE relative to the experimental value. For $N_3^-(H_2O)_5$, despite the near degeneracy between the two lowest-energy isomers (**f1**, **f2**), the **f1** isomer yielded the best VDE in comparison with the experimental data.

Microsolvation of N_3^- by Water. Overall, the DFT data are in excellent agreement with the experiment. In particular, the trend of the solvation structure and the trend of the theoretical VDEs are consistent with the experimental observation. We see that, except for the **e1** structure of $N_3^-(H_2O)_4$, the first four waters interact directly with N_3^- and provide the strongest stabilization, essentially forming the first solvation shell. The fifth water does not directly interact with the solute and thus exerts only small stabilization to the electron binding energy of N_3^-. The fifth water begins to form the second solvation shell. This trend of solvation suggests that the second solvation shell will form asymmetrically along one side of the azide anion and would lead to a surface-solvated N_3^-. This is consistent with our observation for the large solvated clusters and is born out from the MD simulations, as shown below.

In our previous PES studies of hydrated SO_4^{2-} and $C_2O_4^{2-}$, we observed the solute photoemission features to decrease with increasing degree of solvation.[33-35] This observation was interpreted as due to the fact that the solute anion is solvated in the center of the solvated clusters. For $N_3^-(H_2O)_n$, the PES spectra contain only one solute band throughout the investigated cluster size range and it was difficult to evaluate its relative intensity change with the degree of solvation. Nevertheless, we did notice that the electron signals were quite intense for the large clusters ($n > 15$) although their mass intensities decrease significantly, compared to the bare N_3^- and small solvated clusters. This phenomenon was quite similar to PES spectra of hydrated I^- clusters, which represent a typical system with surface solvated anions.[25,45] Therefore, our observation of strong photoemission signals for the large solvated clusters suggest that N_3^- is likely to be on the surface of the large solvated clusters.

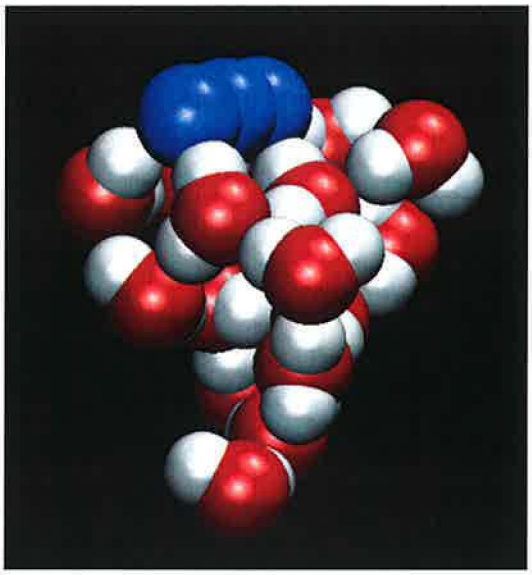

Figure 4. Typical snapshot from a MD simulation of a cluster consisting of 16 water molecules and a single azide anion. Color coding: nitrogen, blue; oxygen, red; hydrogen, white.

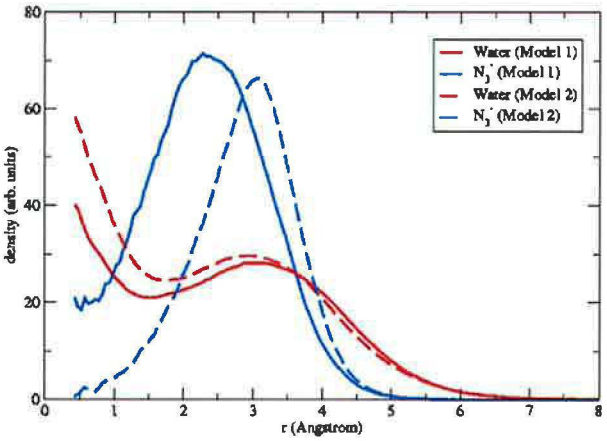

Figure 5. Distributions of distances of water molecules and N_3^- from the center of mass of the water clusters in $N_3^-(H_2O)_{16}$. Model 1: full polarizability of 1.95 Å^3 on nitrogen atoms. Model 2: polarizability on nitrogen atoms reduced to 1.2 Å^3.

MD Simulations of $N_3^-(H_2O)_{16}$. Figure 4 depicts a typical snapshot from a MD simulation of a cluster consisting of 16 water molecules and a single azide anion. The snapshot clearly indicates the preferred surface solvation of N_3^-. This is quantified in Figure 5, which shows the distributions of distances of water molecules and N_3^- from the center of mass of the water cluster. The water signal peaks at the center with a second maximum around 3 Å, which corresponds to "outer shell" water molecules. The distribution of N_3^- peaks exactly in this outer shell—a clear fingerprint of surface solvation. Results for full and reduced polarizabilities of N_3^- are qualitatively similar with the anionic surface effect being slightly more pronounced for the model with full polarizability. A reduction of polarizability by 5−10% can be attributed to solvent effects.[44] However, the reduction necessary to stabilize the slab calculation is more significant (almost 40%). Nevertheless, the effect of such reduction is small and the propensity for surface solvation is preserved. However, a nonpolarizable potential model did not predict a surface solvated N_3^-, but rather an interior solvated structure (results not shown here).

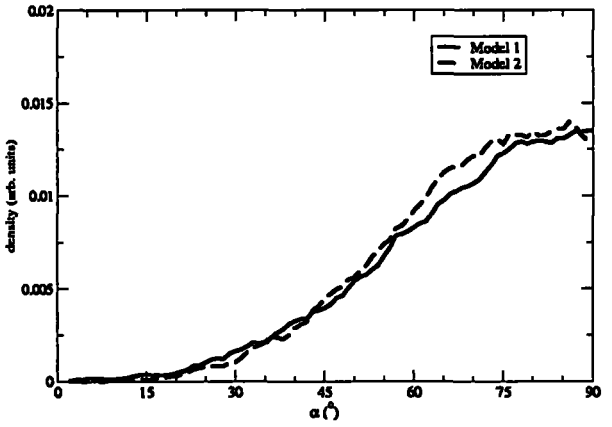

Figure 6. Distribution of angles between the molecular axis of N_3^- and the line connecting the center of mass of the water cluster and that of the azide anion in $N_3^-(H_2O)_{16}$. Model 1: full polarizability of 1.95 Å^3 on nitrogen atoms. Model 2: polarizability on nitrogen atoms reduced to 1.2 Å^3.

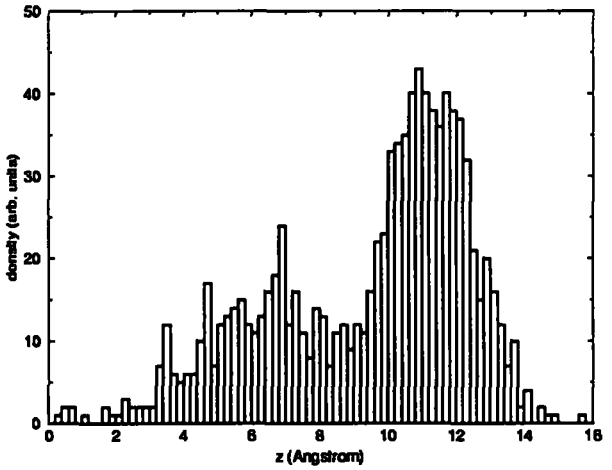

Figure 7. Density profile of the azide anion from the center of an aqueous slab to the vacuum/water interface. The interfacial region lies between 10 and 14 Å.

Figure 6 shows the distribution of angles between the molecular axis of N_3^- and the line connecting the center of mass of the water cluster and that of the azide anion. The angular distribution peaks at 90°, a clear indication of a preferred orientation of N_3^- parallel to the cluster surface. The results for the two values of the azide polarizability almost coincide with each other. The MD results are consistent with the trend predicted from the DFT calculations for the small solvated clusters (Figure 3) and the observation of the strong PES signals for the large solvated species. Both pointed to a surface solvated N_3^- in the hydrated clusters $N_3^-(H_2O)_n$, which is born out nicely from the MD simulations.

MD Simulation of N_3^- at Extended Water/Vacuum Interfaces. It is interesting to address the question whether the surface propensity of the azide anion persists upon moving from the hydrated clusters to extended aqueous systems. Results of MD simulation of N_3^- in/on an aqueous slab are presented in Figures 7 and 8. Figure 7 displays a density profile of N_3^-, i.e., a histogramed distribution of N_3^- from the center of the slab to the vacuum/water interface (the interfacial region corresponds to values of the z-coordinate between roughly 10 and 14 Å). As in the cluster system, the N_3^- distribution strongly peaks at the interface and clearly indicates surface solvation. Note that

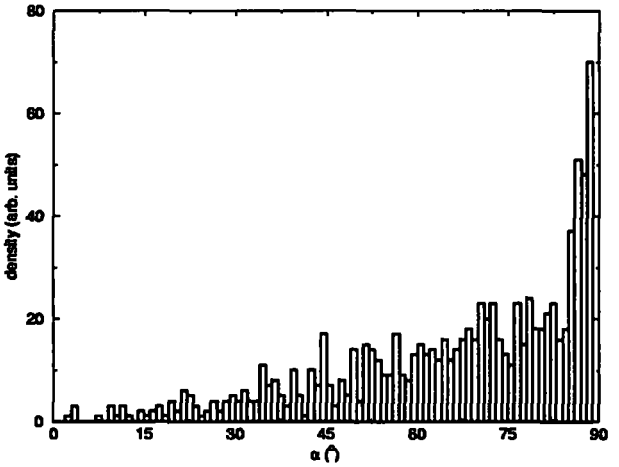

Figure 8. Distribution of angles between the molecular axis of the N_3^- and the normal to the surface of the slab.

this result was obtained for the azide polarizability reduced by 40%. Were we able to circumvent the polarization catastrophe problem and perform the slab calculation with the full polarizability of the anion, the surface propensity of N_3^- would come out even more strongly.

Finally, Figure 8 shows the distribution of angles between the molecular axis of N_3^- and the normal to the surface of the slab. Similar to the cluster system, the angular distribution peaks around 90°. A close inspection of the trajectory reveals that the orientation of N_3^- is strongly correlated with the position of the anion in the slab. On one hand, when the azide anion is at the water/vacuum interface (which is most of the time) it is almost exclusively oriented parallel to the surface. On the other hand, during the short periods when N_3^- "dives" into the subsurface or aqueous bulk, its orientation tends to get randomized, which would be expected if the solvent environment is more or less symmetric.

We note that the behavior of N_3^- at the bulk interface is well represented using a solvated cluster. Both the DFT and MD results confirm the experimental inference of four waters as the first solvation shell of N_3^-. Because the solvent relaxation levels off at seven waters, as observed in the PES data, the MD results also verify the notion that a seven-water cluster can be used as the bare minimum to describe the solvation behavior of N_3^- using cluster models.

Conclusions

Gas-phase photoelectron spectroscopic and computational studies of water-solvated azide anion clusters, $N_3^-(H_2O)_n$ (n = 0−16), were reported. PES spectra of bare and solvated N_3^- were taken at 6.424 eV (193 nm). The spectral features of the solvated clusters are similar to that of the bare N_3^-, except that they become broadened and shifted to the blue due to solvation. The spectral width increases with the solvation number and levels off at $n = 7$. The adiabatic and vertical electron binding energies were measured for each species. The stepwise electron stabilization energies indicated that the first four solvent molecules have the strongest interaction with the solute anion. DFT calculations show how the first five solvent molecules solvate N_3^- one water at a time and revealed numerous low-lying isomers in each solvated species. In general, the first four water molecules were found to directly coordinate to N_3^- along one side of the linear anion, forming the first solvation shell asymmetrically; the fifth water has no direct interactions with

the solute and begins the second solvation shell, consistent with the experimental observation. The leveling off of the spectral width at $n = 7$ suggests that three waters in the second solvation shell are sufficient to capture the solvent relaxation effect upon electron detachment. The asymmetric solvation state in the small clusters was shown to persist in larger solvation systems using MD simulations. MD simulations with a polarizable force field reveal that N_3^- anion clearly prefers interfacial over bulk solvation in large clusters and at the extended vacuum/water interface.

Acknowledgment. This work was supported by The U.S. Department of Energy (DOE), Office of Basic Energy Sciences, Chemical Science Division, and was performed at the W. R. Wiley Environmental Molecular Sciences Laboratory, a national scientific user facility sponsored by DOE's Office of Biological and Environmental Research and located at Pacific Northwest National Laboratory, operated for DOE by Battelle. Support from the Czech Ministry of Education via a grant No. ME644 is gratefully acknowledged.

References and Notes

(1) Patai, S. *The Chemistry of the Azido Group*; Interscience: London, 1971.
(2) Fair, H. D.; Walker, R. F. *Energ. Mater.* **1997**, *1*.
(3) Ingold, C. K. *Structure and Mechanism in Organic Chemistry*; Cornell University Press: Ithaca, New York, 1969.
(4) Jackson, R. L.; Pellerite, M. J.; Brauman, J. I. *J. Am. Chem. Soc.* **1981**, *103*, 1802.
(5) Polak, M.; Gruebele, M.; Saykally, R. J. *J. Am. Chem. Soc.* **1987**, *109*, 2884.
(6) Owrutsky, J. C.; Rosenbaum, N.; Tack, T.; Gruebele, M.; Polak, M.; Saykally, R. J. *Philos. Trans. R. Soc., London A* **1988**, *324*, 23.
(7) Continetti, R. E.; Cyr, D. R.; Metz, R. B.; Neumark, D. M. *Chem. Phys. Lett.* **1991**, *182*, 406.
(8) Dean, K. J.; Wilkinson, G. R. *J. Raman Spectrosc.* **1985**, *16*, 22.
(9) Li, M.; Owrutsky, J. C.; Sarisky, M. J.; Culver, J. P.; Yodh, A.; Hochstrasser, R. M. *J. Chem. Phys.* **1993**, *98*, 5499.
(10) Hamm, P.; Lim, M.; Hochstrasser, R. M. *Phys. Rev. Lett.* **1998**, *81*, 5326.
(11) Le Borgne, C.; Illien, B.; Beignon, M.; Chabane, M. *Phys. Chem. Chem. Phys.* **1999**, 1, 4701.
(12) Waterland, M. R.; Kelley, A. M. *J. Phys. Chem. A* **2001**, *105*, 8385.
(13) Zhong, Q.; Steinhurst, D. A.; Carpenter, E. E.; Owrustsky, J. C. *Langmuir* **2002**, *18*, 7401.
(14) Sherman, W. F.; Wilkinson, G. R. *Vibrational Spectroscopy of Trapped Species*; Hallam, H. E., Ed.; Wiley: London, 1973; pp 245–354.
(15) Zhou, M.; Andrew, L. *J. Phys. Chem. A* **2000**, *104*, 1648.
(16) Andrew, L.; Zhou, M.; Chertihin, G. V.; Bare, W. D.; Hannachi, Y. *J. Phys. Chem. A* **2000**, *104*, 1656.
(17) Peyerimhoff, S. D.; Buencker, R. J. *J. Chem. Phys.* **1967**, *47*, 1953.
(18) Archibald, T. W.; Sabin, J. R. *J. Chem. Phys.* **1971**, *55*, 1821.
(19) Gora, T.; Kemmey, P. J. *J. Chem. Phys.* **1972**, *57*, 3579.
(20) Rossi, A. R.; Bartram, R. H. *J. Chem. Phys.* **1979**, *70*, 532.
(21) Botschwina, P. *J. Chem. Phys.* **1986**, *85*, 4591.
(22) Morita, A.; Kato, S. *J. Chem. Phys.* **1998**, *109*, 5511.
(23) Yarne, D. A.; Tuckerman, M. E.; Klein, M. L. *Chem. Phys.* **2000**, *258*, 163.
(24) Coe, J. V.; Lee, G. H.; Eaton, J. G.; Arnold, S. T.; Sarkas, H. W.; Bowen, K. H. *J. Chem. Phys.* **1990**, *92*, 3980.
(25) Markovich, G.; Pollack, S.; Giniger, R.; Cheshnovsky, O. *J. Chem. Phys.* **1994**, *101*, 9344.
(26) Kim, J.; Becker, I.; Cheshnovsky, O.; Johnson, M. A. *Chem. Phys. Lett.* **1998**, *297*, 90.
(27) Lehr, L.; Zanni, M. T.; Frischkorn, C.; Weinkauf, R.; Neumark, D. M. *Science* **1999**, *284*, 635.
(28) Yang, X.; Wang, X. B.; Wang, L. S. *J. Chem. Phys.* **2001**, *115*, 2889.
(29) Ding, C. F.; Wang, X. B.; Wang, L. S. *J. Phys. Chem. A* **1998**, *102*, 8633.
(30) Yang, X.; Fu, Y. J.; Wang, X. B.; Slavicek, P.; Muncha, M.; Jungwirth, P.; Wang, L. S. *J. Am. Chem. Soc.* **2004**, *126*, 876.
(31) Wang, X. B.; Yang, X.; Wang, L. S.; Nicholas, J. B. *J. Chem. Phys.* **2002**, *116*, 561.
(32) Wang, X. B.; Nicholas, J. B.; Wang, L. S. *J. Chem. Phys.* **2000**, *113*, 10837.
(33) Wang, X. B.; Yang, X.; Nicholas, J. B.; Wang, L. S. *Science* **2001**, *294*, 1322.
(34) Yang, X.; Wang, X. B.; Wang, L. S. *J. Phys. Chem. A* **2002**, *106*, 7607.
(35) Wang, X. B.; Yang, X.; Nicholas, J. B.; Wang, L. S. *J. Chem. Phys.* **2003**, *119*, 3631.
(36) Wang, L. S.; Ding, C. F.; Wang, X. B.; Barlow, S. E. *Rev. Sci. Instrum.* **1999**, *70*, 1957.
(37) Tuma, C.; Boese, A. D.; Handy, N. C. *Phys. Chem. Chem. Phys.* **1999**, *1*, 3939.
(38) High Performance Computational Chemistry Group, *NWChem, A Computational Chemistry Package for Parallel Computers, Version 4.5*; Pacific Northwest National Laboratory, Richland, WA 99352, 2003.
(39) Essmann, U.; Perera, L.; Berkowitz, M. L.; Darden, T.; Pedersen, L. G. *J. Chem. Phys.* **1995**, *103*, 8577.
(40) Ryckaert, J. P.; Ciccotti, G.; Berendsen, H. J. C. *Comput. J. Phys.* **1997**, *23*, 327.
(41) Case, D. A.; Pearlman, D. A.; Caldwell, J. W.; Cheatham, T. E., III; Ross, W. S.; Simmerling, C. L.; Darden, T. A.; Merz, K. M.; Stanton, R. V.; Cheng, A. L.; Vincent, J. J.; Crowley, M.; Tsui, V.; Radmer, R. J.; Duan, Y.; Pitera, J.; Massova, I.; Seibel, G. L.; Singh, U. C. *AMBER6*; University of California: San Francisco, 1999.
(42) Caldwell, J. W.; Kollman, P. A. *J. Phys. Chem.* **1995**, *99*, 6208.
(43) Thole, B. T. *Chem. Phys.* **1981**, *59*, 341.
(44) Morita, A.; Kato, S. *J. Chem. Phys.* **1998**, *109*, 5511.
(45) Coe, J. V. *J. Phys. Chem. A* **1997**, *101*, 2055.

Enhanced Concentration of Polarizable Anions at the Liquid Water Surface: SHG Spectroscopy and MD Simulations of Sodium Thiocyanide

Poul B. Petersen and Richard J. Saykally*

Department of Chemistry, University of California, Berkeley, California 94720

Martin Mucha and Pavel Jungwirth*

Institute of Organic Chemistry and Biochemistry, Academy of Sciences of the Czech Republic and Center for Biomolecules and Complex Molecular Systems, Flemingovo nam. 2, 16610 Prague 6, Czech Republic

Received: February 18, 2005; In Final Form: March 28, 2005

Contrasting current textbook descriptions, a consistent picture of substantial concentration enhancement of highly polarizable anions at the surface of aqueous electrolyte solutions is emerging. Such enhancement may have important implications for chemistry occurring on aqueous aerosols and ocean surfaces. Here we present a combined experimental and theoretical investigation of the liquid/air interface of aqueous sodium thiocyanide at varying salt concentrations. Normalized second harmonic generation intensities fitted to Langmuir isotherms yield a Gibbs free energy of adsorption of −1.80 kcal/mol. These results are in accord with molecular dynamics simulations in slab geometry, which predict an appreciable surface enhancement of SCN^-.

1. Introduction

Recent theoretical and experimental studies have indicated the adsorption of highly polarizable anions to the outermost layer of the liquid water−air interface.[1−9] These findings contradict the textbook description of ions being repelled from the interface and the outermost surface layer being devoid of ions.[10−12] This conventional wisdom is largely based on macroscopic measurements of the increasing surface tension of aqueous solutions with salt concentration. When combined with the Gibbs adsorption equation, such measurements dictate that the ion concentration, integrated over the entire interfacial region, must be depleted with respect to the bulk. This conclusion has been rationalized by electrostatic continuum models dating back to Onsager and Samaras, wherein the interface is described as a discontinuity between two continuous dielectric media.[13] Recent state-of-the-art continuum models have been augmented to include most interfacial forces.[14−19] These modern models mostly depict the outermost liquid layer of the interface as depleted of ions; however, in specific cases (e.g., for highly polarizable ions) some of them predict ion adsorption at the aqueous surface. While being useful in many respects, continuum models still engender several theoretical objections, such as problems with an accurate description of interactions within the first solvation shell, as described in a recent overview.[20]

The picture of an essentially ion-free surface layer was challenged a few years ago by the atmospheric community, which proposed that chemical reactions on aqueous sea salt particles, ocean surfaces, and laboratory aerosol experiments could not be explained without invoking ions at the surface.[21−23] This motivated studies by molecular dynamics simulations with use of polarizable potentials,[1−5,22] followed by indirect experimental investigations by Sum-Frequency Generation (SFG)[8,24] and later by direct measurements with Second Harmonic Generation (SHG)[6,7] of highly polarizable anions at the liquid water−air interface.

It is important to understand that the above theoretical and experimental findings do not contradict the macroscopic surface tension measurements and thermodynamic arguments. The macroscopic measurements offer no detailed molecular description of the surface concentration, but only dictate that the *integrated* ion concentration over the entire interfacial region is depleted. The highly polarizable anions show a very nonmonotonic interfacial distribution, strongly enhanced in the outermost liquid layer but depleted in the subsurface. Qualitatively, this is emerging from the molecular dynamics simulations, although the subsurface depletion is not quantitative due to the finite width of the "bulk" region of the simulated slab systems.[25] The surface propensity of large polarizable anions can be contrasted to the behavior of small nonpolarizable ions (such as alkali cations or fluoride), which are indeed repelled from aqueous surfaces, in accord with the traditional view.

Here we present a combined experimental and theoretical investigation of the surface adsorption of the thiocyanide anion in aqueous solutions of NaSCN of varying concentrations. Our experiments exploit the surface specific nature of SHG spectroscopy and directly probe the SCN^- ions via the strong charge-transfer-to-solvent (CTTS) transitions in the UV. The experimental SHG investigations were designed to measure the surface concentration dependence on the bulk concentration. The surface concentration was then fit to the Langmuir model and the Gibbs free energy of adsorption was determined. It is worth noting that the SHG experiments can only establish a minimum in the Gibbs free energy profile in the interfacial region, and thus a nonmonotonic anion distribution. The actual position of this minimum, at or just below the outermost surface layer, must rely on either anisotropy arguments or theoretical investigations. Our molecular dynamics simulations of solutions in a slab

* Address correspondence to these authors. R.J.S.: phone +1 (510) 642-8269, fax +1 (510) 642-8369, e-mail saykally@berkeley.edu. P.J.: phone +420 (220) 410 314, fax +420 (220) 410 320, e-mail pavel.jungwirth@uochb.cas.cz.

10.1021/jp050864c CCC: $30.25
Published on Web 05/10/2005

geometry provide this detailed molecular insight not obtainable in the experiments. The simulations show the concentration enhancement of the anions occurring in the outermost surface layer of the interface.

2. Experimental Details and the Langmuir Model

A detailed description of our SHG experiments is given elsewhere[26] and only a brief account is given here. The femtosecond laser system consists of a home-built Ti:sapphire oscillator and a commercial regenerative amplifier (Spectra Physics, Spitfire) that pumps two OPAs (Light Conversion, TOPAS). The laser system is capable of generating sub-100 fs laser pulses in the range 290 nm to 10 μm. The output of the TOPAS is purified with dichroic mirrors and optical filters before being focused onto the sample at 45°. The SHG beam is separated from the fundamental by dichroic mirrors and a prism before being collected on a solar blind PMT. Due to the strong SHG response of thiocyanide, pulse energies of only 0.5−3 μJ are needed for the experiments.

The sample is kept in an enclosed box purged with pure nitrogen that also gently stirs the liquid surface. All glassware in contact with the sample is cleaned with Nochromix (a hot chromic acid substitute) and rinsed with 18.2 MΩ water before each experiment. All solutions are made with 99.99% pure NaSCN and ultrapure water (18.2 MΩ and ≤4 ppb total organic content) from a water purification system (Millipore, Milli-Q Gradient).

As a second-order optical process, SHG is forbidden in bulk centrosymmetric media within the dipole approximation, and is thus a surface specific technique for liquids.[27,28] SHG and the related SFG process have been well characterized as direct probes of the liquid water surface structure and surfactants thereon,[29,30] with probing depth of a few molecular layers.[31] The SHG intensity ($I_{2\omega}$) is described in terms of the second-order susceptibility of the surface ($\chi^{(2)}$), which, in turn, is the sum of the molecular hyperpolarizabilities (β) in the interfacial region:

$$I_{2\omega} \propto |\chi^{(2)}|^2 \times I_\omega{}^2 \tag{1}$$

$$\chi^{(2)} = \chi^{(2)}_{\text{water}} + \chi^{(2)}_{\text{SCN-}} \tag{2}$$

$$\chi^{(2)}_{\text{SCN-}} = \sum_i \beta_i = N_S \times \langle\beta\rangle_{\text{Orientation}} \tag{3}$$

Like linear dielectric constants, second-order susceptibilities are real at nonresonant frequencies but become complex near resonances. For the experiments presented here, the water susceptibility is nonresonant (and thus real), but the thiocyanide resonance contains a complex, wavelength-dependent phase. If the orientation of the surface species and the magnitude of the hyperpolarizability are assumed to be constant over the concentration range studied, the change in the SHG intensity can be related to the change in surface concentration. This may seem a strong assumption, given the high concentrations studied, implying significant ion−ion interactions. However, the simulations show identical surface profiles for S, C, and N, implying that the SCN^- anions lie flat at the surface at all concentrations. Furthermore, previous SHG investigations of the Langmuir behavior of surfactants have shown that corrections due to changes in the molecular orientation are relatively small (<25%).[32]

The surface concentration of the ions is represented by the Langmuir adsorption isotherm, which is a standard and well-characterized adsorption model for liquid surfaces.[10,33−35]

$$N_S = N_S^{\max}\frac{Kx}{Kx + C_w} \approx \frac{N_S^{\max} \times x}{x + 55.5M\exp(\Delta G_{Ads}/RT)} \tag{4}$$

Here $N_S^{\max}$ is the maximum surface concentration, K is the equilibrium constant for surface adsorption, x and C_w are the bulk solute and water concentration, respectively, and ΔG_{Ads} is the Gibbs free energy of adsorption.

The Langmuir model assumes a maximum of one monolayer coverage ($N_S^{\max}$) and negligible surfactant−surfactant interactions. At low concentration, ions form a somewhat diffuse layer at the interface, but at higher concentrations, the simulations show the concentration enhancement to occur in a narrow region about 3 Å wide at the outermost surface layer. The enhancement is then followed by depletion in a broader region over deeper layers, with the total interfacial region having a width of more than 10 Å. The probing depth of the experiment is currently not well-known. For the pure water interface with a 90−10 thickness of approximately 5 Å, calculations have shown that almost the entire SHG intensity comes from the outermost surface layer.[31] For the salt solutions, the interface is wider (around 10 Å) and the SHG intensity is, in principle, generated over this entire range that shows a net asymmetry. However, the simulation shows that concentration enhancement in the outermost surface layer coincides with the 90−10 region of the water density profile. This region thus experiences a much higher asymmetry and will dominate the SHG response. The inferred Gibbs free energy should be viewed as a weighted average over the ions within the probing depth of the experiment.

The Langmuir model also assumes negligible surfactant−surfactant interactions or at least similar surfactant−surfactant and surfactant−solvent interactions. For the ions studied here, this assumption is likely not to be fully justified. However, the Debye length is 6 Å for a 0.25 M solution of a 1:1 electrolyte, therefore, long-range electrostatic interactions between ions are well screened at the high concentrations studied here and close range interactions will dominate. Details concerning the close range interactions, such as dispersion and polarization, are not very well understood for electrolyte solutions and the differences between ion−ion and ion−water interactions could prove important at high concentrations.[20] This would result in a concentration-dependent Gibbs free energy of adsorption. Despite these potential obstacles, the Langmuir model is observed to fit the data very well and is, therefore, used due to its simplicity, rather than adopting a more complicated model.

Denoting the real water susceptibility as A and the real and imaginary parts of the thiocyanide susceptibility as B and C, respectively, we incorporate the Langmuir model for the surface concentration into the expression for the SHG intensity:

$$\begin{aligned} I_{SHG} &\propto |A + (B + iC) \times N_S|^2 \\ &= (A + B \times N_S)^2 + (C \times N_S)^2 \\ &= \left(A + \frac{(B \times N_S^{\max}) \times x}{x + D}\right)^2 + \left(\frac{(C \times N_S^{\max}) \times x}{x + D}\right)^2 \end{aligned} \tag{5}$$

Here, D is the Langmuir constant $55.5M\exp(\Delta G_{Ads}/RT)$. The SHG intensities at different wavelengths are fit simultaneously to this equation, allowing the real and imaginary parts of the thiocyanide susceptibility (B and C) to change with the wavelength, while keeping D fixed for all wavelengths.

TABLE 1: Partial Charges, q, Lennard-Jones Radii, R, Lennard-Jones Well Depths, ϵ, and Atomic Polarizabilities, α, of the Atomic Sites for Na^+ and SCN^-

atom	q [au]	R [Å]	ϵ [kcal/mol]	α [Å^3]
Na	+1	1.3190	0.1300	0.24
S	−0.75	2.1500	0.3639	2.0
C	0.49	1.8801	0.1016	2.0
N	−0.74	2.0750	0.0741	2.0

3. Computational Details

The simulated systems consisted of 864 water molecules and 9, 18, or 54 NaSCN ion pairs corresponding to 0.6, 1.2, and 3.5 M solutions, respectively. The ions and molecules were placed in a simulation box with dimensions 30 × 30 × 150 Å^3 and periodic boundary conditions were employed. Due to the elongated z-length of the box an infinite liquid slab was formed in the middle of the z-dimension with two planar liquid−vapor interfaces.[36]

The water model used is the polarizable POL3 water.[37] The Lennard-Jones parameters, partial charges, and atomic polarizabilities for sodium and thiocyanate ions are given in Table 1.

The parameters for the sodium anion are taken from ref 38. The partial charges of thiocyanate were determined by the CHELPG procedure[39] from the wave function calculated at the MP2/aug-cc-pvdz level. The Lennard-Jones parameters were chosen such as to reproduce the ab initio geometry and intermolecular binding energy of the $SCN^-\cdots H_2O$ cluster.[40] Nonbonded interactions were cut off at 12 Å and long-range electrostatics was treated by the Particle Mesh Ewald technique,[41] with a grid size of 1 Å.

The polarizability was first evaluated in the gas phase at the MP2/aug-cc-pvdz level. Diagonal elements of the polarizability tensor are $\alpha_{xx} = \alpha_{yy} = 5.79$ Å^3, and $\alpha_{zz} = 11.6$ Å^3. However, for the sake of the force field implementation, a single value of the isotropic polarizability should be given, which is the average of the diagonal values, $\alpha = 7.7$ Å^3. Moreover, this value should be scaled down by about 10−25% to account for solvent effects[4,42] and distributed among the atoms (see Table 1). Also, to avoid the well-known *polarization catastrophe* during the MD simulation,[43] we adopted a scheme that effectively scales down the atomic polarizability once the instantaneous electric field at the point overcomes a certain limit. To be more specific, the functional dependence, $p = p(E)$, of the induced dipole with respect to the applied electric field strength is no longer linear, $p = \alpha E$, but has a more complex form (see Figure 1). We can divide the induced dipole dependence into three regions: (1) a linear regime for small fields, $E < E_1$, (2) a constant regime for strong fields, $E > E_2$, where the induced dipole does not further rise with increasing electric field, but remains constant at the value p_{max}, and (3) a region of intermediate fields, $E_1 < E < E_2$, where the dependence is quadratic, such that the whole curve is smooth. Then, only two parameters have to be given, to specify the functional form completely, i.e., the maximum induced dipole, αE_{max}, and the induced dipole at the end of linear regime, αE_1. We have used values of $E_{max} = 0.211$ DÅ^{-3}, and $E_1 = 0.19$ DÅ^{-3}. The values were chosen such that the scaling does not affect the behavior of pure POL3 water.

After a period of equilibration of at least 500 ps, production simulations were run for 2 ns with a time step of 2 fs. Temperature was kept constant at 300 K by means of the Berendsen thermostat.[44] All bond lengths were constrained by the SHAKE algorithm.[45] The atomic positions were recorded every 2 ps, and histogramed according to their z-coordinate and atomic type, giving the time-averaged density profiles. The MD simulations were performed with the AMBER 8 program package[46] and the ab initio calculations were done with the Gaussian 03 suite of programs.[47]

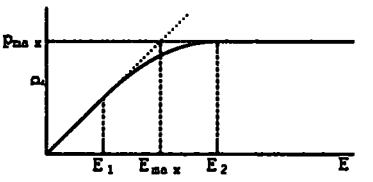

Figure 1. Scaling down of the polarizability, with increasing electric field strength. The induced dipole, p, depends on the electric field strength, E: linear for $E < E_1$, quadratic for $E_1 < E < E_2$, and constant for $E > E_2$. The induced dipole has an upper bound, p_{max}.

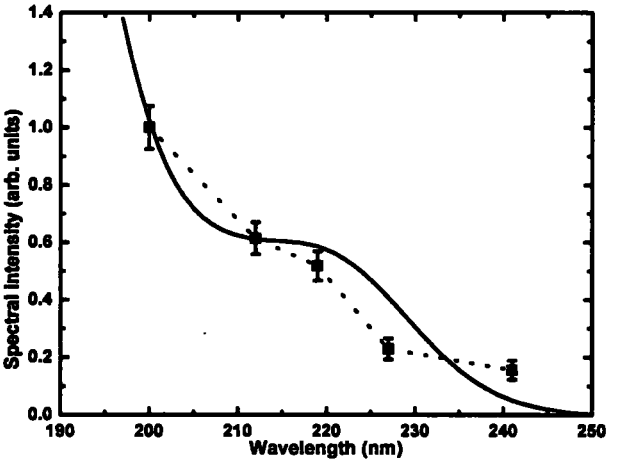

Figure 2. Spectral dependence of the SCN^- CTTS spectrum. The solid line is the bulk absorbance spectrum, showing two CTTS transitions. The solid squares are the magnitudes of the second-order response of thiocyanide ($|\chi^{(2)}_{SCN}|$) and are thus representative of the surface spectrum. A small blue shift (5−10 nm) of the surface spectrum is observed with respect to the bulk due to the interactions occurring in the dense ionic double layer.

4. Experimental Results

The thiocyanide anion exhibits strong ($\epsilon \sim 10^4$ M^{-1} cm^{-1}) charge-transfer-to-solvent (CTTS) transitions in the UV, as shown in Figure 2. CTTS transitions also exhibit a large nonlinear response that can be used to directly probe the surface concentration of the anion as described in Section 2. The concentration dependence of the SHG intensity at different wavelengths is shown in Figure 3. A small initial decrease in the SHG intensity is observed at 227 and 241 nm due to destructive interference of the thiocyanide susceptibility with the water background. This initial decrease is consistent with the high concentration increase and is not indicative of the Jones−Ray effect[48,49] that we observe for iodide[6] and ferrocyanide.[50] That the Jones−Ray effect is not observed for thiocyanide or azide[7] is itself very interesting and could be due to the conjugated bonds of these ions that are not present in the simple ions such as iodide or complex ions such as ferrocyanide. Jones and Ray observed a surface tension minimum for potassium thiocyanide, but the minimum was smaller and occurred at higher concentrations than for the other salts. The small surface tension decrease could be due to an artifact as argued by Langmuir[51,52] or due to some other aspects of the poorly understood Jones−Ray effect. However, a small initial offset in the SHG intensity of these anions of 0.05 due to the Jones−Ray effect cannot be excluded.

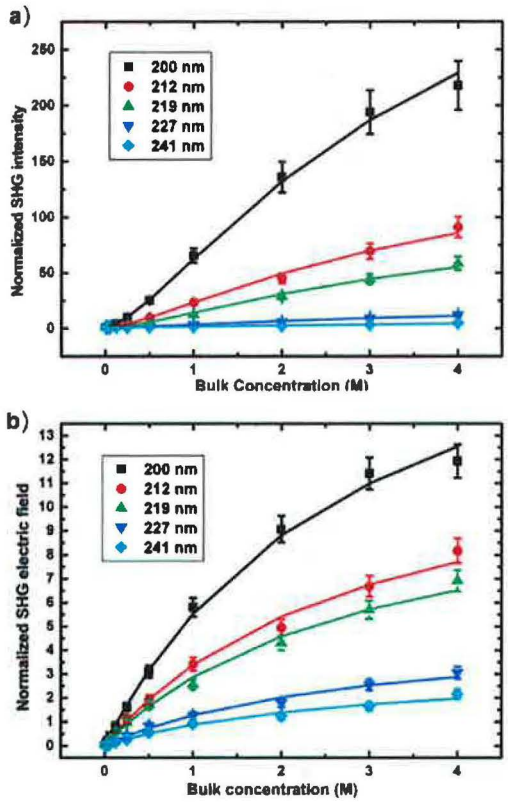

Figure 3. SHG response at five different wavelengths. Panel a shows the SHG intensity of NaSCN solutions normalized to that of pure water. Each wavelength is fit to the Langmuir model, yielding a common Gibbs free energy of adsorption of -1.80 ± 0.03 kcal/mol. The different intensities reflect the spectral dependence, shown in Figure 2. Panel b shows the extracted SHG electric field generated by thiocyanide normalized to the response of pure water. The surface concentration of thiocyanide is proportional to the SHG electric field, and given the (currently unknown) relative second-order cross-section between water and thiocyanide and the water surface concentration, could be calculated in ions/area. The SHG electric field is thus representative of a standard Langmuir plot with the magnitude at each wavelength reflecting the surface spectrum.

The SHG intensity is fit to an expression incorporating the Langmuir model, as described by eq 5. Each wavelength is fit to an individual complex thiocyanide susceptibility, but all are fit with a common Langmuir constant. The magnitude of the thiocyanide susceptibility ($\sqrt{B^2+C^2}$) for the different wavelengths, is shown, along with the bulk absorption spectrum in Figure 2. A blue shift of this high concentration surface spectrum with respect to the bulk is observed. A similar blue shift at high concentrations has been observed for sodium and potassium iodide[6] as well as for hydroiodic acid,[53] but not for azide,[7] and is in contrast to the red shift observed at dilute concentrations due to the less polar nature of the water surface.[54] The high concentration blue shift is thus indicative of significant ion−ion interactions occurring at the interface.

The surface concentration of thiocyanide is proportional to the SHG electric field generated by thiocyanide, which can be extracted from the fit. Panel b in Figure 3 shows the extracted SHG electric field normalized to pure water. The curves thus represent the surface concentration with the magnitude at each wavelength reflecting the second-order cross-section, as seen in Figure 2. From the fitted Langmuir constant, a Gibbs free energy of adsorption for thiocyanide of -1.80 ± 0.03 kcal/mol is extracted. This is less than the energy extracted for azide

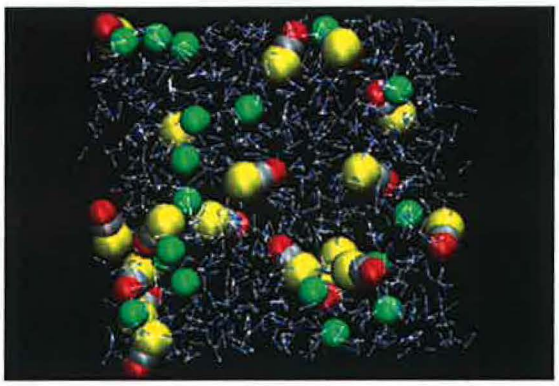

Figure 4. Typical snapshot from the MD simulation. The picture shows a side view of the simulation box, (with solution/air interfaces on the right and on the left) with water molecules depicted as triangles and the atoms of the solvated ions as balls.

(-2.4 ± 0.1 kcal/mol)[7] but more than that for the high concentration iodide adsorption (<1 kcal/mol).[26] The Gibbs free energy of -1.80 kcal/mol for SCN^- is not sufficient to ensure complete saturation of the surface before the solubility limit of the bulk is reached. However, beginning saturation, as manifested by a sublinear increase of the surface concentration with respect to the bulk, of the outermost surface layer is observed above 1 M bulk concentration.

5. Computational Results

A typical snapshot of the MD simulation box (which is periodically repeated in all three dimensions) showing the aqueous slab with dissolved Na^+ and SCN^- ions is depicted in Figure 4. We see qualitatively that in the aqueous bulk the cations and anions are roughly evenly distributed, while at the air/water interface there is an increased concentration of thiocyanide. The figure thus demonstrates the ion-specific behavior at the air/water interface, with large polarizable ions exhibiting a propensity for the surface.

This result is quantified in panels a−c of Figure 5 which show the density profiles across the slab of the 0.6, 1.2, and 3.5 M solution, respectively. All these density profiles represent statistically averaged values over the 2 ns simulations. Each curve corresponds to an individual species, normalized so that the area under all the curves is the same and the bulk water density is equal to unity. Only one-half of the slab is shown, the origin of the z-coordinate corresponding to the center of the slab and the density profiles being averaged over the two halves. The water density is roughly constant for more than 1 nm from the center of the slab, after which it starts to decay to 0, marking the interfacial region. Throughout the concentration range investigated, the highly polarizable SCN^- ions show surface enhancement, whereas the small nonpolarizable Na^+ ions are repelled from the surface. The peak interfacial concentration of SCN^- is about 50% above the bulk value for the lower concentrations but decreases slightly at higher concentrations. This surface peak is accompanied by subsurface depletion and, except for the most dilute system (where the statistics are relatively poor due to the small number of ions), also by a subsurface peak of Na^+.

The value of the surface enhancement of thiocyanide predicted by the present molecular dynamics simulations should be viewed as a lower bound. The reason is that we have reduced the value of the SCN^- gas-phase polarizability by 22% and employed a smooth cutoff scheme for the induced dipoles. The reduction of the gas-phase polarizability can be (at least partly)

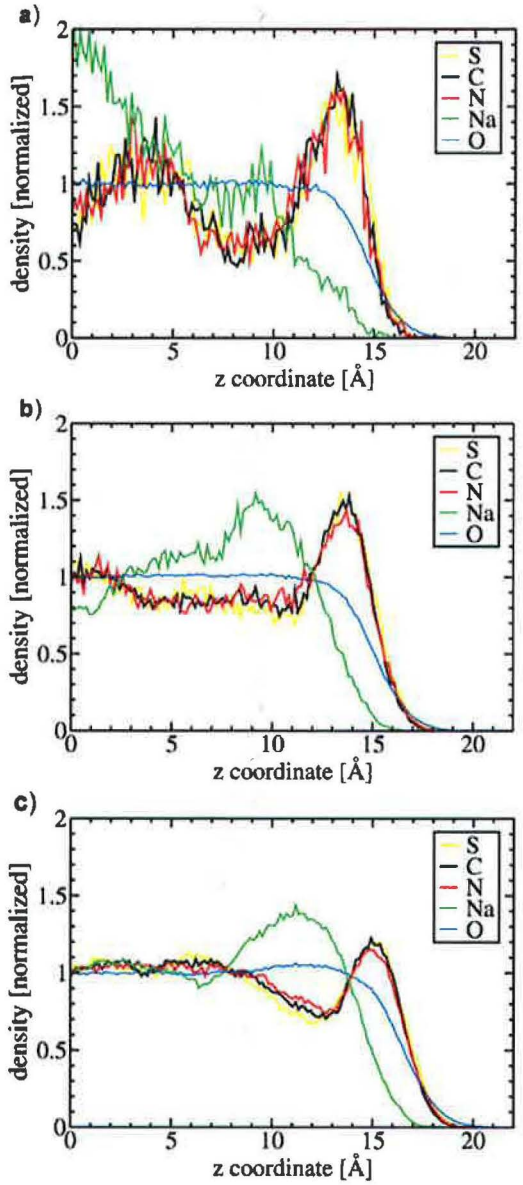

Figure 5. The density profiles of the (a) 0.6, (b) 1.2, and (c) 3.5 M aqueous NaSCN solution. The blue curve is the water oxygen signal, defining the slab. The green color corresponds to the sodium cation. The yellow, black, and red curves correspond to the S, C, and N atoms of the thiocyanate anion. The densities are normalized so that the area under them is equal, with the bulk water density being one.

justified by the solvent effect but the main reason to employ the cutoff procedure was to avoid the polarization catastrophe.[43] Since the propensity of ions for the air/water interface positively correlates with the ion polarizability[25] our simulations tend to somewhat underestimate the surface enhancement of SCN^-.

6. Discussion

Until recently, the description of the distribution of ions at the liquid water surface has been limited to continuum models on the theoretical side and to surface excesses (integrated surface concentrations) derived from surface tension experiments on the experimental side.[55] The original continuum model by Onsager and Samaras[13] described the interface as a discontinuity between two continuous dielectric media and the ions as point charges. The ions are repelled from the interface by image charge repulsion, as first suggested by Wagner.[56] The continuum models have since been refined to include polarizability and ion-specific properties such as ion size and dispersion,[14,15] but these still mostly predict the ions to be repelled from the outermost liquid layer at the surface. Recently, a smooth interface has been incorporated into a continuum model by relaxing the dielectric constant continuously from the bulk water value (79) to air (1) over a few angstroms.[18] Interestingly, this continuum model, as well as another one that employs large values of ionic polarizability,[19] predicts for highly polarizable ions a minimum in the Gibbs energy profile just below the interface, and of about the same magnitude as that following from molecular dynamics simulations.[2,3] However, continuum models inherently lack a description of the asymmetry of water molecules and the directionality of hydrogen bonds, which govern the difference in the interactions of water molecules with anions and cations. Furthermore, they obviously lack the description of the granular nature of the solvent, which engenders surface roughness. These effects are naturally included in the MD simulations.

The surface tension of electrolyte solutions increases roughly linearly with concentration above 0.01 M. By the Gibbs adsorption isotherm,[10] the ions are depleted from the interface accordingly. However, as a thermodynamic relation, the Gibbs equation does not take into account any microscopic structure of the ion distribution, but only the concentration integrated over the whole interfacial region. For electrolyte pairs that include a highly polarizable anion, the concentration is a strongly nonmonotonic function of the distance from the surface. The anions are enhanced, relative to the bulk concentration, at the outermost liquid layer but depleted in subsurface. In turn, small nonpolarizable cations are repelled from the topmost layer but their concentration can be enhanced in the subsurface. Nevertheless, in accord with the surface tension measurements, the total surface ion excess can be negative even though the outermost liquid layer is enhanced with the anions.[25]

Below 0.01 M, surface tension measurements are still controversial due to the accuracy needed to measure very small changes. Jones and Ray measured a minimum in the surface tension at 1 mM for several salts.[48,49] These measurements were later contested[51,52] and remain today as a curiosity. The experimental authors of the present study have recently observed the Jones−Ray effect for iodide[6] and ferrocyanide[50] solutions at dilute concentrations. Straightforward molecular dynamics simulations at such low concentrations are technically hardly feasible, since there would be less than a single ion pair in a reasonably sized unit box. Nevertheless, potential of mean force calculations for a single iodide anion in a box of 1000 water molecules also indicates significant surface propensity.[2]

As discussed above, small nonpolarizable cations typically exhibit different surface behavior than large polarizable anions. However, recent investigations have shown that H_3O^+ is an exception to the general case of cations being repelled from the surface. Recent molecular simulations showed enhanced surface affinity of a single hydronium cation to the aqueous surface, compared, e.g., to alkali cations.[57,58] This prediction has recently been supported by a combined molecular dynamics and SFG investigation[59] and a separate SHG study[53] of concentrated acids (such as HCl, HBr, or HI) which explained why the surface tension of monovalent acid solutions is lower than that of water.[55] The force that brings hydronium to the interface is different from that operating for the anions.[57,59] Hydronium is only capable of forming three hydrogen bonds

since its oxygen is a poor hydrogen bond acceptor, and thus it disrupts the hydrogen bonding network in the bulk. The ion can, in this respect, be qualitatively viewed as a defect in the hydrogen bonding network, and similar to lattice defects in crystals, it is expelled to the surface where it can be accommodated more easily.

7. Conclusions

We have presented a combined description of thiocyanide adsorption at the liquid water−air interface by MD simulations and SHG experiments on aqueous solutions of NaSCN of varying concentrations. The experiments reveal a simple Langmuir behavior of the thiocyanide surface concentration with respect to the bulk. Fit of the experimental data to a Langmuir isotherm yields a Gibbs free energy of adsorption of SCN^- of -1.80 ± 0.03 kcal/mol corresponding to an onset of surface saturation above 1 M. MD simulations in slab geometry confirm the propensity of thiocyanide for the surface of aqueous solutions. Due to the reduced polarizability and cutoff on induced dipoles in the simulations the calculated peak 50% SCN^- enhancement at the surface compared to the bulk concentration should be viewed as a lower limit to the thiocianide surface affinity. The simulations also reveal a slight decrease of the surface peak of thiocyanide with increasing NaSCN concentration, confirming thus the beginning surface saturation observed in the experiment.

The description of inorganic ions in the interfacial region of the water−air interface is becoming more detailed and a consistent new picture is beginning to emerge. Small nonpolarizable (hard) ions are repelled from the aqueous surface in accord with the traditional picture based on continuum solvent models. However, polarizable (soft) anions exhibit a nonmonotonic interfacial distribution, being enhanced at the outermost surface layer, but depleted in the subsurface. At appreciable concentrations, the countercations are then attracted by the anionic surface layer, and become subsequently enhanced in the subsurface. The fact that ions can play an active role at the air−water interface and that such behavior is strongly ion-specific also has important general implications for chemical reactions occurring at surfaces of aqueous electrolytes, such as aerosol particles and ocean surfaces.

Acknowledgment. The Berkeley group is funded by the Experimental Physical Chemistry Division at the National Science Foundation. P.B.P. is funded by the Danish Research Training Council. Support to P.J. via the NSF-funded Environmental Molecular Science Institute (grants CHE 0431312 and 0209719) and from the Czech Ministry of Education (grant LC512) is gratefully acknowledged. Part of the work in Prague was supported via the Research Project Z40550506.

References and Notes

(1) Jungwirth, P.; Tobias, D. J. *J. Phys. Chem. B* **2001**, *105*, 10468.
(2) Dang, L. X.; Chang, T.-M. *J. Phys. Chem. B* **2002**, *106*, 235.
(3) Jungwirth, P.; Tobias, D. J. *J. Phys. Chem. B* **2002**, *106*, 6361.
(4) Salvador, P.; Curtis, J. E.; Tobias, D. J.; Jungwirth, P. *Phys. Chem. Chem. Phys.* **2003**, *5*, 3752.
(5) Yang, X.; Kiran, B.; Wang, X.-B.; Wang, L.-S.; Mucha, M.; Jungwirth, P. *J. Phys. Chem. A* **2004**, *108*, 7820.
(6) Petersen, P. B.; Johnson, J. C.; Knutsen, K. P.; Saykally, R. J. *Chem. Phys. Lett.* **2004**, *397*, 46.
(7) Petersen, P. B.; Saykally, R. J. *Chem. Phys. Lett.* **2004**, *397*, 51.
(8) Liu, D.; Ma, G.; Levering, L. M.; Allen, H. C. *J. Phys. Chem. B* **2004**, *108*, 2252.
(9) Ghosal, S.; Shbeeb, A.; Hemminger, J. C. *Geophys. Res. Lett.* **2000**, *27*, 1879.
(10) Adamson, A. W.; Gast, A. P. *Physical Chemistry of Surfaces*, 6th ed.; Wiley: New York, 1997.
(11) Durand-Vidal, S.; Simonin, J.-P.; Turq, P. *Electrolytes at Interfaces*; Kluwer Academic Publishers: Dordrecht, The Netherlands, 2000.
(12) Fawcett, W. R. *Liquids, Solutions, and Interfaces*; Oxford University Press: Oxford, UK, 2004.
(13) Onsager, L.; Samaras, N. N. T. *J. Phys. Chem.* **1934**, *2*, 528.
(14) Karraker, K. A.; Radke, C. J. *Adv. Colloid Interface Sci.* **2002**, *96*, 231.
(15) Manciu, M.; Ruckenstein, E. *Adv. Colloid Interface Sci.* **2003**, *105*, 63.
(16) Markin, V. S.; Volkov, A. G. *J. Phys. Chem. B* **2002**, *106*, 11810.
(17) Bostrom, M.; Williams, D. R. M.; Ninham, B. W. *Langmuir* **2001**, *17*, 4475.
(18) Frediani, L.; Mennucci, B.; Cammi, R. *J. Phys. Chem. B* **2004**, *108*, 13796.
(19) Levin, Y. Submitted for publication.
(20) Kunz, W.; Lo Nostro, P.; Ninham, B. W. *Curr. Opin. Colloid Interface Sci.* **2004**, *9*, 1.
(21) Hu, J. H.; Shi, Q.; Davidovits, P.; Worsnop, D. R.; Zahniser, M. S.; Kolb, C. E. *J. Phys. Chem.* **1995**, *99*, 8768.
(22) Knipping, E. M.; Lakin, M. J.; Foster, K. L.; Jungwirth, P.; Tobias, D. J.; Gerber, R. B.; Dabdub, D.; Finlayson-Pitts, B. J. *Science* **2000**, *288*, 301.
(23) Laskin, A.; Gaspar, D. J.; Wang, W.; Hunt, S. W.; Cowin, J. P.; Colson, S. D.; Finlayson-Pitts, B. J. *Science* **2003**, *301*, 340.
(24) Raymond, E. A.; Richmond, G. L. *J. Phys. Chem. B* **2004**, *108*, 5051.
(25) Vrbka, L.; Mucha, M.; Minofar, B.; Jungwirth, P.; Brown, E. C.; Tobias, D. J. *Curr. Opn. Colloid Interface Sci.* **2004**, *9*, 67.
(26) Petersen, P. B.; Saykally, R. J. In preparation.
(27) Shen, Y. R. *The Principles of Nonlinear Optics*; Wiley: New York, 1984.
(28) Boyd, R. W. *Nonlinear Optics*, 2nd ed.; Elsevier: Amsterdam, The Netherlands, 2003.
(29) Eisenthal, K. B. *Chem. Rev.* **1996**, *96*, 1343.
(30) Richmond, G. L. *Annu. Rev. Phys. Chem.* **2001**, *52*, 357.
(31) Sokhan, V. P.; Tildesley, D. J. *Mol. Phys.* **1997**, *92*, 625.
(32) Simpson, G. J.; Rowlen, K. L. *Anal. Chem.* **2000**, *72*, 3407.
(33) Dukhin, S. S.; Kretzschmar, G.; Miller, R. *Dynamics of Adsorption at Liquid Interfaces. Theory, Experiment, Application*; Elsevier: Amsterdam, The Netherlands, 1995.
(34) Chang, C.-H.; Franses, E. I. *Colloids Surf. A* **1995**, *100*, 1.
(35) Prosser, A. J.; Franses, E. I. *Colloids Surf. A* **2001**, *178*, 1.
(36) Wilson, M. A.; Pohorille, A. *J. Chem. Phys.* **1991**, *95*, 6005.
(37) Caldwell, J. W.; Kollman, A. *J. Phys. Chem.* **1995**, *99*, 6208.
(38) Perera, L.; Berkowitz, M. L. *J. Chem. Phys* **1991**, *95*, 1954.
(39) Breneman, C. M.; Wiberg, K. B. *J. Comput. Chem.* **1990**, *11*, 361.
(40) Sansone, R.; Ebner, C.; Probst, M. *J. Mol. Liq.* **2000**, *88*, 129.
(41) Darden, T.; York, D.; Pedersen, L. *J. Chem. Phys.* **1993**, *98*, 10089.
(42) Jungwirth, P.; Tobias, D. J. *J. Phys. Chem. A* **2002**, *106*, 379.
(43) Thole, B. T. *Chem. Phys.* **1981**, *59*, 341.
(44) Berendsen, H. J. C.; Postma, J. P. M.; DiNola, A.; Haak, J. R. *J. Chem. Phys.* **1984**, *81*, 3684.
(45) Ryckaert, J. P.; Cicotti, G.; Berendsen, H. J. C. *J. Comput. Phys.* **1977**, *23*, 327.
(46) Case, D. A.; Darden, T. A.; Cheatham, T. E., III; Simmerling, C. L.; Wang, J.; Duke, R. E.; Luo, R.; Merz, K. M.; Wang, B.; Pearlman, D. A.; Crowley, M.; Brozell, S.; Tsui, V.; Gohlke, H.; Mongan, J.; Hornak, V.; Cui, G.; Beroza, P.; Schafmeister, C.; Caldwell, J. W.; Ross, W. S.; Kollman, P. A. *AMBER 8*; University of California: San Francisco, CA, 2004.
(47) Frisch, M. J.; Trucks, G. W.; Schlegel, H. B.; Scuseria, G. E.; Robb, M. A.; Cheeseman, J. R.; Montgomery, J. A., Jr.; Vreven, T.; Kudin, K. N.; Burant, J. C.; Millam, J. M.; Iyengar, S. S.; Tomasi, J.; Barone, V.; Mennucci, B.; Cossi, M.; Scalmani, G.; Rega, N.; Petersson, G. A.; Nakatsuji, H.; Hada, M.; Ehara, M.; Toyota, K.; Fukuda, R.; Hasegawa, J.; Ishida, M.; Nakajima, T.; Honda, Y.; Kitao, O.; Nakai, H.; Klene, M.; Li, X.; Knox, J. E.; Hratchian, H. P.; Cross, J. B.; Bakken, V.; Adamo, C.; Jaramillo, J.; Gomperts, R.; Stratmann, R. E.; Yazyev, O.; Austin, A. J.; Cammi, R.; Pomelli, C.; Ochterski, J. W.; Ayala, P. Y.; Morokuma, K.; Voth, G. A.; Salvador, P.; Dannenberg, J. J.; Zakrzewski, V. G.; Dapprich, S.; Daniels, A. D.; Strain, M. C.; Farkas, O.; Malick, D. K.; Rabuck, A. D.; Raghavachari, K.; Foresman, J. B.; Ortiz, J. V.; Cui, Q.; Baboul, A. G.; Clifford, S.; Cioslowski, J.; Stefanov, B. B.; Liu, G.; Liashenko, A.; Piskorz, P.; Komaromi, I.; Martin, R. L.; Fox, D. J.; Keith, T.; Al-Laham, M. A.; Peng, C. Y.; Nanayakkara, A.; Challacombe, M.; Gill, P. M. W.; Johnson, B.; Chen, W.; Wong, M. W.; Gonzalez, C.; Pople, J. A. *Gaussian 03*; Gaussian, Inc.: Wallingford, CT, 2004.
(48) Jones, G.; Ray, W. A. *J. Am. Chem. Soc.* **1937**, *59*, 187.
(49) Jones, G.; Ray, W. A. *J. Am. Chem. Soc.* **1941**, *63*, 288.
(50) Petersen, P. B.; Saykally, R. J. In preparation.
(51) Langmuir, I. *Science* **1938**, *88*, 430.

(52) Langmuir, I. *J. Chem. Phys.* **1938**, *6*, 873.
(53) Petersen, P. B.; Saykally, R. J. *J. Phys. Chem. B* **2005**, *109*, 7976–7980.
(54) Wang, H.; Borguet, E.; Eisenthal, K. B. *J. Phys. Chem. B* **1998**, *102*, 4927.
(55) Weissenborn, P. K.; Pugh, R. J. *J. Colloid Interface Sci.* **1996**, *184*, 550.
(56) Wagner, V. C. *Phys. Z.* **1924**, *15*, 474.
(57) Petersen, M. K.; Iyengar, S. S.; Day, T. J. F.; Voth, G. A. *J. Phys. Chem. B* **2004**, *108*, 14804.
(58) Dang, L. X. *J. Chem. Phys.* **2003**, *119*, 6351.
(59) Mucha, M.; Frigato, T.; Levering, L.; Allen, H. C.; Tobias, D. J.; Dang, L. X.; Jungwirth, P. *J. Phys. Chem. B* **2005**, *109*, 7617–7623.

FEATURE ARTICLE

Unified Molecular Picture of the Surfaces of Aqueous Acid, Base, and Salt Solutions

Martin Mucha,[†] Tomaso Frigato,[†,‡] Lori M. Levering,[§] Heather C. Allen,[§] Douglas J. Tobias,[∥] Liem X. Dang,[⊥] and Pavel Jungwirth*[,†]

Institute of Organic Chemistry and Biochemistry, Academy of Sciences of the Czech Republic, and Center for Biomolecules and Complex Molecular Systems, Flemingovo nám. 2, 16610 Prague 6, Czech Republic, Max Planck Institute for Biophysics, Marie Curie Strasse 15, D-60439, Frankfurt am Main, Germany, Department of Chemistry, The Ohio State University, 100 West 18th Avenue, Columbus, Ohio 43210, Department of Chemistry and Institute for Surface and Interface Science, University of California, Irvine, California 92697-2025, and Chemical Sciences Division, Pacific Northwest National Laboratory, Richland, Washington 99352

Received: November 30, 2004; In Final Form: January 5, 2005

The molecular structure of the interfacial regions of aqueous electrolytes is poorly understood, despite its crucial importance in many biological, technological, and atmospheric processes. A long-term controversy pertains between the standard picture of an ion-free surface layer and the strongly ion specific behavior indicating in many cases significant propensities of simple inorganic ions for the interface. Here, we present a unified and consistent view of the structure of the air/solution interface of aqueous electrolytes containing monovalent inorganic ions. Molecular dynamics calculations show that in salt solutions and bases the positively charged ions, such as alkali cations, are repelled from the interface, whereas the anions, such as halides or hydroxide, exhibit a varying surface propensity, correlated primarily with the ion polarizability and size. The behavior of acids is different due to a significant propensity of hydronium cations for the air/solution interface. Therefore, both cations and anions exhibit enhanced concentrations at the surface and, consequently, these acids (unlike bases and salts) reduce the surface tension of water. The results of the simulations are supported by surface selective nonlinear vibrational spectroscopy, which reveals among other things that the hydronium cations are present at the air/solution interface. The ion specific propensities for the air/solution interface have important implications for a whole range of heterogeneous physical and chemical processes, including atmospheric chemistry of aerosols, corrosion processes, and bubble coalescence.

1. Introduction

The traditional view of inorganic aqueous salt solution surfaces being devoid of ions[1−3] is yielding gradually to a more complex picture, where ion specificity plays a crucial role.[4] Small, nonpolarizable (hard) ions (e.g., alkali cations and fluoride anions) are repelled from the air/solution interface by the electrostatic image forces, as described already by Onsager and Samaras in the 1930s.[1] However, polarizable (soft) ions, such as the heavier halides, nitrate, or azide, exhibit a propensity for the air/solution interface. This surprising fact, predicted by molecular dynamics simulations[5−8] and supported by various surface sensitive spectroscopic and electron microscopy measurements,[9−13] is not in contradiction with basic thermodynamic arguments based on the Gibbs adsorption equation.[2] Simple inorganic salts raise the surface tension of water, from which an integral net depletion of ions from the interfacial region (i.e., negative surface excess) is inferred.[3] This, however, does not exclude a nonmonotonic ion concentration profile with surface enhancement and subsurface depletion, as observed qualitatively in the simulations, e.g., for bromide and iodide salt solutions.[5,14] It has been shown that such surface ion enhancement can have important atmospheric consequences, for example for the heterogeneous chemistry of seawater aerosols or for tropospheric ozone destruction in the Arctic and Antarctic at polar sunrise due to reactions involving sea spray covered ice pack.[4,15]

Aqueous salt solutions are, however, only one-third of the story concerning the surfaces of electrolytes. It has been known for a long time that salts and bases increase the surface tension of water, whereas adding appreciable amounts of monovalent inorganic acids decreases it.[3,16] However, few experiments have been devoted to the molecular structure of the surfaces of concentrated aqueous acids and bases.[17−20] The corresponding molecular simulations are lacking almost completely, with the notable exception of a recent pioneering study of a single proton and chloride at the extended air/water interface.[21] The present paper aims to close this gap by reporting detailed molecular dynamics (MD) simulations in slab geometries complemented

* Corresponding author. E-mail: pavel.jungwirth@uochb.cas.cz.
† Academy of Sciences of the Czech Republic and Center for Complex Molecular Systems and Biomolecules.
‡ Max Planck Institute for Biophysics.
§ The Ohio State University.
∥ University of California.
⊥ Pacific Northwest National Laboratory.

10.1021/jp0445730 CCC: $30.25
Published on Web 03/23/2005

by surface selective vibrational sum frequency generation (VSFG) spectroscopy of generic concentrated acid, base, and salt solutions. A unified picture with molecular resolution of the air/solution interface of simple aqueous inorganic electrolytes is emerging. Within this picture, hydronium cations and large polarizable anions exhibit a propensity for the interface, in contrast with the traditional view of an ion-free surface layer. This new view not only allows us to rationalize seemingly contradictory macroscopic surface measurements but also has important implications for a variety of heterogeneous chemical processes, e.g., in the atmosphere.[15,22]

2. Computational Method

The air/solution interface was modeled via 1 ns molecular dynamics simulations (after 500 ps of equilibration) at 300 K of water slabs containing HCl, HBr, NaOH, or NaCl at 1.2 M, and HI or NaI at 1.0 M concentration. Simulations in slab geometry were performed using the AMBER (versions 6 and 7) program package[23] with polarizable potentials both for water (POL3[24] and, in the cases of aqueous HI and NaI, DC97[25]) and the alkali, halide, hydronium, and hydroxide ions.[5,6,26-28] The induced electric field was converged in each step using a self-consistent procedure (the convergence was tighter than in our older simulations, which is the main reason for slightly different results for NaCl compared to those obtained previously[4,5]). For aqueous OH^-, where charge-transfer effects can be important and, consequently, a classical force field should be employed carefully, we tested a whole range of potential parameters with van der Waals radii of oxygen ranging from 1.8 to 2.1 Å and polarizabilities between 1.8 and 3 Å.[3] Although the quantitative details of the results depended on the particular parametrization, the weak repulsion of hydroxide anions from the interface was robustly reproduced in all cases. In addition to the classical force field model of H_3O^+ (which should also be used with care because it, e.g., does not allow for proton hopping and for the appearance of the Zundel form), we also employed a quantum hopping model of the hydrated proton.[29] The latter model, which accounts for proton hops between water molecules in a stochastic way, resulted in almost the same surface propensity of hydronium as for the nonpolarizable version of the classical potential.[28]

A slab of 864 (1000 in the cases of aqueous HI and NaI) water molecules was used to construct each system by adding 18 cations and 18 anions. Each slab was placed into a 30 × 30 × 100 Å^3 (32 × 32 × 135 Å^3 in the cases of aqueous HI and NaI) rectangular box, and periodic boundary conditions were applied in three dimensions. For this size of a simulation box we can interchangeably talk about air/solution and vacuum/solution interface, because at atmospheric pressure the number of nitrogen or oxygen molecules in the unit cell is negligible.[4] Note that at these salt concentrations there is only a very small tendency of forming contact ion pairs, both in the bulk and at the interface.[30] The simulations were run at a constant temperature of 300 K. The smooth particle mesh Ewald method[31] was used to calculate the long-range electrostatic energies and forces, and the van der Waals interactions and the real space part of the Ewald sum were truncated at 12 Å. A time step of 1 fs was used in the integration of the equations of motion, and the OH bond vibrations were frozen using the SHAKE algorithm.[32]

3. Experimental Method

The experimental setup of the vibrational SFG scanning system has been described previously.[10] The SFG experiments were carried out using a visible beam at 532 nm and an infrared beam currently tunable from 2500 to 4000 cm^{-1} with a bandwidth of ~8 cm^{-1} generated from a KTP−KTA based optical parametric generator/amplifier (OPG/OPA) system (LaserVision). The 532 nm beam is generated by doubling the frequency (second harmonic) of the 1064 nm pump source from an EKSPLA PL 2143 A/SS Nd:YAG laser (29 ps pulse duration and 10 Hz repetition rate). The energies of the 532 nm and the infrared beams at the sample are ~1.1 mJ and ~350 μJ, respectively. The SFG signal is filtered from the reflected 532 nm light and detected with a charge-coupled device (CCD) (Andor Technology, DV412). The input angles are ~45° and ~53° for the 532 nm and IR beams respectively from the surface normal; the detection angle was set to ~46° from the surface normal for sum frequency. The CCD temperature was set at −42 °C during the experiments and was cooled thermoelectrically.

All of the spectra presented in this paper were acquired in ~60 min using a 20 s exposure time for each data point (from 2800 to 3950 cm^{-1}). VSFG spectra were reproduced several times over the period of several months. Each free OH spectrum (Figure 4 inset) is an average of three spectra and error bars are one standard deviation. At least one air-neat water spectrum was acquired at the beginning and the end of the experiment to ensure the stability of the SFG system and to confirm reproducibility.

The SFG signal is optimized spatially and temporally at 3300 cm^{-1}. The VSFG spectra are normalized by the IR profile because the IR is detected in real time with the SFG intensity. (The SFG spectrum was also obtained from the surface of a GaAs crystal, and was comparable to the IR spectrum.) The polarization combination used for the SFG experiments presented here are s, s, and p for the SFG, 532 nm, and infrared beams, respectively. However, additional polarization spectra were obtained and confirmed lack of orientation changes. All VSFG spectra were acquired at ~23 °C.

Water was obtained from a Millipore Nanopure system (18.3 MΩ·cm). Acid solutions were made volumetrically from concentrated HCl (Fisher Scientific, 36.5 wt %,), HBr (Fisher Scientific, 48 wt %) and HI (Alfa Aesar, 47 wt %). All of the acid solutions were checked for organic contamination by obtaining the SFG spectra of the solution surfaces in the region between 2800 and 3000 cm^{-1}. To prevent the HI solutions from reaction with light, solutions were stored in a dark cabinet and the flasks were covered with aluminum foil.

4. Computational Results

The structure of air/solution interfaces of solutions of generic inorganic salts (sodium chloride and iodide), base (sodium hydroxide), and acids (hydrochloric, hydrobromic, and hydroiodic acid) was investigated by means of MD simulations. The details concerning the calculations are provided in the Methods section. Briefly, extended slabs of concentrated aqueous solutions of HCl, HBr, NaOH, NaCl, NaI, or HI containing a bulk region between two air/solution interfaces were modeled using periodic boundary conditions with a prismatic unit cell.[4,33] A polarizable force field was employed both for water and for the H_3O^+, Na^+, Cl^-, Br^-, I^- and OH^- ions. Nanosecond-length simulations at ambient conditions of well equilibrated systems ensured adequate sampling of structural properties.

The principal results of the MD simulations of aqueous 1.2 M solutions of HCl, HBr, NaOH, and NaCl are summarized in Figure 1. For each of the four solutions we show the density profiles (i.e., averaged distributions of electrolyte ions and water molecules from the bulk region of the slab to the interface)

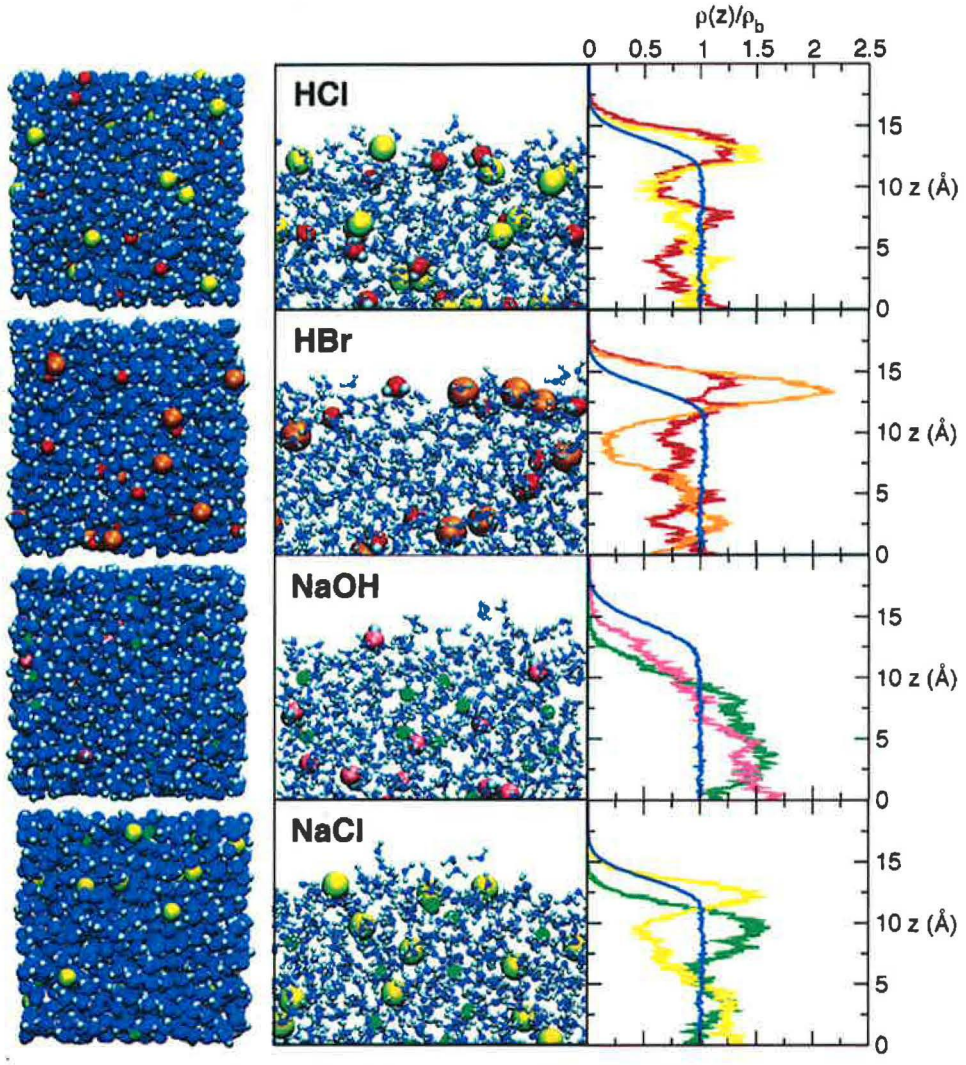

Figure 1. Snapshots from molecular dynamics simulations (side and top view of the slabs) and density profiles (i.e., histogrammed densities of the electrolyte ions and water molecules in layers parallel to the surface, from the center of the slab across the interface into the gas phase) for 1.2 M aqueous HCl, HBr, NaOH, and NaCl. Coloring scheme: water oxygen, blue; hydronium oxygen, red; hydroxide oxygen, pink; hydrogen, gray; sodium ions, green; chloride ions, yellow; bromide ions, orange.

together with typical snapshots from the simulations, depicting top and side views of the systems. Note that in our concentrated systems monitoring the distributions of ions of each type in the slab provides much better statistics than one would get from a potential of mean force of a single ion.

In the case of hydrochloric acid both hydronium cations and chloride anions penetrate into the air/solution interface, and there is actually a slight surface ion enhancement of both ions. For hydrobromic acid the situation is similar, except that bromide is more surface enhanced than chloride or hydronium. Note that the hydronium cations are preferentially oriented at the surface, with hydrogens pointing toward the aqueous phase and oxygen toward the air.

The surface behavior of ions is very different in sodium hydroxide and sodium chloride solutions. On one hand, in aqueous NaOH and NaCl sodium cations are repelled from the surface and never penetrate its topmost layer. On the other hand, hydroxide anions are weakly repelled from and chloride anions weakly attracted to the surface, and both can be found at the surface. We mention in passing that the orientation of OH^- at the surface, with hydrogen pointing into the gas phase (as in the snapshot shown in Figure 1) nicely matches that observed in water clusters.[34]

The effect of added electrolyte on the surface tension of aqueous solutions has been intensely studied for almost a century.[35] Although surface tension measurements do not give direct information about the molecular structure of the surface, they yield, via the Gibbs adsorption equation, information about the net excess of ions in the whole interfacial layer.[2] If surface tension increases compared to neat water, this excess is negative (indicating a net depletion of ions from the interface), whereas a decrease in surface tension is related to a positive surface excess (i.e., a net enrichment of ions in the interfacial layer). It has been known for decades that salts such as alkali halides and bases such as alkali hydroxides increase the surface tension of water, whereas acids such as HCl, HBr, or HI slightly decrease it.[3]

Surface tension can be extracted from MD simulations, albeit with a sizable statistical error due to large pressure fluctuations, from the asymmetry of the pressure tensor.[36] Despite the fact that the calculated numbers are subject to statistical errors of at least 1 mN/m, the experimental trend[3] is reproduced by the

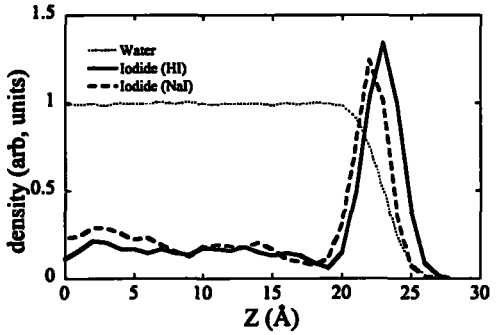

Figure 2. Density profiles of iodide from simulations of a 1.0 M solution of HI and NaI. Note the increased and shifted (toward the gas phase) interfacial peak in the acid. The Gibbs dividing surface is at ~23 Å.

present simulations. Namely, on one hand the calculated surface tension of 1.2 M HCl is within the statistical error equal to that of neat water, whereas that of 1.2 M HBr is smaller by about 1 mN/m. Note that no ion association into a molecular acid is invoked in the simulation to account for the decrease of surface tension, in agreement with the anticipated complete dissociation of these strong acids at molar concentrations, confirmed by earlier VSFG measurements.[17] On the other hand, both 1.2 M NaOH and 1.2 M NaCl increase the surface tension, the calculated numbers being ~4 mN/m in the former case and ~3 mN/m in the latter case. Interestingly, all the investigated systems exhibit the same polarity of the surface potential (negative toward the air).[3] Whereas for NaCl and NaOH this is primarily due to the fact that anions reside closer to the interface than cations, for HCl and HBr there is also a contribution from the hydronium ions that have the electronegative oxygen atom oriented toward the gas phase.

We carried out additional simulations to compare the solvation properties of 1 M HI or NaI at the air/solution interface. In the case of aqueous HI, hydronium is present both in the bulk and at the interface (with appreciable surface enhancement) and iodide exhibits a surface concentration peak, which is larger than that for the lighter halides. In aqueous NaI sodium is repelled from the top surface layer, albeit less than in the case of NaCl, which is due to attractive cation–anion interactions and the stronger surface propensity of iodide compared to chloride. The iodide density profiles for aqueous HI and NaI are plotted in Figure 2. It can be seen from this figure that for HI the interfacial peak of iodide is about 10% larger and shifted by more than 1 Å toward the gas phase, compared to that in the NaI solution. This is in perfect agreement with most recent second harmonic generation spectroscopic measurements,[20] showing an enhanced interfacial iodide signal upon moving from aqueous NaI to HI.

The picture emerging from the simulations is that monovalent inorganic acids have different surface behavior from the corresponding salts and bases in aqueous solutions. In acids both the hydronium cations and the anions exhibit a propensity for the air/solution interface. While the affinity of H_3O^+ for the surface is relatively weak, anions exhibit specificity that correlates with the ion polarizability and size. Br^- and I^- (as well as, e.g., N_3^- or NO_3^-)[7-8,11] show a stronger surface enhancement, whereas the surface propensity of Cl^- is comparable to that of H_3O^+. As a result of the surface propensity of both cations and anions in aqueous HCl, HBr, or HI, there is a net positive surface excess of ions. In bases and salt solutions, the cations, which are small and nonpolarizable spherical ions, are repelled from the surface. OH^- penetrates closer to the

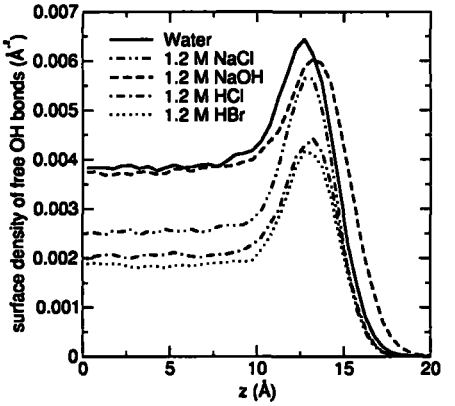

Figure 3. Surface density (number per unit area) of free OH bonds (i.e., water OH bonds that are not hydrogen-bonded to another water molecule or ion) for neat water, HCl, HBr, NaOH, and NaCl, from the center of the slab to the surface.

surface than alkali cations and can be occasionally found in the topmost layer but it does not exhibit any appreciable enhancement at the air/solution interface. The salt anions exhibit ion specific degrees of surface enhancement, similarly as in the case of the corresponding acids. The result of strong cationic repulsion and varying anionic surface propensity is a net depletion of ions from the interfacial layer of aqueous salt solutions and bases.

To connect the simulations to the spectroscopic experiments, we have computed the surface density (number per unit area) of free OH bonds, i.e., OH bonds not serving as hydrogen bond donors, where water–water and water-ion hydrogen bonds have been defined using a geometric criterion.[5] The results for neat water, 1.2 M HCl, HBr, NaOH, and NaCl are shown in Figure 3. In all systems the density of free OH bonds is higher in the interfacial region than in the bulk. Although the density of free OH bonds in the interfacial region is about the same for neat water, NaOH, and NaCl, it is significantly reduced for the two acids, in accord with the spectroscopic data presented next.

5. Experimental Results

Vibrational sum frequency generation spectroscopy (VSFG) is a second-order vibrational spectroscopic technique that is selective to environments lacking inversion symmetry such as interfaces and is used here to directly probe the air/solution interface.[10,17-19,37] The VSFG surface spectra for 1.2 M HCl, HBr, HI, NaOH, and NaCl are shown in Figure 4 under ssp polarization conditions (s and p are perpendicular and parallel to the plane of incidence, respectively), which provide information on molecular orientations,[38] when quantitatively compared to sps VSFG spectra, which showed no signal beyond the noise.

The spectra in Figure 4 reveal very different interfacial behavior for the acids versus sodium hydroxide and sodium halide solutions. The VSFG spectrum of neat water is also shown for comparison. On the basis of the IR and Raman spectra of aqueous acid solutions, the additional VSFG intensity below 3200 cm^{-1} for the HCl, HBr, and HI solutions as compared to the neat water surface spectrum is attributed to the VSFG response from hydronium (Eigen) and Zundel cations.[39] The intensity of the 3400 cm^{-1} band, which is assigned to oscillating dipoles about the tetracoordinated interfacial water molecules in these acid solutions, increases relative to neat water, with $I^- \sim Br^- > Cl^-$. In the 3700 cm^{-1} region, the sharp peak assigned to the dangling OH of water molecules that straddle the air/

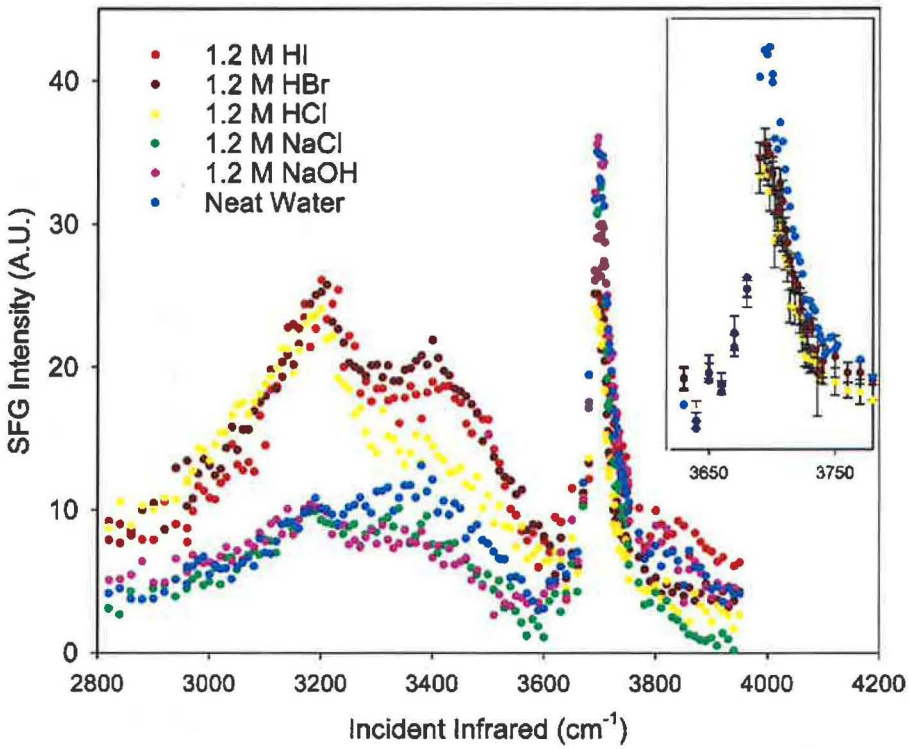

Figure 4. Vibrational sum frequency (ssp polarized) spectra of air/solution interfaces in the OH stretching region of neat water, 1.2 M NaCl, NaOH, HCl, HBr, and HI. Inset: Expanded view of the free OH region for neat water, 1.2 M HCl and HBr (standard deviations shown as error bars).

solution interface decreases for the acids (Figure 4 inset) relative to neat water, although there is a small increase on the higher energy side next to this peak. The 3400 cm^{-1} band increase is consistent with our previous results on sodium halide air/solution interfaces, which indicated that the halides play a dominant role in influencing the 3400 cm^{-1} band similar to observations from Raman spectroscopy of the bulk salt solutions.[10] However, the 3100 cm^{-1} band increases and the 3700 cm^{-1} peak decreases are unique to the acids and are not observed for the base (sodium hydroxide) and the sodium salt air/solution interfaces.

Consistent with the MD simulations, the VSFG data reveal that protonated water exists in the interfacial region. The observed decrease in the dangling OH intensity for HCl and HBr as shown in the inset of Figure 4 is also consistent with the decrease in free OH number densities derived from the MD simulates as stated above (see Figure 3). Changes in the orientation distribution have been ruled out from VSFG polarization data; this is consistent with water dipole orientational distributions calculated from the simulations, which are essentially the same in all the systems considered. The absence of VSFG intensity increases from the aqueous sodium hydroxide surface is consistent with the MD simulations showing a net depletion of OH^- at the surface (see Figure 1). Evidently, spectroscopic experiments and molecular simulations are converging to a unified picture of the interfacial structure of simple electrolyte solutions.

6. Discussion and Broader Implications

The bottom line of the present study is that on one side there are monovalent inorganic acids, where both cations and anions exhibit a propensity for the air/solution interface, whereas on the other side in bases and salt solutions cations are repelled from the interface and anions show a varying surface affinity. Thus, the distinguishing feature is the different surface behavior of hydronium compared to that of other cations. Atomic cations such as alkali ions practically do not penetrate the topmost layer of aqueous solutions. Hydronium cation behaves differently, primarily due to the "hydrophobic" character of its oxygen.[21] Although the three hydrogens of H_3O^+ are good hydrogen bond donors, the oxygen is, due to a significantly reduced negative charge (-0.4 e compared to a charge of -0.8 e of water oxygen), a relatively poor hydrogen bond acceptor. As a result of its amphiphilic character (a term coined for H_3O^+ in ref 21), hydronium can be stabilized at the air/solution interface with its H atoms hydrogen bonded to surrounding water molecules, whereas its oxygen atom remains unbound and pointing into the gas phase. This preferential orientation of H_3O^+ at the air/solution interface of aqueous HCl and HBr, as extracted from our simulations, is plotted in Figure 5.

We have verified the above predictions of classical molecular dynamics by a nonpolarizable quantum hopping molecular dynamics (Q-HOP MD) simulation[29] for a single proton in an aqueous slab. Figure 6a) shows a comparison between density profiles of a single proton and single sodium cation in aqueous slabs (the inferior statistics in Figure 6 compared to Figure 1 is due to sampling over a single ion only). These nonpolarizable calculations confirm that the proton (unlike the sodium cation) penetrates into the interfacial layer, and its density profile across the slab almost coincides with that of a single hydronium in a water slab, described by a classical nonpolarizable force field (see Figure 6b). The addition of polarizability of hydronium and water leads to a further increase of the surface propensity of H_3O^+, as shown in Figure 6b. These results are in perfect agreement with the most recent quantum calculations, which show the surface propensity of a single proton in aqueous clusters and slabs.[21,40,41]

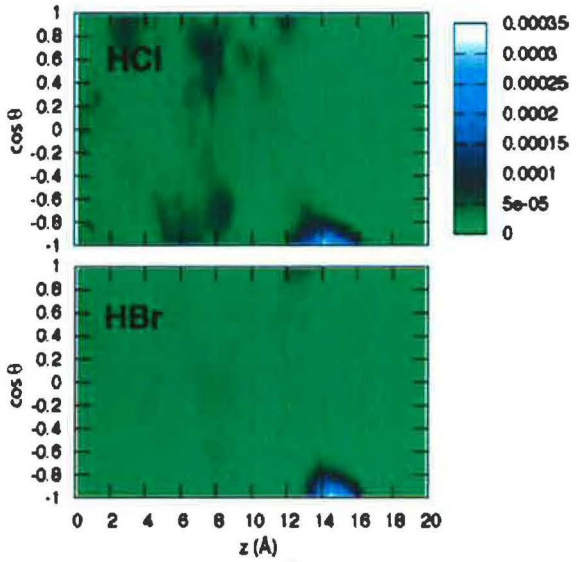

Figure 5. Probability densities of hydronium orientations from molecular dynamics simulations of aqueous solutions of 1.2 M HCl and HBr. Here θ is defined as the angle between the hydronium dipole moment (which points from the oxygen atom to the center of geometry of the hydrogen atoms) and a vector normal to the air−solution interface, and z is the location in the slab ($z = 0$ corresponds to the middle of the slab). The distributions are for the most part uniform (indicating isotropic orientational distributions), except for the pronounced peaks at $\cos\theta = -1$ and $z \sim 14-15$ Å, which correspond to hydronium ions strongly oriented at the air−solution interface with their dipoles pointing toward the interior of the solution.

Recently, the surface of ice doped with NaCl or HCl has been investigated in detail by means of cesium ion sputtering.[42,43] When the ice is heated, the two systems behave very differently from each other. Whereas in the case of NaCl doped ice, heating results in the disappearance of sodium cations (but not chloride anions) from the surface,[43] in the case of HCl doped ice, the elevation of temperature leads to a cationic (i.e., hydronium) and anionic surface enrichment.[42] Despite the fact that these experiments concern ice surfaces, the vastly different behavior of salt vs acid doped systems is indicative also for air/solution interfaces.

The results of the present calculations may shed some light on a long standing problem of the effect of electrolyte on bubble coalescence.[44−46] Though simple inorganic salts tend to inhibit bubble coalescence (which is one of the reasons why foam is formed when waves break in the ocean but not in freshwater lakes), the corresponding acids have no effect.[44,45] It is conceivable that the inhibition of bubble coalescence is related to Coulomb repulsion between interfaces due to separation of cations and anions at the air/solution interface of salts, such as alkali chlorides, bromides, iodides, or nitrates. Due to the surface propensity of hydronium, strong charge separation is not observed at the interfaces of aqueous HCl, HBr, HI, or HNO_3.

Inorganic electrolytes containing multivalent ions are beyond the scope of the present study, but they nevertheless deserve a brief remark. It has been shown both in experiments and calculations that multiply charged inorganic ions are always very strongly repelled from the air/solution interface due to very strong ion−water electrostatic interactions, even when the ion is very polarizable (such as sulfate).[47,48] Taking as an example sulfuric acid, it has been known for a long time that H_2SO_4 increases surface tension at low concentrations, but decreases it at high concentrations.[16] This nonmonotonic behavior of surface tension and, consequently, of the surface excess can be

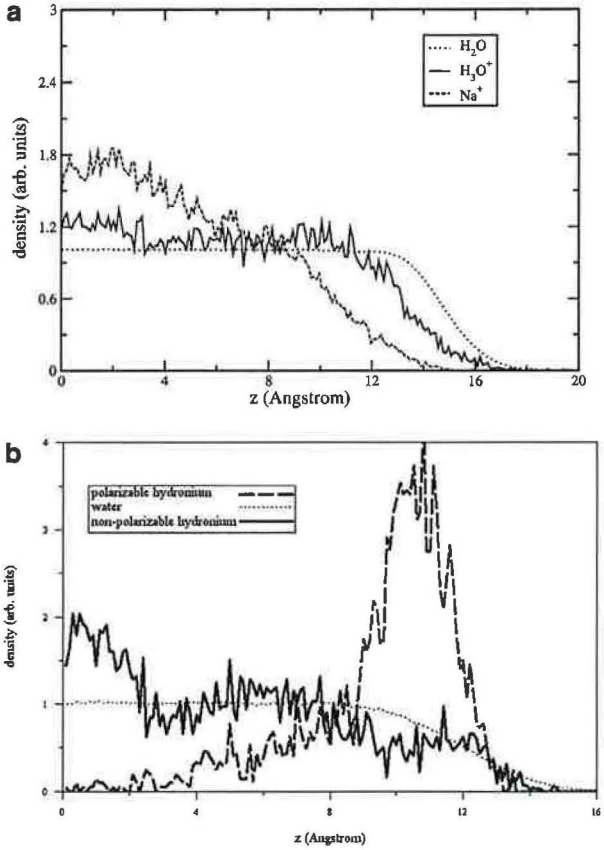

Figure 6. Comparison of density profiles of (a) a single hydrated proton described using the quantum hopping method and sodium and (b) polarizable and nonpolarizable hydronium described using a classical force field.

rationalized within the picture emerging from the present study. Namely, at low concentrations, H_2SO_4 is predominantly dissociated to hydronium and SO_4^{2-} ions. In this situation the weak attraction of hydronium to the surface cannot compete with the strong repulsion of sulfate dianion from the air/solution interface. This results in a net negative surface ion excess (i.e., net depletion of ions from the interface) and, consequently, a surface tension increase. At higher concentrations, H_2SO_4 is no longer fully dissociated and HSO_4^- is becoming the predominant anion. Being a soft monovalent anion, bisulfate is not strongly repelled from the air/solution interface.[14] This allows for a buildup of a positive net surface ion excess (i.e., net enrichment of ions in the interfacial layer), resulting in a surface tension decrease. Moreover, H_2SO_4, which is a weaker acid than HCl, HBr, or HI, can presumably also appear at higher concentrations at the surface in a molecular form, and this could further contribute to the lowering of surface tension.

7. Summary

A new picture of the air/solution interface of simple inorganic electrolytes emerges from the present molecular dynamics calculations and VSFG spectroscopic experiments. In contradiction with the traditional view, ions can play an active role at the interface and strong ionic specificity in surface propensity is the key to understanding macroscopic properties at the molecular level. In particular, the opposite sign of the change in surface tension upon adding bases (e.g., alkali hydroxides) and salts (such as alkali halides) on one side, and the corre-

sponding acids on the other side, can be related to the much stronger propensity of hydronium for the air/solution interface, compared to alkali cations. Although the present large scale molecular simulations necessarily employ a relatively simple polarizable classical force field (which can only approximately describe water molecules, salt ions and, in particular, hydroxide and hydronium), the results are robust and compare well with more accurate calculations on benchmark systems, as well as with most of the surface selective experiments.

The present results not only suggest a conceptual change in the perception of the surfaces of electrolytes, which are still mostly described within the continuum dielectric models,[49-52] but also have important practical implications for interfacial physical processes (such as bubble coalescence) and heterogeneous chemistry, e.g., in the atmosphere. For salts, this has already been recognized in studies of the chemistry of aqueous sea-salt aerosols,[15,53,54] whereas for acids there is a plethora of hitherto unexplored effects, for example, within the realm of the chemistry (e.g., corrosion processes) in the marine boundary layer or droplet and ice nucleation and cloud formation.[55]

Acknowledgment. We thank B. J. Finlayson-Pitts and E. C. Brown for valuable comments. Support via the NSF-funded Environmental Molecular Science Institute (grant CHE 0431512) and from the Czech Ministry of Education (grant ME644) is gratefully acknowledged. Part of the work in Prague was supported via the Research Project Z40550506. The work at PNNL was performed under the auspices of the Division of Chemical Sciences, Office of Basic Energy Sciences, U.S. Department of Energy. Support of the experimental work at Ohio State by NSF (grant ATM-0413893) and Research Corporation (Research Innovation Award) is also gratefully acknowledged.

References and Notes

(1) Onsager, L.; Samaras, N. N. T. *J. Chem. Phys.* **1934**, *2*, 528.
(2) Adam, N. K. *The Physics and Chemistry of Surfaces*; Oxford University Press: London, 1941.
(3) Randles, J. E. B. *Phys. Chem. Liq.* **1977**, *7*, 107.
(4) Jungwirth, P.; Tobias, D. J. *J. Phys. Chem. B* **2002**, *106*, 6361.
(5) Jungwirth, P.; Tobias, D. J. *J. Phys. Chem. B* **2001**, *105*, 10468.
(6) Dang, L. X.; Chang, T.-M. *J. Phys. Chem. B* **2002**, *106*, 235.
(7) Salvador, P.; Curtis, J. E.; Tobias, D. J.; Jungwirth, P. *Phys. Chem. Chem. Phys.* **2003**, *5*, 3752.
(8) Yang, X.; Kiran, B.; Wang, X.-B.; Wang, L.-S.; Mucha, M.; Jungwirth, P. *J. Phys. Chem. A* **2004**, *108*, 7820.
(9) Ghosal, S.; Shbeeb, A.; Hemminger, J. C. *Geophys. Res. Lett.* **2000**, *27*, 1879.
(10) Liu, D.; Ma, G.; Levering, L. M.; Allen, H. C. *J. Phys. Chem. B* **2004**, *108*, 2252.
(11) Petersen, P. B.; Saykally, R. J. *Chem. Phys. Lett.* **2004**, *397*, 51.
(12) Petersen, P. B.; Johnson, J. C.; Knutsen, K. P.; Saykally, R. J. *Chem. Phys. Lett.* **2004**, *397*, 46.
(13) Ghosal, S.; Hemminger, J. C.; Bluhm, H.; Mun, B. S.; Hebenstreit, E. L. D.; Ketteler, G.; Ogletree, D. F.; Requejo, F. G.; Salmeron, M. *Science* **2005**, *307*, 563.
(14) Vrbka, L.; Mucha, M.; Minofar, B.; Jungwirth, P.; Brown, E. C.; Tobias, D. J. *Curr. Opin. Colloid Interface Sci.* **2004**, *9*, 67.
(15) Knipping, E. M.; Lakin, M. J.; Foster, K. L.; Jungwirth, P.; Tobias, D. J.; Gerber, R. B.; Dabdub, D.; Finlayson-Pitts, B.-J. *Science* **2000**, *288*, 301.
(16) Washburn, E. W., Ed. *International Critical Tables*; McGraw-Hill: New York, 1928; Vol. IV.
(17) Baldelli, S.; Schnitzer, C.; Shultz, M. J. *Chem. Phys. Lett.* **1999**, *302*, 157.
(18) Baldelli, S.; Schnitzer, C.; Campbell, D. J.; Shultz, M. J. *J. Phys. Chem. B* **1999**, *103*, 2789.
(19) Schnitzer, C.; Baldelli, S.; Campbell, D. J.; Shultz, M. J. *J. Phys. Chem. A* **1999**, *103*, 6383.
(20) Petersen, P. B.; Saykally, R. J. *J. Phys. Chem. B* **2005**, *109*, 7976.
(21) Petersen, M. K.; Iyengar, S. S.; Day, T. J. F.; Voth, G. A. *J. Phys. Chem. B* **2004**, *108*, 14804.
(22) Foster, K. L.; Plastridge, R. A.; Bottenheim, J. W.; Shepson, J. B.; Finlayson-Pitts, B. J.; Spicer, C. W. *Science* **2001**, *291*, 471.
(23) Case, D. A.; Pearlman, D. A.; Caldwell, J. W.; Cheatham, T. E., III; Ross, W. S.; Simmerling, C. L.; Darden, T. A.; Merz, K. M.; Stanton, R. V.; Cheng, A. L.; Vincent, J. J.; Crowley, M.; Tsui, M.; Radmer, R. J.; Duan, R. Y.; Pitera, J.; Massova, I.; Seibel, G. L.; Singh, U. C. *AMBER6*, University of California, San Francisco, 1999.
(24) Caldwell, J.; Kollman, P. A. *J. Phys. Chem.* **1995**, *99*, 6208.
(25) Dang, L. X.; Chang, T.-M. *J. Chem. Phys.* **1997**,*106*, 8149.
(26) Dang, L. X.; *J. Phys. Chem. B* **2002**, *106*, 10398.
(27) Brodskaya, E.; Lyubartsev, A. P.; Laaksonen, A. *J. Phys. Chem. B* **2002**, *106*, 6479.
(28) Dang, L. X.; *J. Chem. Phys.* **2003**, *119*, 6351.
(29) Liil, M. A.; Helms, V. *J. Chem. Phys.* **2001**, *115*, 7993.
(30) Jungwirth, P.; Tobias, D. J. *J. Phys. Chem. B* **2000**, *104*, 7702.
(31) Essmann, U.; Perera, L.; Berkowitz, M. L.; Darden, T. A.; Pedersen, L. G. *J. Chem. Phys.* **1995**, *103*, 8577.
(32) Ryckaert, J.-P.; Ciccotti, G.; Berendsen, H. J. C. *J. Comput. Phys.* **1977**, *23*, 327.
(33) Wilson, M. A.; Pohorille, A. *J. Chem. Phys.* **1991**, *95*, 6005.
(34) Robertson, W. H.; Diken, E. G.; Price, E. A.; Shin, J.-W.; Johnson, M. A. *Science* **2003**, *299*, 1367.
(35) Heydweiler, A. *Ann. Phys.* **1910**, *33*, 145.
(36) Zhang, Y.; Feller, S. E.; Brooks, B. R.; Pastor, R. W. *J. Chem. Phys.* **1995**, *103*, 10252.
(37) Raymond, E. A.; Richmond, G. L. *J. Phys. Chem. B* **2004**, *108*, 5051.
(38) Moad, A. J.; Simpson, G. J. *J. Phys. Chem. B* **2004**, *108*, 3548.
(39) Buch, V.; Sadlej, J.; Aytemiz-Uras, N.; Devlin, J. P. *J. Phys. Chem. A* **2002**, *106*, 9374.
(40) Iyengar, S. S.; Day, T. J. F.; Voth, G. A. *Int. J. Mass Spectrom.*, in press.
(41) Shin, J. W.; Hammer, N. I.; Diken, E. G.; Johnson, M. A.; Walters, R. S.; Jaeger, T. D.; Duncan, M. A.; Christie, R. A.; Jordan, K. D. *Science* **2004**, *304*, 1137.
(42) Kang, H.; Shin, T.-H.; Park, S.-C.; Kim, I. K.; Han, S.-J. *J. Am. Chem. Soc.* **2000**, *122*, 9842.
(43) Kim, J.-H.; Shin, T.; Jung, K. H.; Kang, H. *J. Chem. Phys.*, in press.
(44) Craig, V. S. J.; Ninham, B. W.; Pashley, R. M. *Nature* **1993**, *364*, 317.
(45) Craig, V. S. J. *Curr. Opin. Colloid Interface Sci.* **2004**, *9*, 178.
(46) Marcelja, S. *Curr. Opin. Colloid Interface Sci.* **2004**, *9*, 165.
(47) Wang, X.-B.; Yang, X.; Nicholas, J. B.; Wang, L.-S. *Science* **2001**, *294*, 1322.
(48) Jungwirth, P.; Curtis, J. E.; Tobias, D. J. *Chem. Phys. Lett.* **2003**, *367*, 704.
(49) Manciu, M.; Ruckenstein, E. *Adv. Colloid Interface Sci.* **2003**, *105*, 63.
(50) Markin, V. S.; Volkov, A. G. *J. Phys. Chem. B* **2002**, *106*, 11810.
(51) Karraker, K. A.; Radke, C. J. *Adv. Colloid Interface Sci.* **2002**, *96*, 231.
(52) Bostrom, M.; Williams, D. R. M.; Ninham, B. W. *Langmuir* **2001**, *17*, 4475.
(53) Finlayson-Pitts, B. J.; Hemminger, J. C. *J. Phys. Chem. A* **2000**, *104*, 11463.
(54) Hu, J. H.; Shi, Q.; Davidovits, P.; Worsnop, D. R.; Zahniser, M. S.; Kolb, C. E. *J. Phys. Chem.* **1995**, *99*, 8768.
(55) Gao, R. S.; Popp, P. J.; Fahey, D. W.; Marcy, T. P.; Herman, R. L.; Weinstock, E. M.; Baumgardner, D. G.; Garrett, T. J.; Rosenlof, K. H.; Thompson, T. L.; Bui, P. T.; Ridley, B. A.; Wofsy, S. C.; Toon, O. B.; Tolbert, M. A.; Kärcher, B.; Peter, T.; Hudson, P. K.; Weinheimer, A. J.; Heymsfield, A. J. *Science* **2004**, *303*, 516.

ELSEVIER

Current Opinion in Colloid and Interface Science 9 (2004) 67–73

Current Opinion in COLLOID and INTERFACE SCIENCE

www.elsevier.com/locate/cocis

Propensity of soft ions for the air/water interface

Lubos Vrbka[a], Martin Mucha[a], Babak Minofar[a], Pavel Jungwirth[a,*], Eric C. Brown[b], Douglas J. Tobias[b,*]

[a]*Institute of Organic Chemistry and Biochemistry, Academy of Sciences of the Czech Republic, and Center for Complex Molecular Systems and Biomolecules, Flemingovo nam. 2, 16610 Prague 6, Czech Republic*

[b]*Department of Chemistry and Institute for Surface and Interface Science, University of California, Irvine, CA 92697-2025, USA*

Abstract

Major recent advances: Results of molecular dynamics simulations with polarizable force fields, supported by surface sensitive experiments, indicate that the propensity of atomic and hydrophilic molecular ions for the air/water interface exhibits strong ion specificity. While hard, non-polarizable ions are repelled from the interface, soft, polarizable ions exhibit surface affinity.

Keywords: Propensity; Soft ions; Air/water interface

1. Introduction

The studies of surface properties of simple electrolytes date back to the early 1900s, when Adolf Heydweiller performed surface tension measurements for a series of aqueous salt solutions [1]. The main findings were as follows: (i) adding simple salts raises surface tension of water; (ii) for cations there is little ion specificity; while (iii) the effect of anions is specific and follows the Hofmeister series [2], with strongly hydrated anions raising surface tension more than weakly hydrated ones. In the 1930s this effect was semi-quantitatively rationalized by Onsager and Samaras [3] via the Gibbs equation [4] in terms of repulsion of ions from the air/water interface by electrostatic image forces. It has since become a common wisdom that surfaces of aqueous solutions of simple salts are formed by an ion-free water layer [5].

The first indication that the above picture is not entirely correct came from cluster studies in the 1990s. Both photoelectron experiments [6,7] and molecular dynamics simulations [8–10] showed ion specificity in the behavior of alkali cations and halide anions in water clusters. While alkali cations and fluoride solvate inside medium sized clusters (with roughly 10–100 water molecules), heavier halides tend to solvate asymmetrically, i.e. to reside on the surface of the cluster. Molecular dynamics simulations showed that this ion specificity is due to the ion polarity, size, and in particular, polarizability. A theoretical study by Stuart and Berne [11] indicated that for chloride the surface effect is primarily due to the finite size and surface curvature of the water cluster. It was, therefore, unclear whether the cluster results can be directly extrapolated to extended, flat surfaces. Note that for aqueous salt droplets with a diameter larger than roughly 1 μm curvature effects become negligible, and consequently, their surface can be viewed as flat. Such particles are ubiquitous, e.g. in the atmosphere (aqueous sea salt aerosols), and their molecular structure and reactivity has been intensely studied recently [12–14]. In the following, we summarize results of molecular dynamics simulations of extended interfaces between air and aqueous solutions of simple salts.

2. Soft ions at the air/water interface

A well established procedure exists for performing molecular dynamics simulations of extended slabs, possessing a liquid bulk region in between two flat air/water interfaces [15]. One simply employs periodic boundary conditions with a unit cell with one dimension significantly elongated. In a typical simulation, an

*Corresponding authors. Tel.: +420-220410314, fax: +420-220410320 (P. Jungwirth); Tel.: +1-949-824-4295, fax: +1-949-824-9920 (D.J. Tobias).

E-mail addresses: pavel.jungwirth@uochb.cas.cz (P. Jungwirth), dtobias@uci.edu (D.J. Tobias).

1359-0294/04/$ - see front matter © 2004 Elsevier Ltd. All rights reserved.
doi:10.1016/j.cocis.2004.05.028

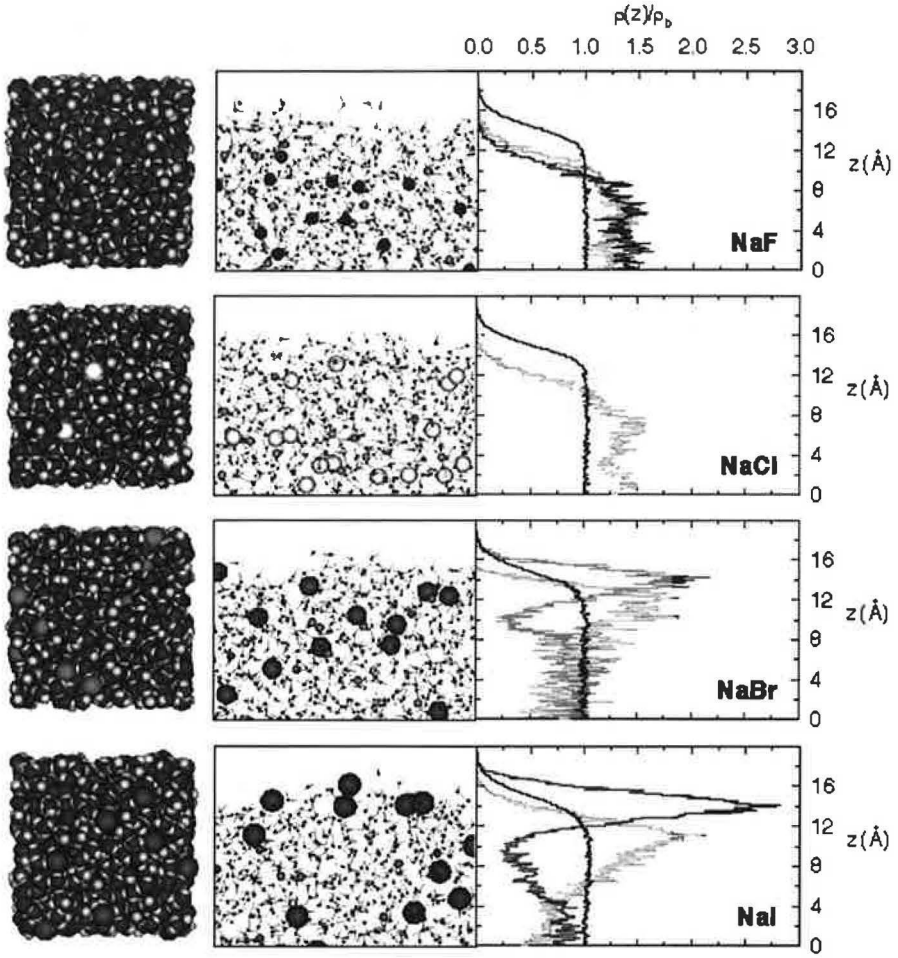

Fig. 1. Left and middle columns: top and side views of snapshots of solution/air interfaces from MD simulations of 1.2 M sodium halide solutions. Right: corresponding number density profiles. Coloring scheme: water oxygen, blue; water hydrogen, gray; sodium ions, green; chloride ions, yellow; bromide ions, orange; iodide ions, magenta.

orthogonal unit cell with dimensions $3\times3\times10$ nm is used, containing a slab of $\sim$900 water molecules and a specific amount of salt ions [16]. Note that under normal atmospheric pressure, less than a single molecule of nitrogen is on average present in the void above or below the aqueous slab. Therefore, for the purpose of the present discussion we can interchangeably use the terms vacuum/water and air/water interfaces.

Early molecular dynamics simulations of slabs containing aqueous NaCl solutions employing a non-polarizable force field showed a certain degree of ion specificity [15]. Namely, chloride penetrated closer to the surface than sodium, however, both ions were effectively repelled from the interface. The surface effects and ion specificity become much more pronounced upon using a polarizable force field [17,18]. This is clearly demonstrated in the composite Fig. 1, which depicts results from molecular dynamics simulations of a series of slabs of 1.2 M aqueous sodium halides. The left and middle columns show top and side views of typical snapshots from the simulations. The right column depicts statistically averaged density profiles of cations, anions, and water oxygens, histogrammed in thin slices parallel with the interface. The water oxygen signal defines the slab extensions, with a constant value (normalized to one) corresponding to the aqueous bulk and the decrease to zero within $\sim$0.4 nm to the interfacial region.

We see from the top pair of pictures that sodium and fluoride behave in our molecular simulations in accord with the traditional continuum dielectric boundary picture [3,5,19], which invokes repulsion from the air/water interface by image forces. However, the situation is very different for heavier halides, with the chloride ions moving all the way to the interface, and bromide and iodide even exhibiting a peak in density at the surface. Note that for the latter two ions, accumulation at the surface is accompanied by depletion from the

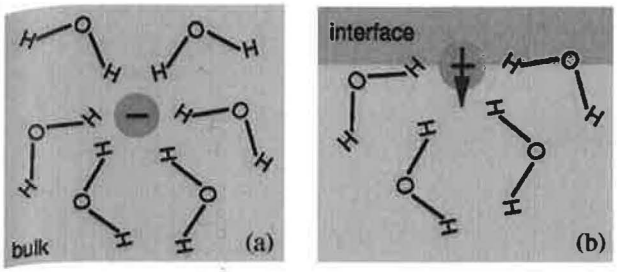

Fig. 2. A schematic picture of interactions between a polarizable anion and water molecules (a) in the aqueous bulk, and (b) at the air/water interface.

subsurface layer, where, as a matter of fact, the sodium cations exhibit a peak in density. As a result, an electric potential develops at the interface with a sign and magnitude correlating with earlier experimental results [5]. In addition, the values of surface tension, which are directly related to the asymmetry of the pressure tensor, have been extracted from the simulations. It is very encouraging that the molecular dynamics simulations succeeded to semi-quantitatively recover the experimental surface tension increase $\Delta\gamma$ with respect to pure water for the whole sodium halide series, including the Hofmeister ordering $\Delta\gamma(F^-) > \Delta\gamma(Cl^-) > \Delta\gamma(Br^-) > \Delta\gamma(I^-)$ [17].

Although the propensity of soft, polarizable anions for the air–water interface is a complicated function of ionic size, polarity and polarizability, simulations performed with polarizable and non-polarizable force fields clearly show that it is the last parameter which to the largest extent determines this effect [13,16]. Fig. 2 schematically shows a polarizable atomic anion in the aqueous bulk and at the air/water interface. In the liquid bulk, water molecules arrange roughly symmetrically around the ion. As a result, the vectorial sum of the dipoles of these water molecules is very small (zero on average). The situation is very different at the interface, where, schematically, water molecules are present only on one side of the ion. Consequently, there is a significant electric field resulting from the sum of water dipoles polarizing the soft anion. This leads to an additional stabilization at the interface, which can, for sufficiently polarizable ions, overwhelm the loss of ion–water electrostatic interactions.

In reality, the picture is more complex than the schematic Fig. 2. The aqueous interface is not perfectly flat but rather corrugated, and the water structure around the ion is thermally disordered. Moreover, water polarizability comes into play, too; not only water dipoles polarize the soft anion but also the ion polarizes water in a complex, non-additive fashion. To explore these effects in detail we performed a series of four simulations of aqueous slabs containing 1.2 M of sodium iodide. In the first simulation, the results of which are depicted in Fig. 3a, a non-polarizable force field was employed. We see from the density profiles that in this case both sodium and iodide ions are repelled from the air/water interface. Still, there is a weak specificity due to ion size and polarity, which results in the iodide signal being shifted closer to the surface than that of sodium. Fig. 3b shows density profiles from a simulation with non-polarizable ions but polarizable water. Including water polarizability results in iodide moving closer to the interface, exhibiting a sizable surface peak and subsurface depletion. Upon performing a simulation with polarizable ions in non-polarizable water (see Fig. 3c), the propensity of iodide for the air/water interface becomes stronger than in the previous case, and the sodium ions start to exhibit a subsurface peak. The combined effect of polarizable ions and water [17], as depicted in Fig. 3d, leads to the strongest surface enhancement (by up to a factor of three) of iodide concentration, with subsurface depletion close to the region where the sodium concentration peaks.

The densities presented in Fig. 3 clearly demonstrate that anion polarizability is an important factor in determining the propensity of an ion for the air–water interface. However, as one moves down the series of halides (F^-, Cl^-, Br^-, I^-), the size of the ion increases along with the polarizability, and it is conceivable that ion size could also play a role in determining adsorption propensity. To test this hypothesis, we have carried out a simulation of a 1.2 M solution of the sodium salt of a hybrid anion that has the size of iodide but the polarizability of chloride, in polarizable water. The simulations were performed with a unit box containing roughly twice as many atoms as in the previous case, in order to explore also the possible effect of the thickness of the slab. The density profile of the hybrid anion is compared to those of polarizable iodide and chloride in Fig. 4. In contrast to the chloride density, which approaches the Gibbs dividing surface but does not exhibit a peak in the interfacial region, the hybrid anion does exhibit a peak, suggesting surfactant activity, albeit not as strongly as iodide. Thus, for the determination of the interfacial propensity of the halide ions, size matters as well as polarizability. In addition, the effect of water polarizability is non-negligible (compare Fig. 3b and Fig. 4).

The polarizability driven surface propensity is not limited to atomic anions. We have investigated the interfacial behavior of three atmospherically relevant hydrophilic molecular anions: nitrate [20], sulfate [21], and bisulfate. The polarizability of nitrate, albeit anisotropic, is roughly of the same mean value as that of bromide. Consequently, NO_3^- exhibits a very similar propensity for the air/water interface as Br^-. Sulfate is even more polarizable than nitrate with polarizability in water (note that SO_4 [2–16] does not exist in the gas

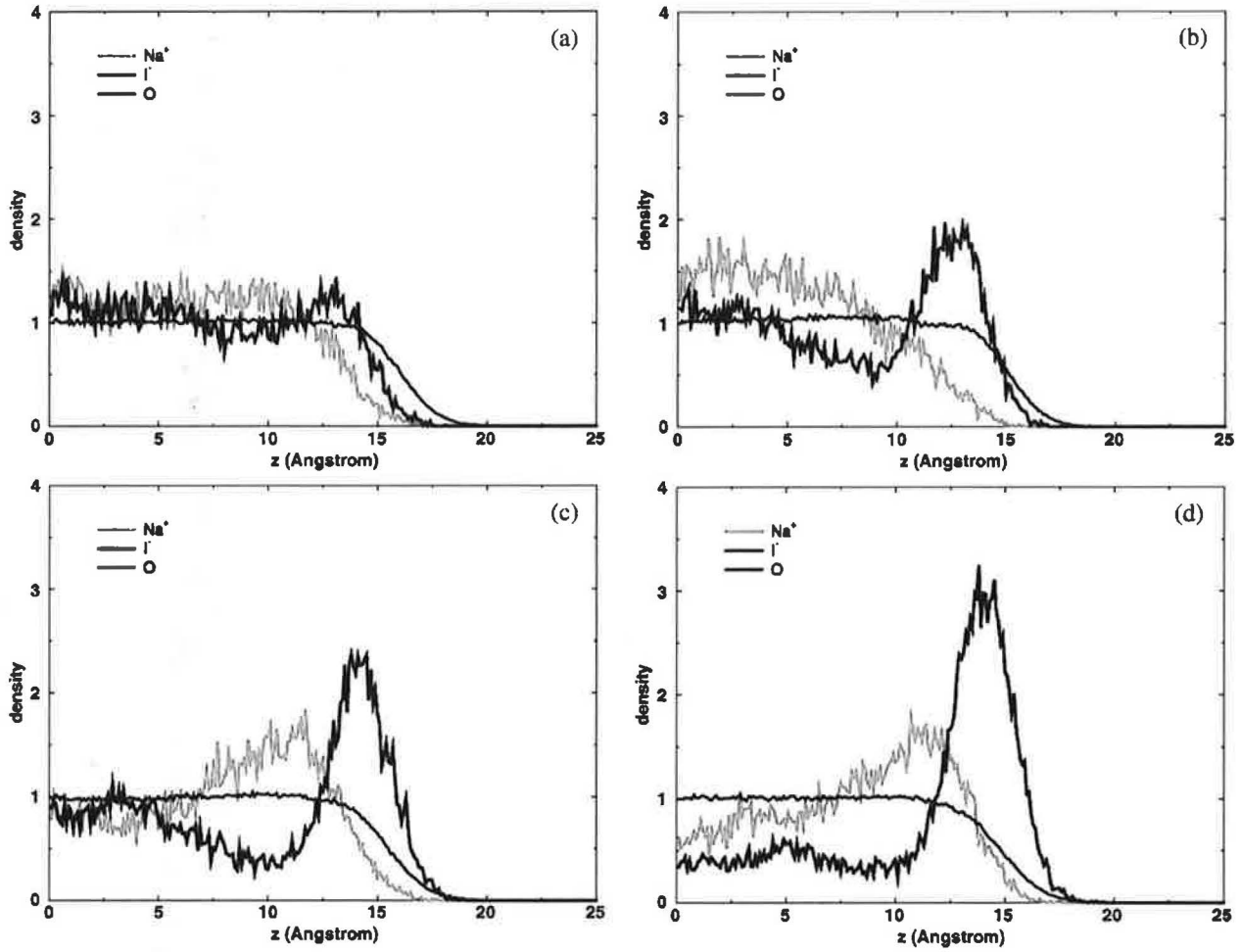

Fig. 3. Density profiles of water oxygen (blue), sodium (green), and iodide (red) from the center to the surface of a 1.2 M aqueous NaI slab. (a) Non-polarizable force field, (b) non-polarizable ions and polarizable water, (c) polarizable ions and non-polarizable water, and (d) polarizable force field.

phase due to a spontaneous electron detachment [22]) equal to 7.1 A^3. Nevertheless, molecular dynamics simulations show that sulfate is repelled from the air/water interface and prefers bulk solvation, in agreement with photoelectron experiments in large aqueous clusters [22–24]. This is due to the multiple charge, which shifts the balance from 'surface-driving' polarization interactions to 'bulk-driving' electrostatic forces. Finally, our most recent simulations show that the rather polarizable monovalent HSO_4^- ion with a strongly hydrophilic OH group turns out to be an intermediate case between bulk and interfacial solvation, behaving similar to chloride.

The force that drives polarizable atomic and hydrophilic molecular ions to the air/water interface is qualitatively different from that acting on hydrophobic ionic surfactants. This is nicely demonstrated on Fig. 5, which depicts our recent results of polarizable and non-polarizable simulations of a single tetra-butyl ammonium iodide ion pair in an aqueous slab. Each of the two ions was initially placed on one of the two air/water interfaces of an aqueous slab. Within a simulation employing a polarizable force field, both ions exhibit surfactant activity and remain at the interface (see Fig. 5a). The behavior of the tetra-butyl ammonium cation does not change significantly upon switching off polarizability. This is due to the fact that the hydrophobic interactions of the alkyl chains dominate. However, as shown in Fig. 5b, a non-polarizable iodide moves from the interface into the aqueous bulk, demonstrating again that its surface affinity is primarily due to polarization interactions.

3. Consistency with experimental observations

The traditional view of an ion-free interface was based largely on analysis of the surface tension of aqueous solutions using the Gibbs adsorption isotherm [25]:

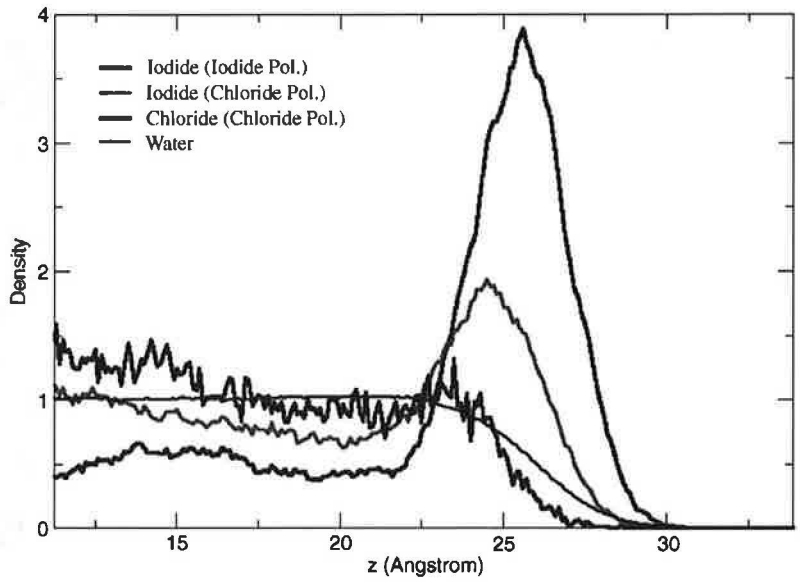

Fig. 4. Density profiles of water oxygen (blue), iodide with its natural polarizability (red), iodide with the polarizability of chloride (brown), and chloride with its natural polarizability (violet) from the center to the surface of a 1.2 M aqueous sodium halide solution.

$$d\gamma = -\Gamma d\mu \tag{1}$$

Here γ is the surface tension, μ is the chemical potential of the solute, and Γ is the surface excess of the solute:

$$\Gamma = \frac{1}{A}(n_{\text{total}} - n_{\text{liq}} - n_{\text{gas}}), \tag{2}$$

where A is the surface area of the interface, n_{total} is the total number of moles of solute, and n_{liq} and n_{gas} are the moles of solute in the liquid and gas phases, respectively. Note that Eq. (1) assumes that there is a single solute, and that the interface is defined by the Gibbs dividing surface, for which the surface excess of the solvent vanishes. Inserting $d\mu = -RT\ln a$ into Eq. (1) and rearranging, we obtain:

$$\left(\frac{d\gamma}{d\ln a}\right)_T = -RT\Gamma \tag{3}$$

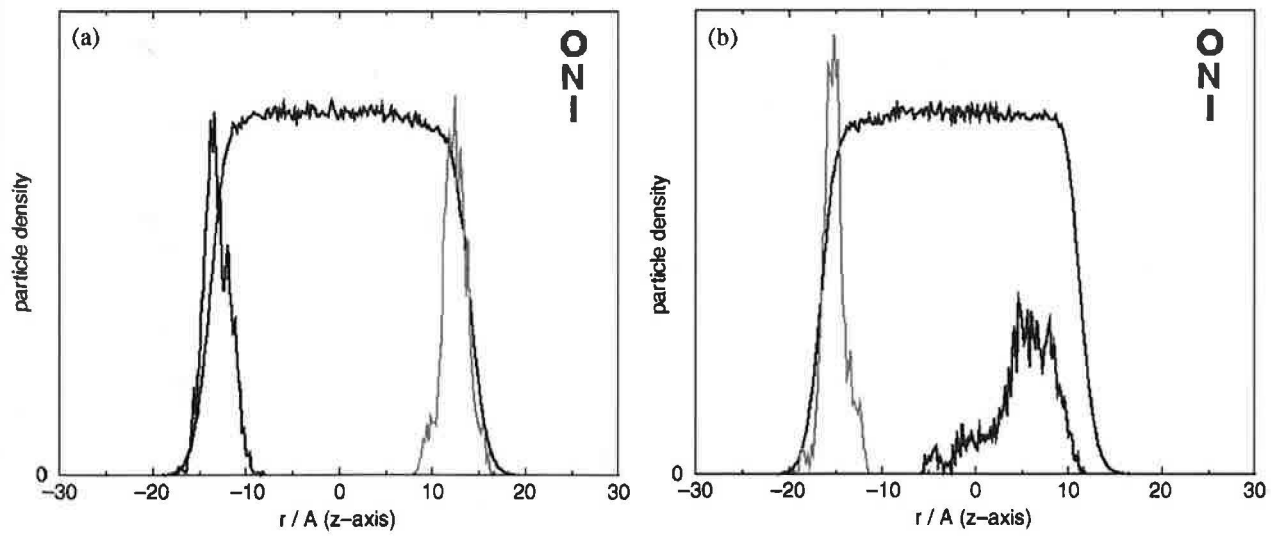

Fig. 5. Density profiles of tetra-butyl ammonium cation (nitrogen – green) and iodide (black) across the whole water slab (oxygen – red). (a) Polarizable force field, and (b) non-polarizable force field.

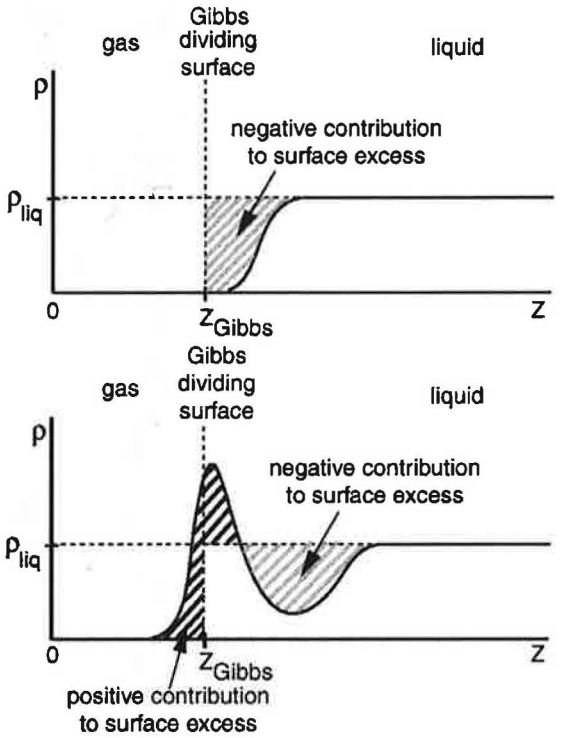

Fig. 6. Schematic depiction of the determination of the Gibbs surface excess from ion density profiles. Top: case of ion repulsion from the interface (e.g. F^-), bottom: case of inhomogeneous ion density profile with a surfactant layer and depletion zone (e.g. Br^-, I^-). The areas shaded green give negative contributions to the Gibbs surface excess, and red give a positive contribution (see text).

where a is the solute activity. Thus, the observed increase of the surface tension with the activity (concentration) of many inorganic salts, including the alkali halides [5], corresponds to a negative surface excess of ions.

Our simulations suggest that there are two ways to get a negative Gibbs surface excess. To illustrate this, we rewrite the definition (Eq. (2)) in terms of an ion density profile, $\rho(z)$:

$$\Gamma = \int_{-\infty}^{\infty} \rho(z)\mathrm{d}z - \rho_{\mathrm{liq}} \int_{z_{\mathrm{Gibbs}}}^{\infty} \mathrm{d}z - \rho_{\mathrm{gas}} \int_{0}^{z_{\mathrm{Gibbs}}} \mathrm{d}z, \tag{4}$$

where ρ_{liq} and ρ_{gas} are the (constant) densities in the bulk liquid and gas phases, respectively. Noting that for ions, $\rho_{\mathrm{gas}} = 0$, we can rearrange Eq. (4) to

$$\Gamma = \int_{0}^{z_{\mathrm{Gibbs}}} \rho(z)\mathrm{d}z + \int_{z_{\mathrm{Gibbs}}}^{\infty} [\rho(z) - \rho_{\mathrm{liq}}]\mathrm{d}z. \tag{5}$$

This equation is the basis of a graphical demonstration in Fig. 6 of two scenarios that can give rise to $\Gamma < 0$ (since atomic cations are repelled from the interface in accord with the traditional view, here we limit the discussion to the more complex case of atomic anions). Fig. 6 (top) depicts the scenario embodied in the traditional view, where anions are repelled from the interface, as exemplified by F^-. Fig. 6 (bottom) depicts the case of the heavier halide salts, e.g. NaBr and NaI, where there is a density enhancement at the surface followed by a depletion in the subsurface region (i.e. an oscillatory density profile). Note that, as long as the depletion is greater than the enhancement, the thermodynamic surface excess is negative. Thus, an increase of surface tension with solute concentration does not rule out the presence of a solute at the interface, and care should be taken when interpreting surface tension data on aqueous electrolyte solutions.

Two well-established experimental techniques for directly probing structure in the inhomogeneous interfacial region of liquid surfaces have recently had mixed success at detecting the presence of ions at the air–water interface. One is specular X-ray reflectometry (XRR) [26], which probes electron density distributions in the direction normal to the surface. In collaboration with experimental colleagues, we recently attempted to use synchrotron XRR to detect the pronounced enhancement of electron density expected at the air–solution interface of aqueous alkali iodides according to the predictions of our simulations (see Fig. 3d). Within experimental uncertainty the reflectivity data for neat water and the alkali iodide salt solutions were indistinguishable, and at first glance this seems to cast doubt on the predicted surface enhancement of iodide anions. However, a plausible explanation is that the surface roughness due to long-wavelength capillary waves (which are not present in the relatively small systems we simulate) wash out the enhancement of electron density due to ion adsorption. This was confirmed by computing reflectivities from the electron density profiles obtained from our simulations, including the roughness due to capillary waves (by Gaussian smoothing using widths extracted from experimental data).

In another set of experiments, Liu et al. [27] used vibrational sum frequency generation (VSFG) to investigate aqueous sodium halide solutions. VSFG is an interface-selective vibrational spectroscopy, which in the application cited focused on probing the water OH stretch, and hence provided information on changes in interfacial water structure upon addition of sodium halide salts. The VSFG data of Liu et al. [27] appear to be essentially consistent with our MD simulations: the spectra for NaF and NaCl solutions are similar to the neat water spectrum, suggesting negligible perturbations of the water structure in the interfacial region, while the spectra of NaBr and NaI solutions suggest significant perturbations of the hydrogen bonding in the interfacial region that increase with increasing concentration. Moreover, a comparison of the SFG data to infrared and Raman spectra obtained in the same study indicates an

increase in the width of the interface of NaBr and NaI solutions compared to neat water, consistent with the predictions of our simulations (cf. Fig. 1).

4. Conclusions

Recent molecular dynamics simulations of slabs of aqueous salt solutions indicate a strong specificity in the propensity of the solvated atomic and small hydrophilic molecular ions for the air/water interface. Small hard (non-polarizable) ions, such as alkali cations or fluoride, are repelled from the surface in accord with the standard Onsager–Samaras theory. However, large soft (polarizable) ions, such as heavier halides or nitrate, exhibit an affinity for the air/water interface. Although the propensity of soft anions for the interface depends on several factors, the main driving forces are the stabilizing polarization interactions in the anisotropic environment of the interface.

Acknowledgments

Support from the Czech Ministry of Education (grant No. ME644) and the US National Science Foundation (grant CHE-0209719) is gratefully acknowledged. We thank Prof. John A. Wheeler for helpful discussions on the Gibbs surface excess, and Prof. Mathias Lösche and Dr Peter Krueger for performing the X-ray reflectivity experiments.

References

[1] Heydweiller A. Ann Physik 1910;33:145.
[2] Hofmeister F. Arch Exp Pathol Pharmakol (Leipzig) 1888; 24:247.
[3] Onsager L, Samaras NNT. J Chem Phys 1934;2:528.
[4] Gibbs JW. The collected works of J. Willard Gibbs. New York: Longmans, 1928.
[5] Randalls JEB. Phys Chem Liq 1977;7:107.
[6] Markovich G, Giniger R, Levin M, Cheshnovsky O. J Chem Phys 1991;95:9416.
[7] Markovich G, Pollack S, Giniger R, Cheshnovsky O. J Chem Phys 1994;101:9344.
[8] Perera L, Berkowitz ML. J Chem Phys 1991;95:1954.
[9] Dang LX, Smith DE. J Chem Phys 1993;99:6950.
[10] Perera L, Berkowitz ML. J Chem Phys 1994;100:3085.
[11] Stuart SJ, Berne BJ. J Phys Chem A 1999;103:10 300.
[12] Oum KW, Lakin MJ, DeHaan DO, Brauers T, Finlayson-Pitts BJ. Science 1998;279:74.
[13] Knipping EM, Lakin MJ, Foster KL, Jungwirth P, Tobias DJ, Gerber RB, et al. Science 2000;288:301.
[14] Laskin A, Gaspar DJ, Wang WH, Hunt SW, Cowin JP, Colson SD, et al. Science 2003;301:340.
[15] Benjamin I. J Chem Phys 1991;95:3698.
[16] Jungwirth P, Tobias DJ. J Phys Chem B 2002;106:6361.
[17] Jungwirth P, Tobias DJ. J Phys Chem B 2001;105:10 468.
[18] Dang LX, Chang TM. J Phys Chem B 2002;106:235.
[19] Adam NK. The physics and chemistry of surfaces. London: Oxford University Press, 1941.
[20] Salvador P, Curtis JE, Tobias DJ, Jungwirth P. Phys Chem Chem Phys 2003;5:3752.
[21] Jungwirth P, Curtis JE, Tobias DJ. Chem Phys Lett 2003;367:704.
[22] Wang X-B, Nicholas JB, Wang L-S. J Chem Phys 2000;113:10 837.
[23] Wang X-B, Yang X, Nicholas JB, Wang L-S. Science 2001;294:1322.
[24] Yang X, Wang X-B, Wang L-S. J Phys Chem A 2002;106:7607.
[25] Defay R, Prigogine I, Bellemans A. Surface tension and adsorption. London: Longmans Green, 1966.
[26] Alsnielsen J, Jacquemain D, Kjaer K, Leveiller F, Lahav M, Leiserowitz L. Phys Rep 1994;246:252.
[27] Liu DF, Ma G, Levering LM, Allen HC. J Phys Chem B 2004;108:2252.

Structure and Vibrational Spectroscopy of Salt Water/Air Interfaces: Predictions from Classical Molecular Dynamics Simulations

Eric C. Brown,† Martin Mucha,‡ Pavel Jungwirth,‡ and Douglas J. Tobias*,†

Department of Chemistry and Environmental Molecular Sciences Institute, University of California, Irvine, Irvine, California 92697-2025, and Institute of Organic Chemistry and Biochemistry and Center for Biomolecules and Complex Molecular Systems, Academy of Sciences of the Czech Republic, Flemingovo nam. 2, 16610 Prague 6, Czech Republic

Received: October 31, 2004; In Final Form: February 22, 2005

We report the sum frequency generation (SFG) spectra of aqueous sodium iodide interfaces computed with the methodology outlined by Morita and Hynes (*J. Phys. Chem. B* **2002**, *106*, 673), which is based on molecular dynamics simulations. The calculated spectra are in qualitative agreement with experiment. Our simulations show that the addition of sodium iodide to water leads to an increase in SFG intensity in the region of 3400 cm^{-1}, which is correlated with an increase in ordering of hydrogen-bonded water molecules. Depth-resolved orientational distribution functions suggest that the ion double layer orders water molecules that are approximately one water layer below the Gibbs dividing surface. We attribute the increase in SFG intensity to these ordered subsurface water molecules that are present in the aqueous sodium iodide/air interfaces but are absent in the neat water/air interface.

1. Introduction

Aqueous aerosols and other particulate matter play an important role in the various chemical reactions that occur in the atmosphere. In the marine boundary layer, aqueous sea-salt aerosols are ubiquitous.[1] The bursting of air bubbles trapped by wave action produces fine aerosols that are comprised primarily of alkali and alkaline earth halide salts dissolved in water. These salt water aerosols serve as a source of reactant and as a substrate for various heterogeneous reactions with polluting gases.

An example of such a reaction is the production of molecular chlorine via the oxidation of chloride by hydroxyl radical. In an aerosol chamber, Knipping et al. monitored the appearance of chlorine and the disappearance of ozone (from which hydroxyl radical was generated by photolysis in the presence of water vapor) and sought to deduce the reaction mechanism(s) by fitting their kinetic data to a sizable battery of known bulk aqueous phase chemical reactions and their respective rates.[2] This particular modeling attempt based on bulk phase chemistry failed to predict the observed production of molecular chlorine under the conditions of the experiment.

Molecular dynamics (MD) simulations predicted that heavier halides may exist at interfaces in surprisingly high abundance.[3−6] The results of the MD simulations suggest that the interface can be rich in reactant chloride, and it is essential to take this into account when proposing a kinetic model that could match experimental data.[2] Indeed, when the aforementioned experimental results were analyzed using an interfacial mechanism that took into account the fact that ions could be present at interfaces, the kinetics data were well-reproduced.[2] Hydroxide, which is predicted to be a product of the interfacial reaction, was subsequently detected in NaCl aerosol particles following exposure to hydroxyl radical.[7]

The notion that atomic ions exist at the interface in surfactant-like excess is seemingly inconsistent with a straightforward application of the Gibbs adsorption relation.[8] If, in accord with experiment and surface electrolyte theory, the surface tension of a salt solution increases relative to that of pure water, then the concentration of solute (in this case, the ions) must decrease at the interface. For example, the surface tension of 1 M NaI in water is higher by roughly 1% than that of pure water,[9] so one might deduce that there should be fewer ions at the interface than in the bulk. However, as we have recently discussed,[10] this behavior can also be rationalized in terms of a nonmonotonic ionic density profile with surface enhancement and subsurface depletion, with a different behavior of cations and anions at the interface.

A simple explanation for the observation that cations and anions associate differently at the air/water interface is that the halide anions are, except for fluoride, larger and more polarizable than the alkali cations and even water molecules.[10] Polarization is an important factor because, qualitatively speaking, the electron clouds of the anions can easily be distorted by the nonvanishing electric field at the interface, which can make the surface location favorable.

Due to their surface specificity, nonlinear spectroscopies[11,12] such as sum frequency generation (SFG) spectroscopy[13,14] are becoming important tools for elucidating molecular structure at solid and liquid surfaces.[12] The surface specificity derives from the fact that the signal averages to zero in centrosymmetric environments. The SFG spectrum of the pure water/air interface has been known for almost a decade,[12] and recently, the SFG spectra of the series of sodium halide/air interfaces have been measured over a range of frequencies spanning the water OH stretching region.[15,16]

The SFG spectrum of pure water is different than the SFG spectra of some of the salt water/air interfaces (e.g., aqueous

* Author to whom correpondence should be addressed. E-mail: dtobias@uci.edu.
† University of California, Irvine.
‡ Academy of Sciences of the Czech Republic.

10.1021/jp0450336 CCC: $30.25
Published on Web 03/29/2005

NaI); hence, one may conclude that the interfaces are different from a structural and/or dynamic point of view. However, there remains uncertainty as to whether these salt water SFG spectra correspond to an environment where some ions exist at the surface in a surfactant-like way (as predicted by classical MD simulations) or whether these spectra correspond to an environment where the interface is perhaps only slightly perturbed by the presence of ions in the subsurface. Thus, the spectra alone have not provided a definitive answer to the question raised by MD simulations: is the concentration of ions such as iodide or bromide in certain regions of the air/water interface higher than the concentration of the salts in the bulk?

The above-mentioned experimental studies of sodium halide/water interfaces that include SFG spectra for the entire sodium halide series revealed that trends in spectral features are enhanced upon moving down the periodic table.[15,16] A similar trend is readily apparent from MD simulations of 1.2 M solutions of NaF, NaCl, NaBr, and NaI, which showed that the probability of finding a halide anion at the interface increased in the order $F^- < Cl^- < Br^- < I^-$.[3] Indeed, this is the trend that one would predict based on the fact that the halide polarizability and ion size increase in the same manner. It is also important to point out that when, in computational experiments based on MD simulations, the particles are prevented from undergoing polarization (i.e., their polarizability parameters are set to be zero), the anions to a large extent lose their tendency to exist at the surface, and except for the heaviest halides, they are repelled from the interface in accord with the classical theory of electrolyte surfaces.[3] Variation of the polarizability parameters allows us to generate molecular dynamics configurations where the ion distribution ranges from being surfactant-like to a situation where the ion distribution is more like that of the bulk solution.[10]

Of all the sodium halides, the SFG spectrum of sodium iodide in water exhibits the largest differences from the SFG spectrum of neat water. The main goal of this work is to compute the SFG spectrum of the aqueous sodium iodide interface from molecular dynamics simulations. Comparison of available experimental SFG spectra[15,16] with our computed spectra, in conjunction with the structures provided by MD simulations, enables us to investigate whether ion adsorption to the air/water interface is manifested in the spectra and, if so, to elucidate the molecular origins of the spectral changes.

2. Computational Methodology

Although other methods for computing SFG spectra exist,[17-20] a straightforward and general way to predict SFG spectra is via time correlation functions computed from classical molecular dynamics trajectories. Morita and Hynes have outlined such a procedure, and the reader is referred to their particularly lucid work[21] for the derivations of the expressions outlined in this section. Here, we adopt their notation and describe only the essential steps that we took to obtain the theoretical spectra reported in this work. While Morita and Hynes have successfully treated the neat water interface with this procedure, we emphasize that we shall focus on *differences* between neat water and salt water solutions computed in a similar way.

Most of the reported experimental investigations of (salt) water interfaces have employed the *ssp* light polarization.[12,15,16] The SFG line shape (I_{ssp}) for this particular polarization is given as:

$$I_{ssp} \propto \left(\frac{\omega_{IR} + \omega_{vis}}{\omega_{IR}}\right)^2 |\chi_{xxz}|^2 \qquad (1)$$

where ω_{IR} and ω_{vis} are the frequencies of the incident infrared and visible radiation, respectively, χ_{xxz} is the second-order nonlinear susceptibility, and x and z are Cartesian coordinates parallel and normal, respectively, to the interface.

The nonlinear susceptibility χ_{xxz} is a complex quantity, being the sum of a complex resonant term, χ^R_{xxz}, and a real nonresonant term, χ^{NR}_{xxz}, that depends on the sum of the molecular hyperpolarizabilities (β)

$$\chi^R_{xxz} = i \int_0^\infty \langle A_{xx}(t) M_z(0) \rangle \, e^{i\omega t} \, dt \qquad (2)$$

$$\chi^{NR}_{xxz} = \frac{1}{2} \left\langle \sum_i^{\text{molecules}} \beta_{xxz}(i) \right\rangle \qquad (3)$$

where A_{xx} and M_z are components of the system polarizability tensor and dipole moment, respectively.[12,17] It is the resonant part (χ^R_{xxz}) of the total susceptibility that gives rise to the features that dominate the corresponding SFG spectrum. Since on long time scales the x and y dimensions are equivalent for a planar interface (i.e., axial symmetry), A_{yy} and M_z also represent a valid combination for describing the SFG intensity I_{ssp}, and we average contributions from the x and y directions for all of the SFG spectra reported in this work. As was pointed out by Morita and Hynes,[21] quantum nuclear effects are not large over the range of the O−H stretching frequencies, and so no attempt was made to modify the spectra due to these affects.

The flexible, SPC/E-like water potential of Ferguson[22] was chosen for this study because it has been previously shown to reproduce the experimental SFG spectrum of neat water reasonably well.[21] For the ions, the polarizable potentials for sodium and iodide of Markovich et al. were employed.[23] All of the MD simulations were performed with the AMBER 7[24] suite of programs, modified by us to implement the cubic (anharmonic) O−H stretch terms required by the Ferguson model. The dimensions of the prismatic unit cell were chosen to be 30 Å in the x and y dimensions and 160 Å in the z dimension, resulting in a slab geometry with two solution/vapor interfaces. Particle-mesh Ewald summation was performed to account for long-range electrostatic effects.[25] Initial configurations for the trajectories were taken from evenly spaced snapshots from a previous 1 ns molecular dynamics simulation.[4] Systems containing pure water had 864 molecules, and systems containing water and ions had 864 waters, 18 cations, and 18 anions, giving 1.2 M NaI solutions. The initial velocities for each configuration were randomly sampled from a Maxwellian distribution corresponding to 300 K.

The first studies of aqueous salt water interfaces that employed polarizability in the molecular dynamics force fields considered polarization effects on the ions and on the waters.[4-6,26] In those studies, the water molecules had rigid O−H bonds, whereas in this study the O−H bonds were allowed to undergo vibration. Because the simultaneous incorporation of polarizability, flexibility of the water O−H bonds, and a lack of a Lennard-Jones repulsion term for hydrogen leads to the well-known "polarization catastrophe",[27,28] we were not able to augment the Ferguson model of water with the atom-based polarizability model as implemented in AMBER 7. Nevertheless, as we have previously shown,[10] most of the surface excess of ions such as iodide can be obtained using force fields with polarizablity only on the ions and nonpolarizable water molecules, and hence this is the treatment also adopted in this work.

For the SFG modeling, for each of the runs we used a 0.6 fs time step and performed equilibration for 15 ps with the Berendsen thermostat, followed by a 15 ps acquisition time in

the NVE ensemble. From these latter trajectories, the time-dependent system dipole and polarizability were evaluated with the inclusion of the local field corrections. We removed the effect of rotational drift on this short time scale by smoothing the resulting $M(t)$ and $A(t)$ with a broad Gaussian function and then subtracting this result from the initial values to obtain $M(t)$ and $A(t)$ solely as a result of water vibrational motions.

A simple sum over the permanent gas-phase dipole moments and polarizabilities is only an approximate description of the system dipole and polarizability. It neglects several important factors: (1) the condensed phase effect on molecular properties, (2) the fact that the interfacial region is a different chemical environment than the bulk phase, and (3) the fact that the interaction of a water molecule with a nearby ion is likely to be strong. To account for these effects, each of the dipole moments and polarizabilities were corrected with a many-body approach.[21,29,30]

Equations 4 and 5 represent the simultaneous linear equations that must be solved to correlate the dipoles and charges for each MD configuration

$$(1 + \mathbf{T}\alpha)\mathbf{E} = \mathbf{E}^{cd} - \mathbf{T}\mathbf{p}^0 \tag{4}$$

$$(1 + \mathbf{T}\alpha)\mathbf{f} = \mathbf{h} \tag{5}$$

where $\mathbf{T}$ is the dipole field tensor, α is a polarizability matrix, $\mathbf{E}^{cd}$ is the term that accounts for the field due to the permanent charges on the dipoles, $\mathbf{p}^0$ is the polarization (dipole moment) vector, $\mathbf{f}$ is a local field correction, and $\mathbf{h}$ is a vector of identity matrices.

The linear equations describing the effects of induced polarization[21] were solved iteratively with the GMRES algorithm.[31] The construction and solution of these equations accounts for the vast majority of the time required to perform the spectral calculations.

The quantities A and M are represented as the sum of the molecular quantities at each time step of the MD simulation, where $\alpha_i(t)$ and $\mu_i(t)$ are the polarizability tensor and dipole moment, respectively, of an individual molecule i at time t. The perturbed molecular dipole moments and polarizabilities from eqs 6 and 7

$$A(t) = \sum_{i}^{\text{molecules}} \alpha_i(t) \cdot f_i(t) \tag{6}$$

$$M(t) = \sum_{i}^{\text{molecules}} \mu_i(t) + \alpha_i(t) E_i(t) \tag{7}$$

and the nonresonant susceptibility was modified as

$$\chi^{NR}_{xxz} = \frac{1}{2} \left\langle \sum_{i}^{\text{molecules}} \sum_{q,r}^{x-z} \beta_{xxz}(i) f_{qx}(i) f_{rz}(i) \right\rangle \tag{8}$$

and are then used in eq 2.

Since we are interested in vibrational spectroscopy, these simulations must be performed with a flexible force fields, i.e., water molecules must be free to undergo stretching and bending motion. At each instantaneous molecular position, the dipole moment and polarizability for each molecule is determined from ab initio data. Specifically, each water molecule is rotated from its laboratory frame orientation into a standard orientation, where the properties are mapped onto functions representing the center of charge, dipole, polarizability, and hyperpolarizability. These functions were determined by fitting ab initio values at various

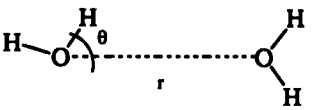

Figure 1. Schematic description of the distances and angles involved in the definition of the "free O−H" bond. The angle criterion is 30°, and the distance criterion is 3.5 Å.

grid points computed at the B3LYP/d-aug-cc-pVDZ level of theory[32−36] with the Gaussian 03 suite of programs.[37] Whereas Morita and Hynes represented these molecular quantities via O−H bond additivity, we chose to represent the dipole functions over the internal coordinate space of the entire molecule. Since at the grid point geometries both our treatment and theirs[21] yield fitted values that are virtually identical to the ab initio quantities, we conclude that these two approaches are equivalent for water.[38−40] These interpolated quantities enter into the summations in eqs 6 and 7. The mapping is done using configurations generated by MD simulations based on empirical force fields.

While we expect that the actual vibrational frequencies depend mostly on the chemical environments that arise from the molecular dynamics force field, the intensities of these transitions are affected by the magnitudes of the dipole moments and polarizabilities that enter eq 2.[21] While the average dipole moment of a gas-phase water molecule is 1.8 D (taken from the B3LYP calculations, in excellent agreement with experiment[41]), the most probable dipole moment in these systems, after application of eqs 6 and 7, is 2.2 D, which is closer to the ab initio estimate for liquid water of about 2.6 D.[42] On the basis of the work of Markovitch et al.,[23] the polarizability of the iodide ion and the sodium polarizability were chosen to be 6.9 Å^3 and 0.24 Å^3, respectively.

Since these slabs possess two interfaces ("top" and "bottom"), averaging may be performed over both. However, straightforward summation over the entire slab would lead to the cancellation of surface-normal components since the two interfaces "point" in opposite directions. Therefore, one must choose one interface to have the positive normal direction and appropriately reflect the other interface such that its normal direction is the same as the other. At the beginning of each trajectory, the molecules were assigned to a particular interface for the duration of the 15 ps run and were counted as being in a particular slab side when accumulating properties.

Correlation functions were computed using the Wiener−Kinchin method.[43] The resulting correlation functions were exponentially damped with a damping constant of 0.0025 ps^{-1}. Last, the Fourier transform of each damped correlation function yields the corresponding frequency spectrum. During the course of the calculation of an SFG spectrum, we may readily compute the infrared and Raman spectra since they are related to the Fourier transforms of the appropriate autocorrelation functions, $\langle M(0) \cdot M(t) \rangle$ and $\langle \mathrm{Tr}[A(0) \cdot A(t)] \rangle$, respectively.[44,45]

Spectral convergence was assessed by comparing the average results of the top of the slab to the average results from the bottom of the slab. The resonant susceptibilities of each of the systems considered herein were well-converged in 128 trajectories.

In addition to computed SFG spectra, we report the results of several standard structural diagnostics. Density profiles and orientational distribution functions of the angle bisector of each water molecule with respect to the surface-normal direction were computed. Free O−H bonds were defined as those not acting as hydrogen bond donors, with hydrogen bonds defined by using a geometric criterion; the oxygen atom of a potential hydrogen bond donor is less than 3.5 Å from the oxygen on a potential

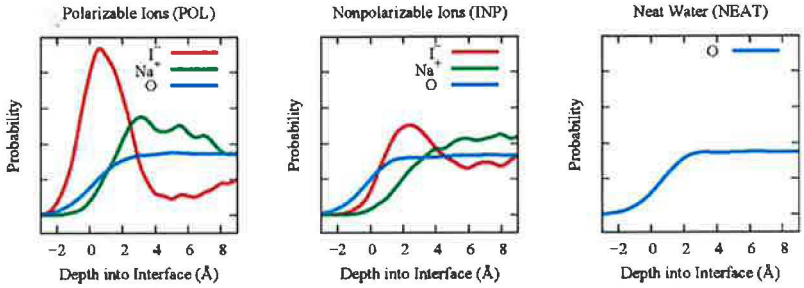

Figure 2. Density profiles of IPOL (left panel), INP (center panel), and NEAT (right panel). Zero on the x-axis corresponds to the Gibbs dividing surface.

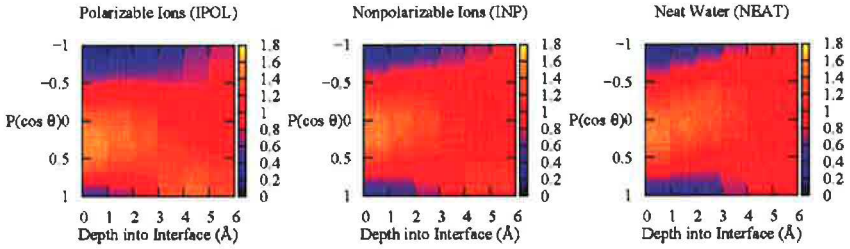

Figure 3. Orientational distribution functions as a function of depth into the interface. The values have been scaled such that a unit value corresponds to an isotropic environment.

hydrogen bond acceptor, and the angle between the donor hydrogen, donor oxygen, and acceptor oxygen is less than 30° (Figure 1).

3. Results and Discussion

First, we characterize the various systems by analyzing the structures obtained from the molecular dynamics simulations, and susbsequently, we report predictions of the IR, Raman, and SFG spectra. We consider three systems: (1) neat water (NEAT), (2) 1.2 M sodium iodide in water with polarizable ions (IPOL), and (3) a system analagous to IPOL, but with the polarizabilities "switched off" (INP). As expected, the ion distribution for IPOL is surfactant-like for iodide, with the sodium ions broadly peaking in the subsurface. The ion distribution for INP is more homogeneous, although it does exhibit a small surface anion enhancement (Figure 2).[10]

3.1. Structure. As stated in the Introduction, we aim to resolve, from structural and spectroscopic considerations, how changes in the SFG spectrum correlate with the presence of halide ions near the air/water interface. SFG spectroscopy, within the dipolar approximation, gives intensities corresponding to oscillators that are in anisotropic environments. Therefore, it is reasonable to begin this discussion by identifying which regions in the slab correspond to such environments. A convenient way to visualize this anisotropy is to plot the orientational distribution function (ODF) of the water dipole moments (i.e., the distribution of angles between the H−O−H angle bisector and the surface-normal vector). At the Gibbs dividing surface ($Z = 0$ Å), the ODF of the neat water system (NEAT) has a maximum corresponding to an angle of ~78° (Figure 3), which is in good agreement with the value obtained by Benjamin for SPC/E water (upon which the Ferguson model is based).[45,46]

Figure 3 also shows the ODFs of the IPOL and INP systems, respectively. Despite the fact that in IPOL there is an appreciable ion concentration at the surface, the largest difference (Figure 4) between neat water and IPOL and between neat water and INP is in the region 4−5 Å below the Gibbs dividing surface. In this subsurface region, the ODF difference plots (Figure 4) reveal that in IPOL and INP there is a significant ordering of

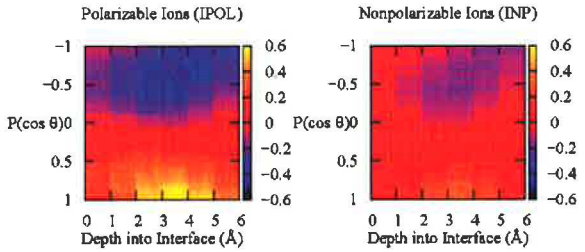

Figure 4. Orientational distribution functions of IPOL and INP, less the ODF profile of NEAT.

waters corresponding to an angle of ~0° between the water dipole moments and the surface-normal vector. We speculate that this (time-averaged) ordering is due to the separation of anions and cations in the interfacial layer. This conclusion is supported by the fact that a greater subsurface water ordering is found in the case of IPOL than in the case of INP (Figure 4), coupled with the fact that the density profile of IPOL exhibits a more pronounced ion double layer than does that of INP (Figure 2). At this concentration (1.2 M and a roughly 2.5 M effective peak surface ion concentration in IPOL), the orientation of the water molecules is caused by interaction with at most one anion and one cation rather than by an electric field caused by a dense "plate" of ions.

Comparison of the ODFs of the three systems does not reveal a large difference between NEAT, IPOL, and INP in water orientation at the Gibbs dividing surface. Water molecules in this region give rise to the so-called "dangling O−H" or "free O−H" band in the SFG spectrum (ca. 3750 cm^{-1}, vide infra).[47] Because the SFG spectrum depends significantly on the number density of oscillators of this type, it is useful to compare the number of molecules that contain a free O−H bond between each of the systems. As is evident in Figure 5, there are no large differences, and hence one would not expect there to be large differences in the SFG spectra due to a change in the number density of free O−H oscillators.

3.2. Spectroscopy. As a way of highlighting the usefulness of SFG spectroscopy, we begin the discussion of our spectroscopic calculations by demonstrating the limitations of IR and

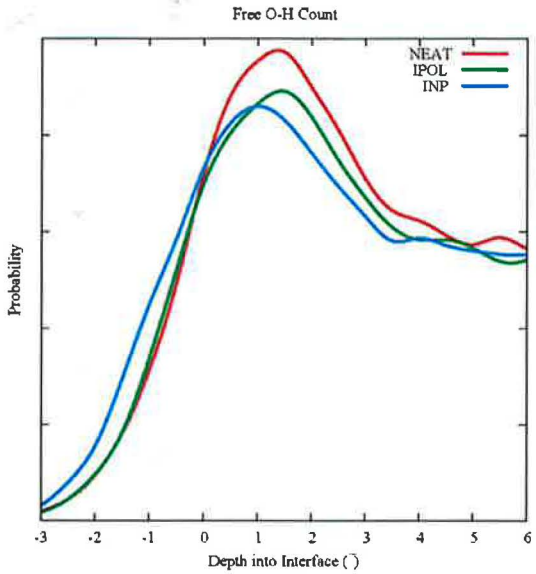

Figure 5. Number of O−H bonds characterized as being a "free O−H" bond, resolved into depth into the interface.

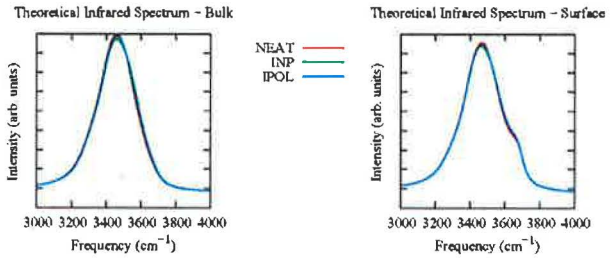

Figure 6. Theoretical infrared spectrum of the bulk (left panel) and topmost layer (right panel; $Z < 0$) of IPOL, INP, and NEAT.

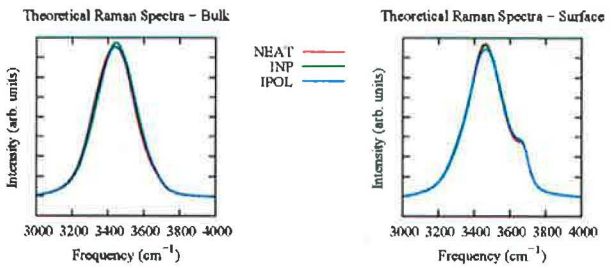

Figure 7. Theoretical Raman spectrum of the bulk (left panel) and topmost layer (right panel; $Z < 0$) of IPOL, INP, and NEAT.

Raman spectroscopies for differentiating between the salt water solutions and the neat water system. Because the SFG intensity arises from the quantities also required to compute the IR and Raman spectra,[44] the latter are readily computed during the course of the computation of the SFG spectrum.

Linear spectroscopies (e.g., IR and Raman) give rise to features corresponding to both bulk and interfacial waters (i.e., isotropic and anisotropic environments). As expected, there is almost no difference between the theoretical IR (Figure 6) or Raman (Figure 7) spectra of the NEAT, IPOL, and INP systems. Benjamin has pointed out that hypothetical IR spectra of only the topmost layer can be calculated.[45] We also report the theoretical, topmost layer IR and Raman spectra for each of the systems in Figures 6 and 7. These spectra yield two important details: (1) the appearance of the "free O−H" oscillator as a shoulder at ca. 3750 cm^{-1} and (2) the fact that there is only a small difference between the IR and Raman spectra in terms of the relative intensities of the hydrogen-bonded region and the "free O−H" region. We conclude from these spectra that there is either not much difference between the oscillators of the different systems or that the spectral differences between NEAT, IPOL, and INP are masked by bulklike contributions.

In contrast to the linear spectroscopies, in SFG spectroscopy, bulklike contributions vanish, leaving only the anisotropic environments visible in the spectrum. The computation of SFG spectra involves a large amount of sampling over many trajectories to average the bulklike components to zero.[21] Since these calculations are rather time-consuming, it is desireable to find a way to reduce the required effort. The ODFs give some clue as to which regions of the bulk are anisotropic and which are isotropic. The computed susceptibilities converge at about $Z = 9$ Å, where the ODF profiles strongly suggest that the environment is isotropic. Therefore, the computed susceptibilities and SFG spectra involve the summation of molecules that are no more than 9 Å below the Gibbs dividing surface.

The resonant susceptibilities of NEAT, IPOL, and INP are similar in the region around 3750 cm^{-1} (Figure 8). However, the salt water solutions have a clear "onset" at 3300 cm^{-1}, which gives rise to the features in the SFG spectrum corresponding to a peak maximum of ~3400 cm^{-1}. Since the main structural difference between NEAT and the salt water interfaces (INP and IPOL) is the presence of the subsurface water ordering in the latter systems, we attribute this feature to water oscillators that are ordered by the ion double layer. Unfortunately, the phase information corresponding to this feature is lost in the actual SFG spectrum, since the intensity is related to the square modulus of the susceptibility according to eq 1.[12]

The theoretical SFG spectrum given by eq 1 involves the sum of the resonant and nonresonant susceptibilites. Although we originally attempted to compute the frequency-independent nonresonant susceptibility of each system following the prescription of Morita and Hynes, the values turned out to be orders of magnitude off from what would be required to generate a reasonable SFG spectrum from the simple addition of this term to the resonant contribution.[21] Therefore, we simply optimized the fit of our spectra for NEAT with those obtained by Morita and Hynes and then multiplied this value by the experimentally determined ratio (0.154 IPOL/ 0.105 NEAT) of the nonresonant susceptibilities that were reported by Richmond and Raymond. Whereas we are confident that the chosen values of the nonresonant term yield computed SFG spectra that are "realistic", we point out that a weakness of this approach is that the accurate, first-principles calculation of this term remains elusive.[21] Consequently, we cannot compare absolute intensities (e.g., of the free O−H band) between the different systems, and we will therefore focus on changes in the relative intensities of the two main bands.

Figure 9 shows our computed SFG spectra (ssp polarization) for NEAT, IPOL, and INP. The computed SFG spectra of the three systems exhibit similar features: a broad band around 3400 cm^{-1} corresponding to stretching of waters in the hydrogen-bonded region and a sharp intensity at 3750 cm^{-1} that corresponds to the "free O−H" stretch. Our computed SFG spectrum for neat water is in excellent agreement with that reported by Morita and Hynes for a somewhat smaller system.[21] The main difference between the predicted SFG spectrum of the neat water system and the predicted spectra of the salt water systems is that in the salt water systems there is, in qualitative agreement with experiment, a considerable increase in intensity

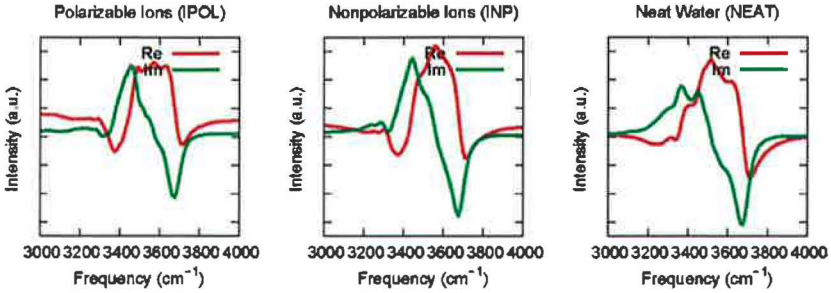

Figure 8. Theoretical resonant susceptibilities (*xxz*, *yyz*) of IPOL (left panel), INP (center panel), and NEAT (right panel).

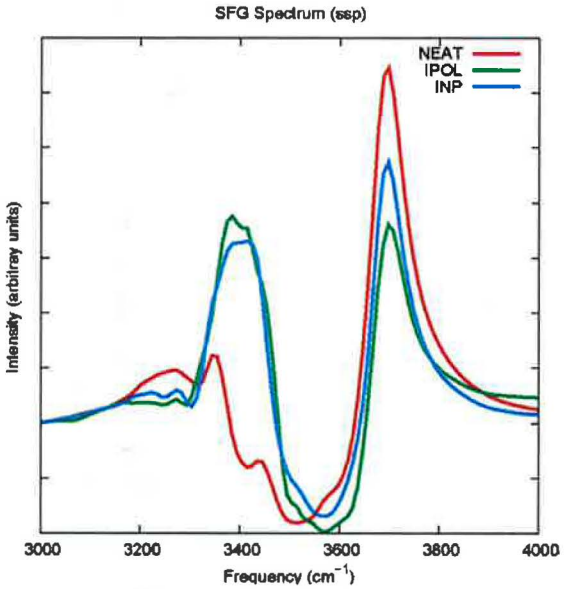

Figure 9. Theoretical vibrational sum frequency generation spectra (ssp) of IPOL, INP, and NEAT.

of the region around 3400 cm^{-1} relative to the "free O−H" stretch in the salt water systems.

It is interesting to note that the intensities of the 3400 cm^{-1} region of IPOL and INP are very similar in magnitude (Figure 9). Indeed, the comparison of the ODFs of IPOL and INP (Figure 4) reveal that the latter does not possess as much anisotropy as the former. It is possible that more sampling would lead to spectral features that have a more direct correspondence to the orientational distribution functions. However, it is reassuring that the magnitude of the 3400^{-1} region of IPOL is greater than that in INP, in accord with the ODF profiles. It is clear that additional studies that probe the quantitative sensitivity of the computed SFG signal to the presence of ions are of interest.

4. Conclusions

On the basis of the results of molecular dynamics simulations, we predict that iodide ions exist at the air/water interface with a surfactant-like excess. When polarizability is included in the force field of the ions (IPOL), this excess is much greater than the case where the ion polarizability is neglected (INP). This is in agreement with our previous simulations that employed a somewhat different (i.e., polarizable, rigid) model for the water molecules.[4]

Comparison of the time-averaged orientational distribution functions of the water dipoles with respect to the surface-normal vector in IPOL and NEAT reveals that there is a significant subsurface ordering in IPOL that does not appear in the case of NEAT. Because the excess ordering corresponds to an angle of ~0° with respect to the surface-normal vector and the depletion of ordering corresponds to an angle of ~150°, we postulate that these deviations from time-averaged isotropic orientation are due to electrostatically favorable (~0°) and electrostatically unfavorable (~150°) interactions of water with a time-averaged ionic double layer. This assumption is supported by the fact that INP, which has a less-pronounced ion double layer, also shows less subsurface water ordering than IPOL.

We have computed the theoretical SFG spectra of these systems using the approach outlined by Morita and Hynes.[21] The simulation models predict that there is a significant enhancement in the SFG intensity at 3400 cm^{-1} upon the addition of sodium iodide. This is in qualitative agreemeent with the experimental results of the groups of Richmond[16] and Allen.[15] There is no significant difference in absolute intensities in the 3400 cm^{-1} region between IPOL and INP, despite the stronger ion separation and water ordering in the interfacial layer in the former case. The increase (vs neat water) of the intensity of the 3400 cm^{-1} band relative to the 3750 cm^{-1} band is slightly larger in the IPOL system compared to the INP system. Taken together, our computed spectra and structural analysis suggest that the changes in the experimentally measured SFG spectra accompanying the addition of sodium iodide to water could be consistent with the adsorption of anions and the presence of a diffuse double layer at the solution/air interface, with a concomitant increase in ordering of the interfacial water molecules.

The correlation that we have demonstrated between the changes in the SFG spectrum of NaI versus pure water and the presence of anions at the air/solution interface is consistent with the conclusions drawn by Liu et al.,[15] which were based on the comparison of SFG data with bulk IR and Raman data of sodium halide solutions.[15] However, it is in contrast to the interpretation of the essentially identical SFG spectra of sodium halide solutions by Raymond and Richmond,[16] which relied on spectral fitting and an assignment of bands in the 3200 cm^{-1} region to tetrahedrally coordinated water and the 3400 cm^{-1} band to the donor OH (the hydrogen-bonded OH of a three-coordinated water with a free OH). The insensitivity of the fitted parameters of the donor OH band to addition of salt led Raymond and Richmond to conclude that there are few ions in the surface region, where the donor OH resides. However, this conclusion needs to be viewed with some skepticism, because the spectral assignment is questionable in light of a computational analysis of the IR spectrum of ice nanoparticles,[48] which demonstrated that the lowest frequency feature (i.e., the 3200 cm^{-1} band in the SFG spectrum) is due to the donor OH, and the intermediate frequency features (the bands around 3400 cm^{-1} in the SFG spectrum) are due to the tetrahedrally coordinated water molecules. Clearly, more work will be required before the

features in the hydrogen-bonded OH region of the SFG spectra can be unambiguously assigned. In ongoing work, we are seeking to improve the agreement between computed and experimentally measured SFG spectra to the point where an assignment of the SFG spectral features based on MD trajectories could be made with confidence.

SFG spectroscopy, which directly probes the water oscillators, is an indirect probe of the presence and structure of the ions in the interfacial layer. Moreover, quantitative characterization of the water subsurface ordering (presumably caused by interaction with the interfacial ion double layer) via SFG spectroscopy might be difficult due to the fact that all phase information is lost. However, subsurface ordering is predicted to be visible in the resonant susceptibility, which does exhibit strong sensitivity to the orientation of the water molecules as manifested in the phase of this complex quantity. Shen and co-workers have recently reported experimental resonant susceptibilities for aqueous systems, although these studies involved a solid surface.[49] Alternatively, SFG spectra that employ different polarizations (e.g., ppp) might reveal the existence of subsurface water ordering. It would be interesting to see the results of further experiments that probe salt solution/air interfaces.

Acknowledgment. We are grateful to Professor A. Morita, Professor J. T. Hynes, Professor B. Space, Professor B. J. Finlayson-Pitts, Professor V. Buch, Dr. J. S. Vieceli, and Dr. J. A. Freites for fruitful discussions. The applicability of the iterative solver used in this work was demonstrated by Miss O. Mandelshtam and Professor V. Mandelshtam. Professor H. C. Allen and Professor G. S. Richmond are acknowledged for providing us with their experimental SFG spectra prior to publication. All calculations were performed on the Medium Performance Cluster at the University of California. We thank the National Science Foundation (Grant No. CHE 0431512) and the Czech Ministry of Education (Grant Nos. ME644 and LC512) for financial support. Part of the work in Prague was completed within the framework of research project Z40550506.

References and Notes

(1) Finlayson-Pitts, B. J.; Pitts, J. N. *Chemistry of the Upper and Lower Atmosphere*; Academic Press: San Diego, 2000.

(2) Knipping, E. M.; Lakin, M. J.; Foster, K. L.; Jungwirth, P.; Tobias, D. J.; Gerber, R. B.; Dabdub, D.; Finlayson-Pitts, B. J. *Science* **2000**, *288*, 301.

(3) Jungwirth, P.; Tobias, D. J. *J. Phys. Chem. B* **2002**, *106*, 6361.

(4) Jungwirth, P.; Tobias, D. J. *J. Phys. Chem. B* **2001**, *105*, 10468.

(5) Dang, L. X. *J. Phys. Chem. B* **2002**, *106*, 10388.

(6) Dang, L. X.; Chang, T. M. *J. Phys. Chem. B* **2002**, *106*, 235.

(7) Laskin, A.; Gaspar, D. J.; Wang, W.; Hunt, S. W.; Cowin, J. P.; Colson, S. D.; Finlayson-Pitts, B. J. *Science* **2003**, *301*, 340.

(8) Defay, R.; Prigogine, I.; Bellemans, A. *Surface Tension and Adsorption*; Longmans Green: London, 1966.

(9) Washburn, E. W. *International Critical Tables*; McGraw-Hill: New York, 1928; Vol. IV.

(10) Vrbka, L.; Mucha, M.; Minofar, B.; Jungwirth, P.; Brown, E. C.; Tobias, D. J. *Curr. Opin. Colloid Interface Sci.* **2004**, *9*, 67.

(11) Mukamel, S. *Principles of Nonlinear Optical Spectroscopy*; Oxford University Press: Oxford, 1995.

(12) Shen, Y. R. In *Proceedings of the International School of Physics "Enrico Fermi"*; Hansch, T.; Ingusio, M., Eds.; North-Holland: Amsterdam, 1994; Vol. 120.

(13) Eisenthal, K. B. *Chem. Rev.* **1996**, *96*, 1343.

(14) Richmond, G. L. *Chem. Rev.* **2002**, *102*, 2693.

(15) Liu, D.; Ma, G.; Levering, L. M.; Allen, H. C. *J. Phys. Chem. B* **2004**, *108*, 2252.

(16) Raymond, E. A.; Richmond, G. L. *J. Phys. Chem. B* **2004**, *108*, 5051.

(17) Pouthier, V.; Hoang, P. N. M.; Girardet, C. *J. Chem. Phys.* **1999**, *110*, 6963.

(18) Morita, A.; Hynes, J. T. *Chem. Phys.* **2000**, *258*, 371.

(19) Brown, M. G.; Walker, D. S.; Raymond, E. A.; Richmond, G. *J. Phys. Chem. B* **2003**, *107*, 237.

(20) Perry, A.; Ahlborn, H.; Space, B.; Moore, P. *J. Chem. Phys.* **2003**, *118*, 8411.

(21) Morita, A.; Hynes, J. T. *J. Phys. Chem. B* **2002**, *106*, 673.

(22) Ferguson, D. M. *J. Comput. Chem.* **1995**, *15*, 501.

(23) Markovich, G.; Perera, L.; Berkowitz, M. L.; Cheshnovsky, O. J. *J. Chem. Phys.* **1996**, *105*, 2675.

(24) Case, D. A. et al. *AMBER*, version 7; University of California: San Francisco, 2002.

(25) Essmann, U.; Perera, L.; Berkowitz, M. L.; Darden, T.; Petersen, L. G. *J. Chem. Phys.* **1995**, *103*, 8577.

(26) Jungwirth, P.; Tobias, D. J. *J. Phys. Chem. B* **2000**, *104*, 7702.

(27) Thole, B. T. *Chem. Phys.* **1981**, *59*, 341.

(28) van Duijnen, P. T.; Swart, M. *J. Phys. Chem. A* **1998**, *102*, 2399.

(29) Applequist, J.; Carl, J. R.; Fung, K.-K. *J. Am. Chem. Soc.* **1972**, *94*, 2952.

(30) Silberberg, L. *Philos. Mag.* **1917**, *33*, 521.

(31) van der Vorst, H. A.; Vuik, C. *Numer. Linear Algebra Appl.* **1994**, *1*, 369.

(32) Becke, A. D. *J. Chem. Phys.* **1993**, *98*, 5648.

(33) Lee, C.; Yang, W.; Parr, R. G. *Phys. Rev. B* **1988**, *37*, 785.

(34) Kendall, R.; T.H. Dunning, J.; Harrison, R. *J. Chem. Phys.* **1992**, *96*, 6796.

(35) Dunning, T. H. *J. Chem. Phys.* **1994**, *100*, 2975.

(36) Basis sets were obtained from the Extensible Computational Chemistry Environment Basis Set Database, version 02/25/04, as developed and distributed by the Molecular Science Computing Facility, Environmental and Molecular Sciences Laboratory, which is part of the Pacific Northwest Laboratory, P.O. Box 999, Richland, Washington 99352, and funded by the U. S. Department of Energy. The Pacific Northwest Laboratory is a multiprogram laboratory operated by Battelle Memorial Institute for the U. S. Department of Energy under contract DE-AC06-76RLO 1830. Contact David Feller or Karen Schuchardt for further information.

(37) Frisch, M. J.; Trucks, G. W.; Schlegel, H. B.; Scuseria, G. E.; Robb, M. A.; Cheeseman, J. R.; Montgomery, J. A., Jr.; Vreven, T.; Kudin, K. N.; Burant, J. C.; Millam, J. M.; Iyengar, S. S.; Tomasi, J.; Barone, V.; Mennucci, B.; Cossi, M.; Scalmani, G.; Rega, N.; Petersson, G. A.; Nakatsuji, H.; Hada, M.; Ehara, M.; Toyota, K.; Fukuda, R.; Hasegawa, J.; Ishida, M.; Nakajima, T.; Honda, Y.; Kitao, O.; Nakai, H.; Klene, M.; Li, X.; Knox, J. E.; Hratchian, H. P.; Cross, J. B.; Adamo, C.; Jaramillo, J.; Gomperts, R.; Stratmann, R. E.; Yazyev, O.; Austin, A. J.; Cammi, R.; Pomelli, C.; Ochterski, J. W.; Ayala, P. Y.; Morokuma, K.; Voth, G. A.; Salvador, P.; Dannenberg, J. J.; Zakrzewski, V. G.; Dapprich, S.; Daniels, A. D.; Strain, M. C.; Farkas, O.; Malick, D. K.; Rabuck, A. D.; Raghavachari, K.; Foresman, J. B.; Ortiz, J. V.; Cui, Q.; Baboul, A. G.; Clifford, S.; Cioslowski, J.; Stefanov, B. B.; Liu, G.; Liashenko, A.; Piskorz, P.; Komaromi, I.; Martin, R. L.; Fox, D. J.; Keith, T.; Al-Laham, M. A.; Peng, C. Y.; Nanayakkara, A.; Challacombe, M.; Gill, P. M. W.; Johnson, B.; Chen, W.; Wong, M. W.; Gonzalez, C.; Pople, J. A. *Gaussian 03*, revision A.1; Gaussian, Inc.: Pittsburgh, PA, 2003.

(38) Denbigh, K. G. *Trans. Faraday Soc.* **1940**, *36*, 936.

(39) LeFevre, C. G.; LeFevre, R. J. W. *Rev. Pure Appl. Chem.* **1955**, *5*, 261.

(40) Miller, K. J. *J. Am. Chem. Soc.* **1990**, *112*, 8543.

(41) Clough, S. A.; Beers, Y.; Klein, G. P.; Rothman, L. S. *J. Chem. Phys.* **1973**, *59*, 2254.

(42) Silvestrelli, P. L.; Parrinello, M. *Phys. Rev. Lett.* **1999**, *82*, 3308.

(43) Press, W. H.; Teukolsky, S. A.; Flannery, B. P.; Vetterling, W. T. *Numerical Recipes in Fortran: The Art of Scientific Computing*; Cambridge University Press: New York, 1992.

(44) Gordon, R. G. *Adv. Magn. Reson.* **1968**, *3*, 1.

(45) Benjamin, I. *Phys. Rev. Lett.* **1994**, *73*, 2083.

(46) Benjamin, I. *Chem. Rev.* **1996**, *96*, 1449.

(47) Wei, X.; Shen, Y. R. *Phys. Rev. Lett.* **2001**, *86*, 4799.

(48) Devlin, J. P.; Joyce, C.; Buch, V. *J. Phys. Chem. A* **2000**, *104*, 1974.

(49) Shen, Y. R. Sum-frequency vibrational spectroscopy of water/quartz interfaces: Crystalline vs. fused quartz. In *Abstracts of Papers*, 227th National Meeting of the American Chemical Society, Anaheim, CA, March 28−April 1, 2004; American Chemical Society: Washington, DC, 2004.

J|A|C|S
ARTICLES
Published on Web 01/03/2004

Solvent-Mediated Folding of a Doubly Charged Anion

Xin Yang,[†,‡] You-Jun Fu,[†,‡] Xue-Bin Wang,[†,‡] Petr Slavíček,[§] Martin Mucha,[§,∥] Pavel Jungwirth,[*,§,∥] and Lai-Sheng Wang[*,†,‡]

Contribution from the Department of Physics, Washington State University, 2710 University Drive, Richland, Washington 99352, W. R. Wiley Environmental Molecular Sciences Laboratory, Pacific Northwest National Laboratory, P.O. Box 999, Richland, Washington 99352, and J. Heyrovsky Institute of Physical Chemistry, Academy of Sciences of the Czech Republic and Center for Complex Molecular Systems and Biomolecules, Dolejskova 3, 18223 Prague 8, Czech Republic

Received August 25, 2003; E-mail: pavel.jungwirth@jh-inst.cas.cz; ls.wang@pnl.gov

Abstract: The microsolvation of the suberate dianion, $^{-}O_2C(CH_2)_6CO_2^{-}$, with two separate charge centers was studied by photoelectron spectroscopy and molecular dynamics simulation one solvent molecule at a time for up to 20 waters. It is shown that the two negative charges are solvated in the linear suberate alternately. As the solvent number increases, the negative charges are screened and a conformation change occurs at 16 waters, where the cooperative hydrogen bonding of water is large enough to overcome the Coulomb repulsion and pull the two negative charges closer through a water bridge. This conformation change, revealed both from the experiment and from the simulation, is a manifestation of the hydrophilic and hydrophobic forces at the molecular level.

Introduction

Understanding the behavior of ions, especially multiply charged species, in aqueous solution is essential to obtain insight into many processes in chemistry and biochemistry. Many textbook multiple-charged anions (MCAs), such as SO_4^{2-}, owe their existence to their hydration shell and would spontaneously emit an electron in free space.[1,2] For biological macromolecules, solvation of their charged groups plays an important role in determining their structures and functions.[3-5] Studying the microhydration of complex multiply charged anions in the gas phase provides a unique vantage point to understand at the molecular level the solvation effect on the structure of the solute molecules.

Photoelectron spectroscopy (PES) is a sensitive probe for the solvation environment of MCAs and their intramolecular electrostatic interactions. We have developed an experimental technique to study gaseous MCAs using electrospray ionization (ESI) and PES.[6] The ESI technique is a powerful soft ionization method to produce MCAs, or any ionic species and solvated clusters, from solution to the gas phase.[7-10] Using these techniques, we have investigated the hydration of two common inorganic dianions, SO_4^{2-} and $C_2O_4^{2-}$, with up to 40 water molecules[11-14] and a series of dicarboxylate dianions, $^{-}O_2C-(CH_2)_x-CO_2^{-}$ ($x = 2-10$), with one and two water molecules.[15]

Carboxylate is an important negative charge carrier in proteins, present in the C-terminal of polypeptides and the side chains of aspartic and glutamic acids. Linear dicarboxylate dianions $^{-}O_2C-(CH_2)_n-CO_2^{-}$ have two distinct charged groups ($-CO_2^{-}$) linked by a flexible aliphatic chain and can be viewed as a simple model for peptide chains. Here, we report the first observation of solvent-mediated folding of suberate dianion $^{-}O_2C-(CH_2)_6-CO_2^{-}$. We studied the microsolvation of the suberate dianion using PES and molecular dynamics simulations. We observed that water molecules solvate the two negative charges in the linear suberate alternately at the two ends, but not the middle hydrophobic aliphatic chain. As the solvent number increases, the negative charges are screened and a folding occurs at about 16 waters, where the cooperative hydrogen bonding of water is large enough to overcome the Coulomb repulsion and pull the two negative charges closer through a water bridge. The current work provides a simple

[†] Washington State University.
[‡] Pacific Northwest National Laboratory.
[§] Academy of Sciences of the Czech Republic and Center for Complex Molecular Systems and Biomolecules.
[∥] Present address: Institute of Organic Chemistry and Biochemistry, Academy of Sciences of the Czech Republic and Center for Complex Molecular Systems and Biomolecules, Flemingovo nam. 2, 16610 Prague 6, Czech Republic.

(1) Boldyrev, A. I.; Simons, J. *J. Phys. Chem.* **1994**, *98*, 2298.
(2) Wang, X. B.; Nicholas, J. B.; Wang, L. S. *J. Chem. Phys.* **2000**, *113*, 10837.
(3) Ohtaki, H.; Radnai, T. *Chem. Rev.* **1993**, *93*, 1157.
(4) Israelachvili, J.; Wennerstrom, H. *Nature* **1996**, *379*, 219.
(5) Otting, G.; Liepinsh, E.; Wüthrich, K. *Science* **1991**, *254*, 974.
(6) Wang, L. S.; Ding, C. F.; Wang, X. B.; Barlow, S. E. *Rev. Sci. Instrum.* **1999**, *70*, 1957.
(7) Blades, A. T.; Kebarle, P. *J. Am. Chem. Soc.* **1994**, *116*, 10761.
(8) Baldes, A. T.; Klassen, J. S.; Kebarle, P. *J. Am. Chem. Soc.* **1995**, *117*, 10563.
(9) Blades, A. T.; Ho, Y.; Kebarle, P. *J. Phys. Chem.* **1996**, *100*, 2443.
(10) Lau, T. C.; Wang, J.; Guevremont, R.; Siu, K. W. M. *J. Chem. Soc., Chem. Commun.* **1995**, 877.
(11) Wang, X. B.; Nicholas, J. B.; Wang, L. S. *J. Chem. Phys.* **2000**, *113*, 10837.
(12) Wang, X. B.; Yang, X.; Nicholas, J. B.; Wang, L. S. *Science* **2001**, *294*, 1322.
(13) Yang, X.; Wang, X. B.; Wang, L. S. *J. Phys. Chem. A* **2002**, *106*, 7607.
(14) Wang, X. B.; Yang, X.; Nicholas, J. B.; Wang, L. S. *J. Chem. Phys.* **2003**, *119*, 3631.
(15) Ding, C. F.; Wang, X. B.; Wang, L. S. *J. Phys. Chem. A* **1998**, *102*, 8633.

10.1021/ja038108c CCC: $27.50

and clean model system to study the hydrophilic and hydrophobic effects,[16,17] as well as solvent-mediated formation of like-ion pairs in solution,[18−20] and is likely to be important for understanding the hydration and conformation changes of biological molecules.[21−23]

Experimental Methods

The experiment was carried out using an experimental apparatus equipped with a magnetic-bottle time-of-flight photoelectron analyzer and an ESI source. Details of the experimental method have been given elsewhere.[6] Briefly, solvated suberate dianions with a wide range of solvent number, $^{-}O_2C(CH_2)_6CO_2^{-}(H_2O)_n$, were produced from electrospray of a mixed solution of 10^{-3} M suberic acid and 2×10^{-3} M NaOH in water−acetonitrile (1:4 volume ratio). Anions produced from the ESI source were guided into a room-temperature ion-trap, where ions were accumulated for 0.1 s before being pulsed into the extraction zone of a time-of-flight mass spectrometer.

During the PES experiment, the bare and solvated suberate dianions were mass-selected and decelerated before being intercepted by a probe laser beam in the photodetachment zone of the magnetic-bottle photoelectron analyzer. In the current study, the detachment photon energy used was 193 nm (6.424 eV). Experiments were performed at 20 Hz repetition rate with the ion beam off at alternating laser shots for background subtraction, which was critical for high photon energy experiments due to background noises. Photoelectrons were collected at nearly 100% efficiency by the magnetic-bottle and analyzed in a 4-m long electron flight tube. Photoelectron time-of-flight spectra were collected and then converted to kinetic energy spectra, calibrated by the known spectra of I^- and O^-. The electron binding energy spectra presented here were obtained by subtracting the kinetic energy spectra from the detachment photon energies. The energy resolution ($\Delta E/E$) was about 2%, that is, ~10 meV for 0.5 eV electrons, as measured from the spectrum of I^- at 355 nm.

Theoretical Methods

The calculations involved a combination of classical molecular dynamics simulations aimed at a Boltzmann sampling of geometries of the $^{-}O_2C(CH_2)_6CO_2^{-}(H_2O)_n$ clusters and ab initio quantum chemistry for evaluation of detachment energies. Very long (microsecond) simulations were performed at constant temperatures (ranging from 150 to 230 K) with a time step of 1 fs. This temperature range encompasses the estimated experimental temperatures. Also, from the technical point of view, reduced temperatures help to avoid problems connected with evaporation of water molecules from the clusters. Note that at these temperatures the cluster is not solid but liquidlike and rather flexible, which is due to both the presence of the suberate dianion and the small size of the system. We employed the SPCE model of water,[24] while for the suberate dianion, we used the Cornell force field[25] with fractional charges evaluated at the HF/6-31G* level. These Mulliken charges have been evaluated for the MP2/6-31$_{+O}$G* (the subscript +O denotes diffuse functions on oxygen atoms) fully optimized geometry of the dianion. All molecular dynamics calculations were performed using the GROMACS 3.1 program package.[26]

Ab initio calculations were employed to evaluate the vertical detachment energies (VDE) of $^{-}O_2C(CH_2)_6CO_2^{-}(H_2O)_n$ (n = 0, 1, 2, and 21). For complexes with up to two water molecules, we performed a full geometry optimization, while for the large cluster we did ab initio calculations for a set of 52 snapshots taken from the MD simulation. While for geometry parameters the performance of the Hartree−Fock method was satisfactory (i.e., optimized HF and MP2 geometries of the smallest complexes were very close to each other), correlation effects had to be included for reliable calculations of the VDEs. From the basis set point of view, a modest 6-31$_{+O}$G* provided already almost converged results, which was checked against calculations at the MP2 level with the 6-311$_{+}$G* basis set. For the bare suberate dianion and small clusters, we calculated their VDEs using CCSD(T)/6-31$_{+O}$G* and MP2 levels of theory. For larger clusters, explicit inclusion of water molecules into the ab initio calculation became computationally unfeasible. We, therefore, replaced the water molecules by fractional charges of −0.82 e (oxygen) and +0.41 e (hydrogen). This replacement almost did not change the value of VDEs; for example, the increase of VDE of suberate by two water molecules changed from 0.83 to 0.89 eV by this procedure. All ab initio calculations were performed using the Gaussian 98 program.[27]

Experimental Results

Mass Spectra. Typical mass spectra of $^{-}O_2C(CH_2)_6CO_2^{-}(H_2O)_n$ from our ESI source are shown in Figure 1. Because of the perpendicular extraction configuration of ions in our time-of-flight mass spectrometer, we can only optimize ion signals for a limited mass range. Figure 1 shows three separately optimized mass spectra, covering the full mass range of interest for the present study. Solvated suberate dianion clusters with up to 30 water molecules were readily produced. In general, the mass intensities of $^{-}O_2C(CH_2)_6CO_2^{-}(H_2O)_n$ decreased monotonically as n increased. Strong mass signals of two singly charged ion pairs, $NaO_2C(CH_2)_6CO_2^{-}$ and $HO_2C(CH_2)_6CO_2^{-}$, were observed, as labeled in the second panel of Figure 1. Most of the unlabeled mass peaks were due to the mixed solvent species, $^{-}O_2C(CH_2)_6CO_2^{-}(H_2O)_x(CH_3CN)_y$.

Photoelectron Spectra. Figure 2 displays the photoelectron spectra of $^{-}O_2C(CH_2)_6CO_2^{-}(H_2O)_n$ for n = 0−20. The two intense overlapping bands in the spectrum of the bare dianion were due to electron detachment from the $-CO_2^-$ groups.[28] The small bump centered at ~4.6 eV for n = 0 and a similar weak feature at higher binding energies for n = 1 were due to detachment of the singly charged product anions by a second photon. Several observations can be made about the spectra of the small solvated species (n = 1−9). First, the electron binding energies increase as a function of solvent number due to stabilization of the negative charges by water. Second, the spectral features showed an odd−even effect: those with even solvent numbers were similar to those of the bare dianion, while those with odd solvent numbers exhibit an extra band. Third, for $n \geq 2$, a new band emerged at the high binding energy side. Its relative intensity reached the maximum at n = 4, then decreased gradually and disappeared for $n > 8$. Similar spectral features were observed in our previous PES studies of $SO_4^{2-}(H_2O)_n$, $C_2O_4^{2-}(H_2O)_n$, and $F^-(H_2O)_n$ systems, and they were found to be due to ionization of the solvent.[12−14,29] The ionization potential of water was significantly

(16) Ben-Naim, A. *Hydrophobic Interactions*; Plenum Press: New York, 1980.
(17) Cheng, Y. K.; Rossky, P. J. *Nature* **1998**, *392*, 696.
(18) Pettitt, B. M.; Rossky, P. J. *J. Chem. Phys.* **1986**, *84*, 5836.
(19) Jungwirth, P.; Zahradnik, R. *J. Phys. Chem.* **1994**, *98*, 1328.
(20) Wallqvist, A.; Covell, D. G. *J. Phys. Chem.* **1995**, *99*, 5705.
(21) Makarov, V.; Pettitt, B. M.; Feig, M. *Acc. Chem. Res.* **2002**, *35*, 376.
(22) Gross, D. S.; Schnier, P. D.; Rodriguez-Cruz, S. E.; Fagerquist, C. K.; Williams, E. R. *Proc. Natl. Acad. Sci. U.S.A.* **1996**, *93*, 3143.
(23) Jarrold, M. F. *Acc. Chem. Res.* **1999**, *32*, 360.
(24) Berendsen, H. J. C.; Grigera, J. R.; Straatsma, T. P. *J. Phys. Chem.* **1987**, *91*, 6269.
(25) Cornell, W. D.; Cieplak, P.; Bayly, C. I.; Gould, I. R.; Merz, K. M., Jr.; Ferguson, D. M.; Spellmeyer, D. C.; Fox, T.; Caldwell, J. W.; Kollman, P. A. *J. Am. Chem. Soc.* **1995**, *117*, 5179.
(26) Lindahl, E.; Hess, B.; van der Spoel, D. *J. Mol. Model.* **2001**, *7*, 306.
(27) Frisch, M. J.; Trucks, G. W.; Schlegel, H. B.; Scuseria, G. E.; Robb, M. A.; Cheeseman, J. R.; Zakrzewski, V. G.; Montgomery, J. A., Jr.; Stratmann, R. E.; Burant, J. C.; Dapprich, S.; Millam, J. M.; Daniels, A. D.; Kudin, K. N.; Strain, M. C.; Farkas, O.; Tomasi, J.; Barone, V.; Cossi, M.; Cammi, R.; Mennucci, B.; Pomelli, C.; Adamo, C.; Clifford, S.; Ochterski, J.; Petersson, G. A.; Ayala, P. Y.; Cui, Q.; Morokuma, K.; Malick, D. K.; Rabuck, A. D.; Raghavachari, K.; Foresman, J. B.; Cioslowski, J.; Ortiz, J. V.; Stefanov, B. B.; Liu, G.; Liashenko, A.; Piskorz, P.; Komaromi, I.; Gomperts, R.; Martin, R. L.; Fox, D. J.; Keith, T.; Al-Laham, M. A.; Peng, C. Y.; Nanayakkara, A.; Gonzalez, C.; Challacombe, M.; Gill, P. M. W.; Johnson, B. G.; Chen, W.; Wong, M. W.; Andres, J. L.; Head-Gordon, M.; Replogle, E. S.; Pople, J. A. *Gaussian 98*; Gaussian, Inc.: Pittsburgh, PA, 1998.
(28) Wang, L. S.; Ding, C. F.; Wang, X. B.; Nicholas, J. B. *Phys. Rev. Lett.* **1998**, *81*, 2667.

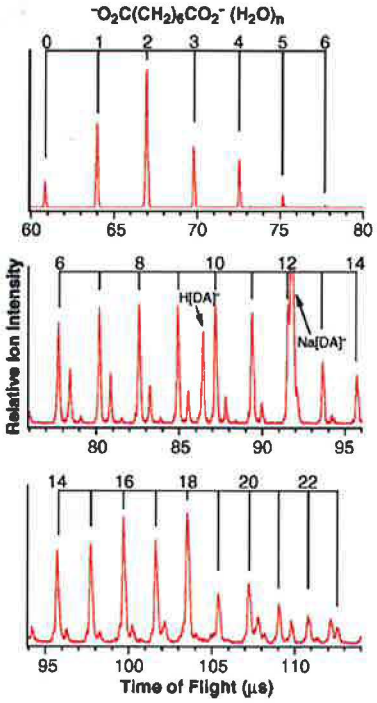

Figure 1. Typical mass spectra of $^-O_2C(CH_2)_6CO_2^-(H_2O)_n$ from electrospray ionization of a suberate solution, that were optimized for three mass ranges. $H[DA]^-$ and $Na[DA]^-$ indicated the singly charged protonated and sodiated suberate ion pairs, respectively.

lowered in the presence of the negative ions due to the strong Coulomb repulsion. Fourth, spectral features on the high binding energy side were cut off as a result of the repulsive Coulomb barrier (RCB), which exists universally in multiply charged anions and essentially prohibits slow electrons from being emitted.[28] The cutoff point in each spectrum provides a rough estimate of the barrier height (photon energy minus the cutoff energy), which has been shown to be approximately equal to the magnitude of the intramolecular Coulomb repulsion.[28]

For the large solvated clusters ($n = 10-20$), the even−odd effect of the spectral features became smeared out. With increasing solvent number, the spectral features moved steadily to high binding energies until $n = 16$, where the spectrum suddenly shifted to lower binding energies. For $n > 16$, the spectral features moved again to high binding energies. In addition to the sudden change of the binding energies, we also observed a backward shift of the spectral cutoff at the high binding energy side. This spectral cutoff at the high binding energy side is characteristic of PES of MCAs and is a direct consequence of the RCB, which prohibits low kinetic energy electrons to be emitted. The cutoff, which increased slowly with the solvent number for $n < 16$ (Figure 1, right column), is clearly shifted to lower binding energies in the spectra of $n > 16$ relative to those of $n < 16$, giving rise to the appearance of a sharper peak for these large clusters.

Adiabatic and Vertical Detachment Energies. The adiabatic detachment energy (ADE) and VDE determined from the spectrum of each cluster are listed in Table 1. Because of the lack of vibrational resolution, the ADEs were measured by drawing a straight line along the leading edge of the threshold band and then adding a constant to the intersection with the binding energy axis to take into account the instrumental resolution at the given energy range. Despite the approximate nature of this procedure, a consistent set of ADEs with reasonable uncertainties could be obtained. The VDE was measured from the maximum of the first band. However, due to the overlap between the first band and the higher binding energy band in the large solvated clusters, the VDEs could not be determined precisely, as reflected by the large uncertainties given for the reported VDEs in Table 1.

The measured ADEs are also plotted in Figure 3A (the blue curve) as a function of solvent number. The odd−even effect and the sudden drop of ADE at $n = 16$ are revealed readily. These effects can be seen more dramatically in Figure 3B, which showed the differential ADE [ΔADE = ADE(n) − ADE($n - 1$)] as a function of solvent number. The ADE of $n = 16$ shows a decrease of ~0.3 eV relative to that of $n = 15$.

Discussion

Solvation at Linear Conformation. The suberate dianion has two equivalent $-CO_2^-$ groups. The Coulomb repulsion between the two charges keeps them as far as possible from each other in the free dianion, that is, in a quasi-linear conformation, as we showed previously.[28] For small solvated clusters, both the PES features and the electron binding energies show clearly an odd−even effect (Figures 2 and 3). This observation suggests that the solute dianion maintains its linear conformation in the small solvated clusters and the two $-CO_2^-$ groups are solvated alternately with increasing solvent number: the first water solvates one of the two $-CO_2^-$ groups on one end of the suberate dianion, while the second water solvates the other one independently. For $n = 1$, only one side of the dianion is solvated (stabilized), leaving the other $-CO_2^-$ group relatively unaffected. The asymmetric solvation lifts the degeneracy of the two $-CO_2^-$ groups and gives rise to three PES bands, which are due to the superposition of detachment from a solvated $-CO_2^-$ and a free $-CO_2^-$. It is thus understandable that only a small increase of ADE (0.19 eV) was observed for the $n = 1$ case relative to the bare suberate dianion. For $n = 2$, both $-CO_2^-$ groups are stabilized by one water, resulting in an extremely large ΔADE (0.62 eV), as shown in Figure 3B. For even solvent numbers, the two negative charges are solvated symmetrically and maintain their equivalence. Thus, their PES spectra are similar to that of the bare dianion. For odd solvent numbers, however, the two charges are solvated asymmetrically and become inequivalent, thus giving rise to the extra band in their PES spectra. The odd−even effect becomes smeared out beyond $n = 9$ because the inequivalence due to the difference of one water becomes insignificant. The odd−even effects due to the alternating solvation of the two $-CO_2^-$ groups were also observed previously in the free energies of hydration of the dicarboxylate dianions.[8]

Control Experiments. The observation of a decrease in ADE at $n = 16$ in the hydrated suberate was totally unexpected. In all previous PES studies of solvated anions,[11−14,30,31] the ADEs were always observed to increase with solvent numbers. A decrease of ADE with increasing solvent numbers has never been observed before. To confirm our observation, we performed two control experiments using two isomers of the benzene-dicarboxylate (BDC), in which the $-CO_2^-$ groups are connected by the rigid phenyl ring. The first experiment was the hydrated *o*-BDC dianions, in which the two $-CO_2^-$ groups are next to each other. The ADEs of the hydrated *o*-BDC in the same range of solvent numbers ($n = 0-20$) are also plotted in Figure 3A (the green curve). In contrast to the hydrated

(29) Yang, X.; Wang, X. B.; Wang, L. S. *J. Chem. Phys.* **2001**, *115*, 2889.
(30) Markovich, G.; Pollack, S.; Giniger, R.; Cheshnovesky, O. *J. Chem. Phys.* **1994**, *101*, 9344.
(31) Coe, J. V.; Earhart, A. D.; Cohen, M. H.; Hoffman, G. J.; Sarkas, H. W.; Bowen, K. H. *J. Chem. Phys.* **1997**, *107*, 6023.

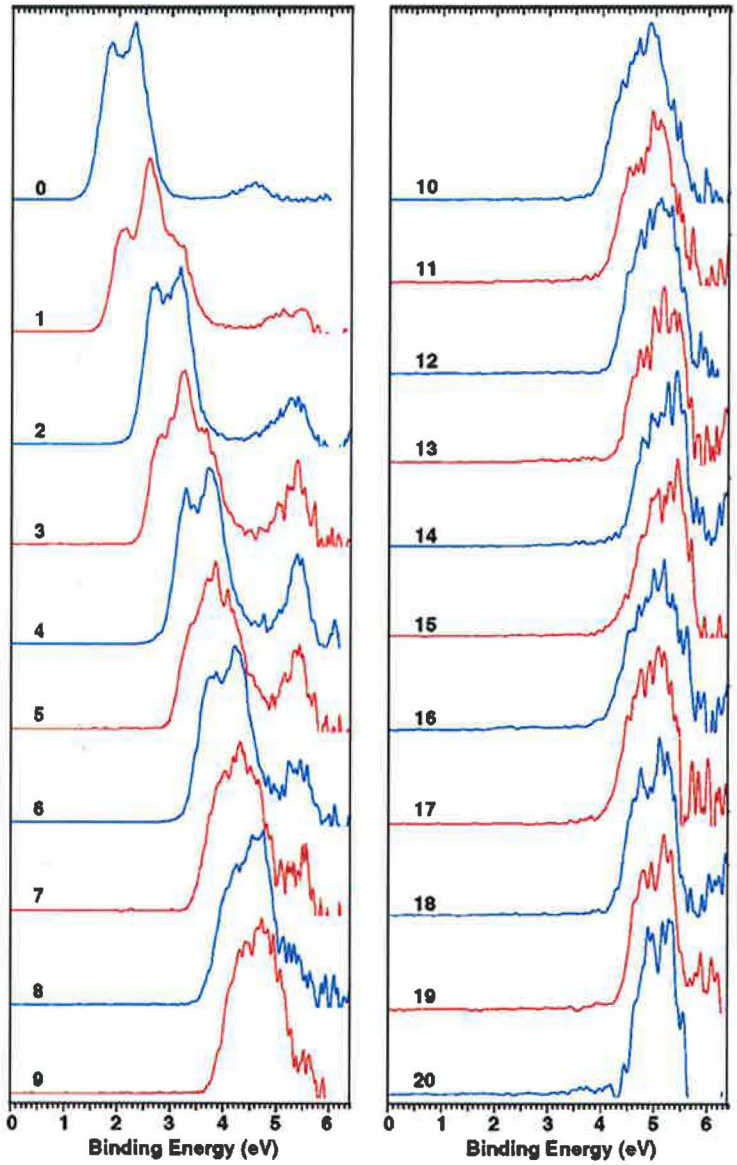

Figure 2. Photoelectron spectra of $^{-}O_2C(CH_2)_6CO_2^{-}(H_2O)_n$ (n = 0–20) at 193 nm (6.424 eV).

suberate dianions, no odd–even effect was observed (Figure 3B, the green curve) because each solvent molecule can interact with the two $-CO_2^-$ groups at the same time due to their proximity. Our second control experiment used hydrated *p*-BDC, in which the two $-CO_2^-$ groups are on the opposite site of the phenyl ring in a linear configuration. The ADEs of the hydrated *p*-BDC (Figure 3A, red curve) are higher than those of the *o*-BDC due to the reduced Coulomb repulsion. Unlike the *o*-BDC system, the hydrated *p*-BDC dianions displayed an odd–even effect (Figure 3B, red curve), because water solvates the two carboxylate groups in *p*-BDC separately and independently in a fashion similar to that in the hydrated suberate. The magnitude of the odd–even effect is much smaller for the *p*-BDC system because the aromatic phenyl ring between the two charges is much more polarizable than the aliphatic chain in suberate. However, both the *o*-BDC and the *p*-BDC systems exhibit only a monotonic increase in their ADEs as a function of solvent number, and no drop was observed at $n = 16$ (Figure 3A).

Solvent-Mediated Folding. Thus, the ADE decrease at $n = 16$ for the hydrated suberate must indicate a conformation change of the dianion caused by solvation. In contrast to the rigid phenyl ring, the aliphatic chain in the suberate is flexible. As water is added one molecule at a time, there are two major forces acting in the hydrated dianions: the Coulomb repulsion and the hydrophilic hydration. The Coulomb repulsion dominates in the bare dianion and smaller hydrated clusters, keeping the two negative charges as far as possible in the linear confirmation. The first few waters provide enormous stabilization to the negative charges, on average by ~0.4 eV per water for the first four waters in all three dicarboxylates (Figure 3B). As the negative charges are further solvated, the stabilization

Table 1. The Experimental Adiabatic (ADE) and Vertical (VDE) Detachment Energies of $^{-}O_2C(CH_2)_6CO_2^{-}(H_2O)_n$

solvent number	ADE (eV)	VDE (eV)
0	1.55 ± 0.05	1.86 ± 0.06
1	1.74 ± 0.05	2.02 ± 0.06
2	2.36 ± 0.05	2.71 ± 0.06
3	2.53 ± 0.05	2.81 ± 0.06
4	2.96 ± 0.05	3.3 ± 0.1
5	3.07 ± 0.06	3.4 ± 0.1
6	3.35 ± 0.06	3.8 ± 0.1
7	3.50 ± 0.06	3.9 ± 0.1
8	3.72 ± 0.06	4.2 ± 0.1
9	3.80 ± 0.06	4.3 ± 0.2
10	3.96 ± 0.06	4.5 ± 0.2
11	4.07 ± 0.08	4.6 ± 0.2
12	4.23 ± 0.08	4.9 ± 0.2
13	4.34 ± 0.08	5.0 ± 0.2
14	4.39 ± 0.08	5.0 ± 0.2
15	4.41 ± 0.08	5.1 ± 0.2
16	4.13 ± 0.08	4.7 ± 0.2
17	4.20 ± 0.08	4.8 ± 0.2
18	4.3 ± 0.1	5.0 ± 0.2
19	4.4 ± 0.1	5.1 ± 0.2
20	4.5 ± 0.1	5.2 ± 0.2

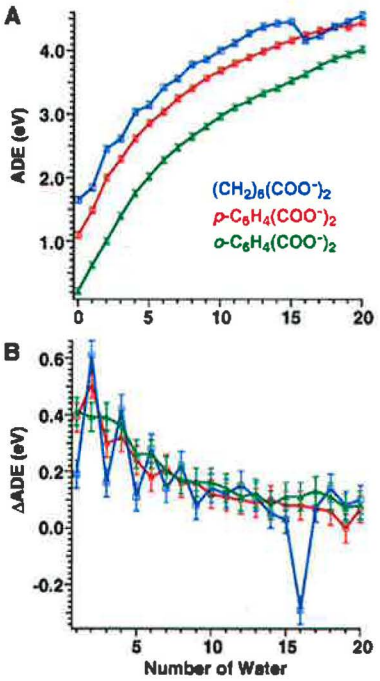

Figure 3. Comparisons of the adiabatic electron detachment energies (ADE) of $^{-}O_2C(CH_2)_6CO_2^{-}(H_2O)_n$ (n = 0−20) with those of p-$C_6H_4(CO_2^{-})_2$ (n = 0−20) and o-$C_6H_4(CO_2^{-})_2$ (n = 0−20). (A) The ADE as a function of solvent number (n). (B) Differential ADE, defined as ΔADE = ADE(n) − ADE(n − 1). Blue curve, hydrated suberate; red curve, hydrated p-benzene dicarboxylate; green curve, hydrated o-benzene dicarboxylate.

of adding an extra water steadily decreases. Beyond n = 8, the differential ADE is less than 0.2 eV and drops to about 0.1 eV per water for n > 12 (Figure 3B). This is because the negative charges become fully solvated at certain solvent number, and additional waters have no direct interactions with them.

As more water is added, the two negative charges are screened and it becomes thermodynamically less favorable to have two separate solvation centers. The merge of the two separated water droplets would result in a significant energy gain due to the cooperative hydrogen-bonding effect in the resulting larger water droplet. However, the formation of a single water droplet would require pulling the two negative charges closer and excluding the hydrophobic aliphatic chain by folding. This causes unfavorable Coulombic interaction between the two negative charges in the folded conformation. Hence the merging of the two water droplets only becomes possible when there are enough water molecules to provide a sufficiently high stabilization due to the cooperative hydrogen bonding to overcome the resulting increase in Coulomb repulsion. For suberate, our data suggest this happens at $n \approx 16$. The extra Coulomb repulsion upon folding can be estimated to be approximately the ADE drop from n = 15 to 16, that is, ~0.3 eV. Thus, the cooperative hydrogen-bonding effect resulting from the merge of the two water droplets must be higher than 0.3 eV.

The increase of Coulomb repulsion in the hydrated suberate for n > 16 can also be inferred from the spectral cutoff at the high binding energy side in the PES spectra (Figure 2).[28] This cutoff is clearly shifted to lower binding energies in the spectra of n > 16 relative to those of n < 16, indicating that the RCB in the larger solvated clusters has increased. We note that in the spectrum of n = 15, there is a small tail at the lower binding energy side, which could indicate that there might already be a small population of folded clusters. The fact that the spectral cutoff of n = 16 is similar to that of n = 15 also suggests that there might be a small amount of linear isomers in the n = 16 solvated clusters. Yet for n = 17 and higher, the folded isomers seem to dominate.

NMR experiments on the hydration of polypeptides[32] showed that the aspartate and glutamate anions (each contains one $-CO_2^{-}$ group) are commonly hydrated by 6 or 7 waters under normal solution conditions at −35 °C and pH 6−9. These numbers are strikingly similar to our current observations, implying that folding only occurs once each carboxylate is fully hydrated and screened.

Molecular Dynamics Simulations. Molecular dynamics simulations at the microsecond time scale confirm the above interpretation of the PES spectra in terms of folding of the suberate dianion upon solvation, and the consequent close approach of the two anionic centers and the merge of the two water structures around them. Our simulations revealed that the folding depends on both the cluster size and the temperature. In Figure 4A, we show the distribution of distances between the carbon atoms of the two $-CO_2^{-}$ groups of the dianion for n = 15 at 230 K. This distribution strongly peaks around 9 Å, which is a clear signature of the linear suberate dianion. There is also a very weak signal at around 5.5 Å, which corresponds to the folded geometries. A very similar picture emerges from a simulation for n = 18 at the same temperature, as depicted in Figure 4B. Upon further solvation, however, the folded geometries start to be significantly populated, as shown by the rise of a peak around 5.5 Å for n = 21 (Figure 4C). We see in Figure 4C a coexistence of folded (5.5 Å) and linear (9 Å) structures with small fractions of almost unfolded (7−8 Å) geometries. Further increasing the cluster size to 24 waters leads to a continuing population shift toward the folded geometries (Figure 4D), such that at this cluster size the folded structures clearly dominate. These simulation results are already in qualitative agreement with the PES observation.

(32) Kuntz, I. D. *J. Am. Chem. Soc.* **1971**, *93*, 514.

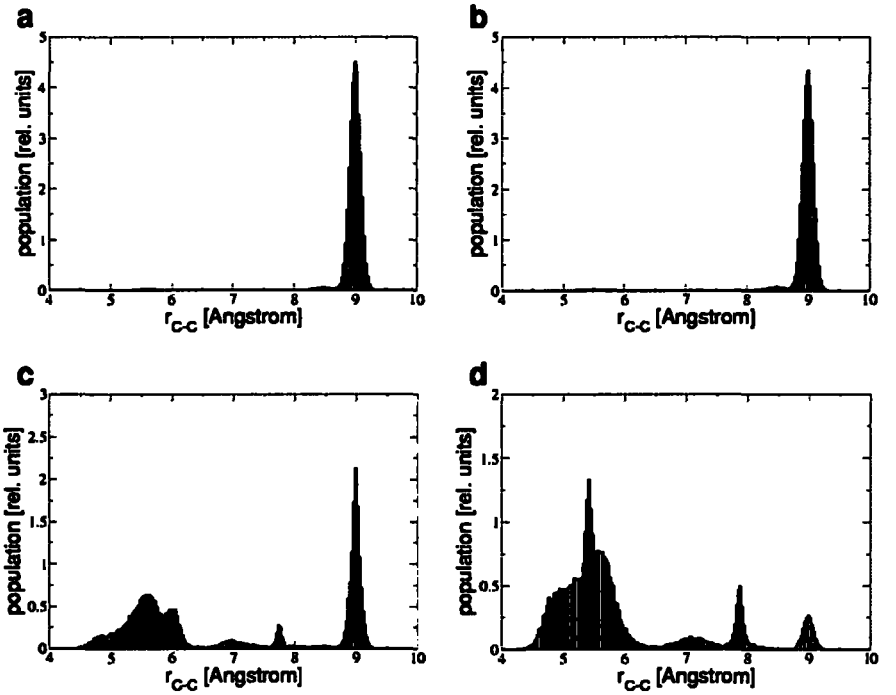

Figure 4. Distributions of distances between the carbon atoms of the two $-CO_2^-$ groups of hydrated suberate at 230 K. (A) Suberate with 15 water molecules. (B) Suberate with 18 water molecules. (C) Suberate with 21 water molecules. (D) Suberate with 24 water molecules. Note the appearance and rise of folded suberate (peak around 5.5 Å) and decrease of unfolded suberate (peak around 9 Å) upon increasing solvent number.

To assess the influence of temperature, we also performed simulations at 150 K. Unlike the run at 230 K, we were not able to obtain fully thermodynamically converged results within a microsecond simulation due to increasing nonergodicity of the system at 150 K. Nevertheless, the results indicate that the effect of decreasing temperature is nonnegligible, shifting the critical cluster size for folding to smaller values. While at 230 K folding of the suberate dianion only starts around $n = 15-18$, at 150 K clusters of these sizes have already significant fractions of folded structures. Clearly, the entropy term, which is more important at higher temperatures, shifts the balance toward the more floppy linear geometries, disfavoring the more rigid folded structures. Note that the temperatures of the clusters in the experiment were not precisely defined. However, due to evaporative cooling during the long trapping time (~0.1 s), the cluster temperatures could lie significantly below the room temperature, at which the ion trap was held. On the basis of a previous estimate of protonated water clusters under evaporative cooling,[33] the temperatures of our hydrated suberate clusters could be below 200 K. Within this uncertainty, we conclude that the simulation results not only strongly support the above interpretation of the solvent-induced folding based on the PES data, but are also in semiquantitative agreement with the experimental observations.

Figure 5 shows snapshots from the molecular dynamics simulations for several clusters. The first three snapshots display an unfolded suberate dianion for $n = 1, 2, 15$. The last snapshot (Figure 4D) shows a folded suberate dianion fro $n = 18$. Comparing Figure 5C and 5D, we see that for the linear structure a separate water cluster is formed around each of the two $-CO_2^-$ groups, while in the folded structure a single water cluster is formed, bringing to close contact the two anionic centers. In the Supporting Information, we include two short movies made from the simulation, showing how a linear solvated suberate comes to the folded configuration at two solvent numbers and two different temperatures.

Ab Initio Calculations. To further support this interpretation, we carried out additional ab initio calculations for the VDEs. At the CCSD(T)/6-31+oG* level, the VDE of the bare suberate dianion amounts to 1.63 eV, which compares favorably with the experimental value (1.86 eV, Table 1), while at the MP2 level the value is only 1.14 eV. However, the differential detachment energies between the bare anion and clusters with different numbers of water molecules are well described already at the MP2 level, presumably due to the dominant electrostatic effect. For example, two water molecules increase the MP2 VDE by 0.83 eV as compared to the bare suberate, the experimental value being 0.85 eV (Table 1). The only exception is the complex with a single water molecule, where this differential detachment energy is hard to converge due to its very low value (~0.2 eV). We evaluated the differences between VDEs for a set of 20 folded, 20 linear, and 12 almost unfolded structures for $n = 21$, taken from the simulations. Although the VDEs in each set exhibit a certain spread (~0.2 eV), the detachment energies for the set of folded geometries lie on average 0.5 eV (or 0.4 eV) below those of the linear (or almost unfolded) structures. The 0.5 eV decrease in VDE of the folded structures is due to the increased Coulomb repulsion between the two negative charges relative to the linear isomers. This theoretical result confirms the PES observation that the decrease of detachment energies at $n = 16$ signified a conformation change.

(33) Klots, C. E. *J. Chem. Phys.* **1985**, *93*, 5854.

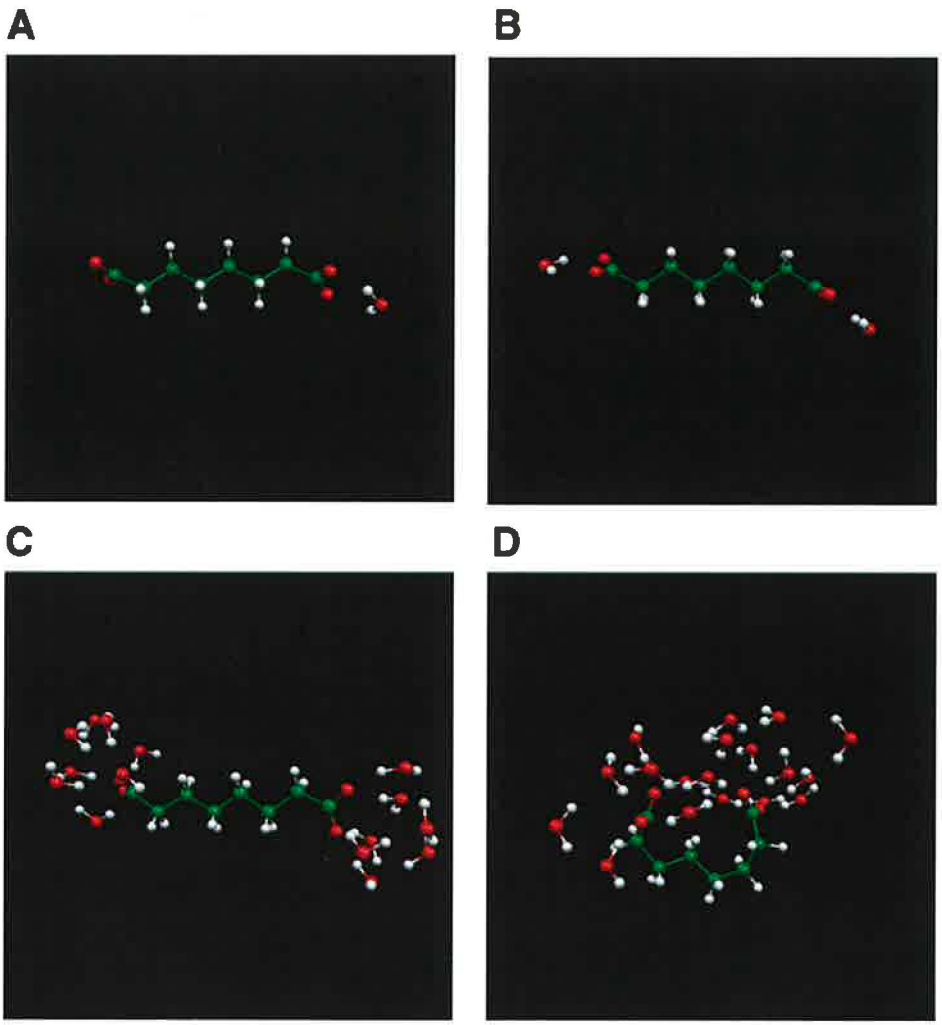

Figure 5. Snapshots from simulations of the suberate dianion in selected water clusters. (A) Suberate with one water molecule. (B) Suberate with two water molecules. (C) Suberate with 15 water molecules. (D) Suberate with 18 water molecules (folded structure).

Despite the increase of intramolecular Coulomb repulsion in the folded structure, the total energy of the system is decreased due to the enhanced solvent interaction, giving the appearance of an "attraction" between the two negative charges as they are pulled closer in the folded conformation. Thus, the solvated suberate dianions not only provide a detailed molecular picture of hydrophilic and hydrophobic salvation, but also demonstrate how these forces operate synergically to dictate the molecular configuration and give rise to an overall effective attractive interaction between the two negative charges.

Conclusions

Using photoelectron spectroscopy and molecular dynamics simulation, we studied the microsolvation of the suberate dianion, $^{-}O_2C(CH_2)_6CO_2^{-}$, one solvent molecule at a time for up to 20 waters. Both the PES spectral feature and the ADE show an odd−even effect, revealing that the suberate dianion keeps its linear conformation in the small solvated clusters, and water molecules solvate the two negative charges alternately and independently at the two ends. As the solvent number increased, we observed surprisingly that the ADE for suberate solvated with 16 water molecules decreased relative to that for the 15-water solvated suberate, indicating a solvent-mediated conformation change. For the large solvated clusters, the negative charges are screened and a folding occurs at 16 waters, where the cooperative hydrogen bonding of water is large enough to overcome the Coulomb repulsion and pull the two negative charges closer through a water bridge. Molecular dynamics simulations and ab initio calculations strongly supported the experimental observations and further revealed the temperature effect on the critical size for folding. We found that at higher temperatures the critical size for folding shifts to larger solvent numbers due to the entropic effect, which is more important at higher temperatures. The current experimental and theoretical methods provide a new tool to probe solvent-mediated conformation changes and the electrostatic environments in multiply charged macromolecules, and hydrophobic and hydrophilic interactions at a molecular level.[21−23,34,35]

Acknowledgment. This work was supported by the U.S. Department of Energy (DOE), Office of Basic Energy Sciences,

(34) Pratt, L. R.; Phohorille, A. *Chem. Rev.* **2002**, *102*, 2671.
(35) Sorenson, J. M.; Hura, G.; Soper, A. K.; Pertsemlidis, A.; Head-Gordon, T. *J. Phys. Chem. B* **1999**, *103*, 5413.

Chemical Science Division, and was performed at EMSL, a national scientific user facility sponsored by DOE's Office of Biological and Environmental Research and located at Pacific Northwest National Laboratory, operated for DOE by Battelle. Support (to P.J.) from the Czech Ministry of Education (Grant LN00A032) and the National Science Foundation (Grant CHE-0209719) is gratefully acknowledged.

Supporting Information Available: Two short movies showing the folding of a linear suberate dianion with 18 water molecules at 150 K and 24 water molecules at 230 K (MPG). This material is available free of charge via the Internet at http://pubs.acs.org.

JA038108C

J|A|C|S
ARTICLES
Published on Web 08/25/2004

Bulk versus Interfacial Aqueous Solvation of Dicarboxylate Dianions

Babak Minofar,† Martin Mucha,† Pavel Jungwirth,*,† Xin Yang,‡ You-Jun Fu,‡ Xue-Bin Wang,‡ and Lai-Sheng Wang*,‡

Contribution from the Institute of Organic Chemistry and Biochemistry, Academy of Sciences of the Czech Republic and Center for Complex Molecular Systems and Biomolecules, Flemingovo nam. 2, 16610 Prague 6, Czech Republic, Department of Physics, Washington State University, 2710 University Drive, Richland, Washington 99352, and W. R. Wiley Environmental Molecular Sciences Laboratory, Pacific Northwest National Laboratory, P.O. Box 999, Richland, Washington 99352

Received April 29, 2004; E-mail: pavel.jungwirth@uochb.cas.cz; ls.wang@pnl.gov

Abstract: Solvation of dicarboxylate dianions of varying length of the aliphatic chain in water clusters and in extended aqueous slabs was investigated using photoelectron spectroscopy and molecular dynamics simulations. Photoelectron spectra of hydrated succinate, adipate, and tetradecandioic dianions with up to 20 water molecules were obtained. Even−odd effects were observed as a result of the alternate solvation mode of the two negative charges with increasing solvent numbers. The competition between hydrophilic interactions of the charged carboxylate groups and hydrophobic interactions of the aliphatic chain leads to conformation changes in large water clusters containing dicarboxylates bigger than adipate. It also leads to a transition from bulk aqueous solvation of small dicarboxylates to solvation at the water/vapor interface of the larger ones. Whereas oxalate and adipate solvate in the inner parts of the aqueous slab, suberate and longer dicarboxylate dianions have a strong propensity to the surface. This transition also has consequences for the folding of the flexible aliphatic chain and for the structure of aqueous solvation shells around the dianions.

1. Introduction

The propensity of certain atomic and small molecular ions for the water/vapor interface has important implications for heterogeneous chemistry at aqueous surfaces. In particular, important tropospheric reactions involving polluting gases such as ozone or OH and leading to the production of reactive halogen compounds take place at the surface of aqueous sea salt aerosols in the lower marine troposphere[1,2] or salt solution films sprayed over the polar snowpack.[3] There is mounting computational and experimental evidence that heavier halides (iodide, bromide, and, to a lesser extent, chloride) penetrate the aqueous surface, where they can react with atmospheric gases.[4] Among small molecular ions, nitrate and azide were also shown to exhibit a similar surface behavior.[5,6] Note that the propensity for the water/vapor interface of these ions cannot be attributed to hydrophobicity since they lack any hydrophobic center. Results of molecular dynamics (MD) simulations indicate that in these cases the main force that drives the above anions to the aqueous surface is their large polarizability (softness).[4,7,8]

Small *multiply* charged ions exhibit a more pronounced hydrophilicity than those bearing a single elementary charge. Because of the strong electrostatic interactions with surrounding water molecules, they tend to organize in the bulk liquid one to two solvation shells around themselves. These ions are repelled from the water/vapor interface because of huge image forces. As a result, they never penetrate into the topmost surface layer of aqueous systems. Typical examples of positively charged ions are alkali earth dications such as Mg^{2+} or Ca^{2+}, while SO_4^{2-} represents a textbook hydrophilic dianion.[9]

Gas-phase solvated clusters provide ideal molecular models for investigating the solvation behaviors of atomic and molecular ions and can provide valuable information pertaining to the question of bulk vs interfacial solvation.[10−15] For the heavier

† Academy of Sciences of the Czech Republic and Center for Complex Molecular Systems and Biomolecules.

‡ Washington State University and Pacific Northwest National Laboratory.

(1) Oum, K. W.; Lakin, M. J.; DeHaan, D. O.; Brauers, T.; Finlayson-Pitts, B. J. *Science* **1998**, *279*, 74−77.
(2) Knipping, E. M.; Lakin, M. J.; Foster, K. L.; Jungwirth, P.; Tobias, D. J.; Gerber, R. B.; Dabdub, D.; Finlayson-Pitts, B. J. *Science* **2000**, *288*, 301−306.
(3) Foster, K. L.; Plastridge, R. A.; Bottenheim, J. W.; Shepson, P. B.; Finlayson-Pitts, B. J.; Spicer, C. W. *Science* **2001**, *291*, 471−474.
(4) Jungwirth, P.; Tobias, D. J. *J. Phys. Chem. B* **2002**, *106*, 6361−6373.
(5) Salvador, P.; Curtis, J. E.; Tobias, D. J.; Jungwirth, P. *Phys. Chem. Chem. Phys.* **2003**, *5*, 3752−3757.
(6) Yang, X.; Kiran, B.; Wang, X. B.; Wang, L. S.; Mucha, M.; Jungwirth, P. *J. Phys. Chem. A*, published online May 8, 2004, http://dx.doi.org/10.1021/jp0496396.
(7) Jungwirth, P.; Tobias, D. J. *J. Phys. Chem. B* **2001**, *105*, 10468−10472.
(8) Dang, L. X.; Chang, T. M. *J. Phys. Chem. B* **2002**, *106*, 235−238.
(9) Jungwirth, P.; Curtis, J. E.; Tobias, D. J. *Chem. Phys. Lett.* **2003**, *367*, 704−710.
(10) Greenblatt, B. J.; Zanni, M. T.; Neumark, D. M. *Science* **1997**, *276*, 1675−1678.
(11) Cabarcos, O. M.; Weinheimer, C. J.; Lisy, J. M.; Xantheas, S. S. *J. Chem. Phys.* **1999**, *110*, 5−8.

10.1021/ja047493l CCC: $27.50

halogen ions (Cl^-, Br^-, and I^-) and azide (N_3^-), which have a propensity for the water/vapor interface of extended systems, studies of their hydrated clusters demonstrate that they also prefer a "surface" solvation state.[6,16-21] An interesting class of systems are multiply charged ions.[22-26] Recent experimental advances using photoelectron spectroscopy and electrospray have allowed multiply charged anions to be studied in the gas phase.[27,28] Hydrated clusters of small multiply charged anions including SO_4^{2-} have been produced and shown that these species prefer to be in the center of the solvated clusters,[29-31] anticipating their absence from the air/water interface in extended systems or nanodroplets.[9]

In contrast to the above small multiply charged ions, dicarboxylate dianions $^-O_2C-(CH_2)_n-CO_2^-$ have two distinct charged groups ($-CO_2^-$) linked by a flexible hydrophobic aliphatic chain. Recently, we have investigated the sequential solvation of an example of dicarboxylate dianions, $^-O_2C-(CH_2)_6-CO_2^-$ (suberate), in clusters with 1−25 water molecules in a combined photoelectron spectroscopy and computational study.[32] The main finding is that for up to about 16 water molecules, both carboxylate charge centers of the linear gas phase dianion are separately solvated, one water molecule after another in an alternating pattern. However, upon adding more waters, the suberate dianion folds and a single water cluster forms around and between the two $-CO_2^-$ groups. At the same time, the hydrophobic $(CH_2)_6$ chain is not solvated by water molecules at all, regardless of the cluster size.

Dicarboxylate dianions play important roles in many natural environments. For example, carboxylate is an important negative charge carrier in proteins, which is present in the C-terminal of polypeptides and the side chains of aspartic and glutamic acids. As another example, dicarboxylate dianions originating from small, water soluble acids (such as oxalic, malonic, or succinic acid) were recently suggested to play an important role in controlling the chemical and physical properties of organic aerosols in the polluted troposphere.[33] Understanding the solvation behavior in aqueous interfaces of the dicarboxylate dianions may be essential to elucidate the chemistry of the organic aerosols containing these species.

These dianions with a varying length of the $(CH_2)_n$ chain also represent ideal systems for studying the competition between hydrophilic electrostatic forces due to the $-CO_2^-$ groups and the hydrophobic interactions between the connecting aliphatic chain and water.[34,35] In the current work, we report a comprehensive experimental and theoretical study on a series of dicarboxylate dianions with different numbers of CH_2 spacer groups. Experimentally, we have obtained photoelectron spectra for hydrated $^-O_2C-(CH_2)_n-CO_2^-$ for $n = 2$, 4, 12, and up to 20 water molecules. There are two questions that we would like to address. Previous work has shown that the smallest member of the series, the oxalate ($C_2O_4^{2-}$), prefers to be in the center of the solvated clusters.[30,31] As the aliphatic chain length is increased, the size of the dianion increases and the hydrophobic interactions with water also increase. What is the largest dicarboxylate that can still have the interior solvation behavior? Second, we want to examine how the solvation-induced conformation change would depend on the aliphatic chain length, as well as on the number of solvent molecules.

Despite the above cluster results, there is little direct information about the character of solvation of dicarboxylate dianions in extended aqueous systems. While, as discussed above, a lot of valuable information is gained from cluster studies, solvation at the extended water/vapor interface differs somewhat from that in and on aqueous clusters with a diameter smaller than about 100 nm because of the finite size and surface curvature of the latter. In particular, the curved surface of the aqueous cluster represents a possible additional surface driving factor for the solute species, which is missing at the planar interface of extended systems.[36] Extensive molecular dynamics simulations have thus been carried out within the current study concerning the solvation and, in particular, the interfacial behaviors of the dicarboxylates with different aliphatic chain lengths. The main questions addressed, in conjunction with the experimental work, which focused on small- and medium-sized solvated clusters, are as follows: Do small dicarboxylate dianions solvate in the aqueous bulk, and do the larger ones solvate at the water/vapor interface? At what length of the aliphatic chain do the hydrophobic interactions overwhelm the hydrophilic ones, leading to a crossover between bulk and surface solvation? To what extent is the dicarboxylate dianion folded and unfolded at the surface and in the aqueous bulk? What is the solvent structure around the charged carboxylate groups and around the aliphatic chain? In addition, the experiment addresses the issues of sequential hydration and possible folding of dicarboxylate dianions upon increasing the number of solvent water molecules, as observed recently for suberate.[32]

In our previous work on clusters containing a suberate dianion and up to 20 water molecules,[32] quantitative agreement between computer simulations and results of photoelectron spectroscopy measurements was established. Building on this success, in the present study we employ experiment and computations primarily in a complementary way, the former focusing on extracting

(12) Ayotte, P.; Weddle, G. H.; Johnson, M. A. *J. Chem. Phys.* **1999**, *110*, 7129−7132.
(13) Lehr, L.; Zanni, M. T.; Frischkorn, C.; Weinkauf, R.; Neumark, D. M. *Science* **1999**, *284*, 635−638.
(14) Weber, J. M.; Kelley, J. A.; Nielsen, S. B.; Ayotte, P.; Johnson, M. A. *Science* **2000**, *287*, 2461−2463.
(15) Patwari, G. N.; Lisy, J. M. *J. Chem. Phys.* **2003**, *118*, 8555−8558.
(16) Perera, L.; Berkowitz, M. L. *J. Chem. Phys.* **1991**, *95*, 1954−1963.
(17) Perera, L.; Berkowitz, M. L. *J. Chem. Phys.* **1992**, *96*, 8288−8294.
(18) Perera, L.; Berkowitz, M. L. *J. Chem. Phys.* **1993**, *99*, 4222−4224.
(19) Stuart, S. J.; Berne, B. J. *J. Phys. Chem.* **1996**, *100*, 11934−11943.
(20) Markovich, G.; Pollack, S.; Giniger, R.; Cheshnovsky, O. *J. Chem. Phys.* **1994**, *101*, 9344−9353.
(21) Choi, J. H.; Kuwata, K. T.; Cao, Y. B.; Okumura, M. *J. Phys. Chem. A* **1998**, *102*, 503−507.
(22) Kalcher, J.; Sax, A. F. *Chem. Rev.* **1994**, *94*, 2291−2318.
(23) Freeman, G. R.; March, N. H. *J. Phys. Chem.* **1996**, *100*, 4331−4338.
(24) Boldyrev, A. I.; Gutowski, M.; Simons, J. *Acc. Chem. Res.* **1996**, *29*, 497−502.
(25) Stefanovich, E. V.; Boldyrev, A. I.; Truong, T. N.; Simons, J. *J. Phys. Chem. B* **1998**, *102*, 4205−4208.
(26) Dreuw, A.; Cederbaum, L. S. *Chem. Rev.* **2002**, *102*, 181−200.
(27) Wang, L. S.; Wang, X. B. *J. Phys. Chem. A* **2000**, *104*, 1978−1990.
(28) Wang, X. B.; Yang, X.; Wang, L. S. *Int. Rev. Phys. Chem.* **2002**, *21*, 473−498.
(29) Yang, X.; Wang, X. B.; Wang, L. S. *J. Phys. Chem. A* **2002**, *106*, 7607−7616.
(30) Wang, X. B.; Yang, X.; Nicholas, J. B.; Wang, L. S. *J. Chem. Phys.* **2003**, *119*, 3631−3640.
(31) Wang, X. B.; Yang, X.; Nicholas, J. B.; Wang, L. S. *Science* **2001**, *294*, 1322−1325.
(32) Yang, X.; Fu, Y. J.; Wang, X. B.; Slavicek, P.; Mucha, M.; Jungwirth, P.; Wang, L. S. *J. Am. Chem. Soc.* **2004**, *126*, 876−883.
(33) Kawamura, K.; Umemoto, N.; Mochida, M.; Bertram, T.; Howell, S.; Huebert, B. J. *J. Geophys. Res., D: Atmos.* **2003**, *108* 8639.
(34) Wang, L. S.; Ding, C. F.; Wang, X. B.; Nicholas, J. B. *Phys. Rev. Lett.* **1998**, *81*, 2667−2670.
(35) Ding, C. F.; Wang, X. B.; Wang, L. S. *J. Phys. Chem. A* **1998**, *102*, 8633−8636.
(36) Stuart, S. J.; Berne, B. J. *J. Phys. Chem. A* **1999**, *103*, 10300−10307.

electron binding energies and inferring structures of dicarboxylate dianions in and on water clusters, while the latter aiming at elucidating directly the thermodynamically averaged structures of these dianions in the aqueous bulk or at the extended water/vapor interface.

2. Experimental and Computational Methods

2.1. Photoelectron Spectroscopy. The experiment was carried out using an apparatus equipped with a magnetic-bottle time-of-flight photoelectron analyzer and an ESI source.[37] Details of the experimental method have been given elsewhere,[37] and the procedures were the same as our previous study on the solvated suberate dianions.[32] Briefly, solvated dianions with a wide range of solvent molecules, $^{-}O_2C(CH_2)_n$-$CO_2^{-}(H_2O)_x$, were produced from electrospray of mixed solutions of 10^{-3} M of the corresponding acids, $HO_2C(CH_2)_nCO_2H$ and 2×10^{-3} M NaOH in a water–acetonitrile mixture (1:4 volume ratio). Anions produced from the ESI source were guided into a room-temperature ion trap, where ions were accumulated for 0.1 s before being pulsed into the extraction zone of a time-of-flight mass spectrometer. During photoelectron spectroscopic experiments, the dianions of interest were mass-selected and decelerated before being intercepted by a probe laser beam in the photodetachment zone of the magnetic-bottle photoelectron analyzer. In the current study, the detachment photon energy was 193 nm (6.424 eV). Photoelectron time-of-flight spectra were collected and then converted to kinetic energy spectra, calibrated by the known spectra of I^- and O^-. The electron binding energies (EB) were obtained by subtracting the kinetic energy (KE) spectra from the detachment photon energy (EB = 6.424 eV − KE). The energy resolution (ΔKE/KE) was about 2%, i.e., ~10 meV for 0.5 eV electrons, as measured from the spectrum of I^- at 355 nm.

2.2. Computational Methods. The calculations involved classical molecular dynamics simulations aimed at a Boltzmann sampling of solvation structures of $^{-}O_2C(CH_2)_nCO_2^{-}$, n = 0, 4, 6, and 12 (i.e., oxalate, adipate, suberate, and tetradecandioic dianion) in and on aqueous slabs. To construct the slab, a rectangular box of 3.5 × 3.5 × 17.5 nm^3 was used, containing 1400 water molecules, a single dicarboxylate dianion, and two sodium cations as counterions. Application of periodic boundary conditions at constant volume with such a unit cell yields an infinite slab with two open surfaces, perpendicular to the z-axis. A cutoff of 16 Å was used for nonbonded interactions. Long-range electrostatic interactions were accounted for using a standard particle mesh Ewald procedure.[38]

The systems were first equilibrated at 300 K for at least 0.5 ns, after which very long (~5 ns) production runs at the same temperature followed. A time step of 1 fs was adopted, and all bonds containing hydrogen atoms were constrained using the standard SHAKE procedure.[39] We employed the SPCE model of water,[40] while for the dicarboxylate dianions, we used the Cornell force field[41] with fractional charges evaluated (as is the standard for force field parametrizations[42]) at the HF/6-31G* level using the natural population analysis for structures optimized at the MP2/6-31+G* level. All molecular dynamics calculations were performed using the GROMACS 3.1 program package.[43]

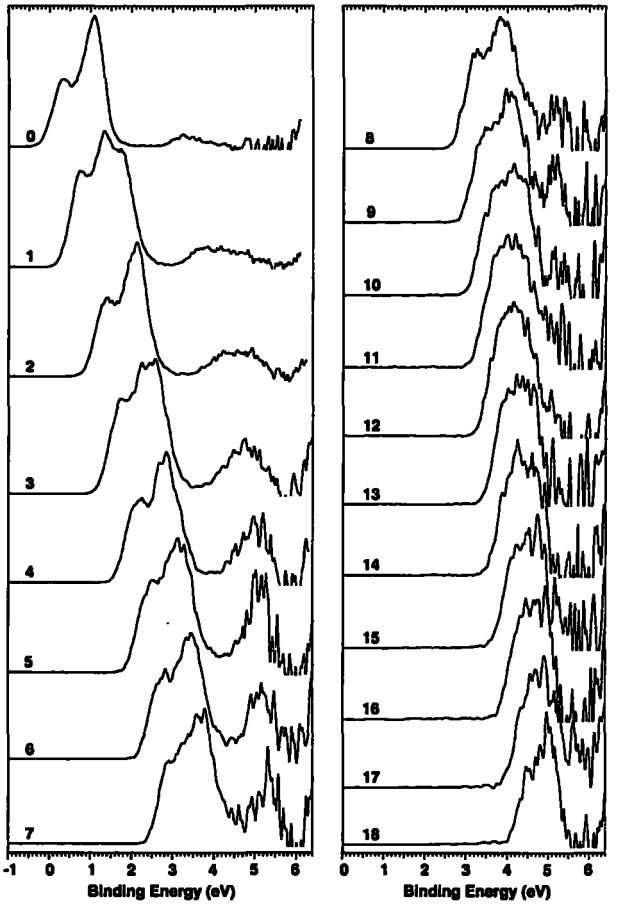

Figure 1. Photoelectron spectra of $^{-}O_2C-(CH_2)_2-CO_2^{-}(H_2O)_x$ (x = 0–18) at 193 nm (6.424 eV). Note the low electron binding energies of the bare anion at x = 0.

3. Experimental Results and Discussion

3.1. The Bare Dianions and the Observation of the Smallest Stable Dicarboxylate Dianions: The Succinate. The photoelectron spectra of $^{-}O_2C(CH_2)_nCO_2^{-}(H_2O)_x$ (x = 0–20) for n = 2, 4, 12 are displayed in Figures 1–3, respectively. The spectra of the bare dianions all exhibited two bands, consistent with our previous study carried out at two lower photon energies.[34] The weak band at higher binding energies in the spectra of the bare dianions was due to detachment of the singly charged anions by a second photon. The succinate dianion was observed for the first time here and was found to be barely stable with an adiabatic detachment energy (ADE) estimated as ~0.0 eV. We were not able to observe this dianion in our previous study,[44] likely because of a harsher desolvation condition in the electrospray source. The observed vanishing value of ADE for succinate qualitatively agrees with a previous ab initio calculation, which gives an ADE of −0.086 eV.[44] We have shown previously that the oxalate dianion ($C_2O_4^{2-}$) is not stable in the gas phase,[30,31] similarly to the sulfate dianion (SO_4^{2-}).[45,46] The succinate dianion turns out to be the smallest electronically stable dicarboxylate dianion in the gas phase, if

(37) Wang, L. S.; Ding, C. F.; Wang, X. B.; Barlow, S. E. *Rev. Sci. Instrum.* **1999**, *70*, 1957–1966.
(38) Essmann, U.; Perera, L.; Berkowitz, M. L.; Darden, T.; Lee, H.; Pedersen, L. G. *J. Chem. Phys.* **1995**, *103*, 8577–8593.
(39) Allen, M. P.; Tildesley, D. J. *Computer Simulations of Liquids*; Clarendon: Oxford, 1987.
(40) Berendsen, H. J. C.; Grigera, J. R.; Straatsma, T. P. *J. Phys. Chem.* **1987**, *91*, 6269–6271.
(41) Cornell, W. D.; Cieplak, P.; Bayly, C. I.; Gould, I. R.; Merz, K. M.; Ferguson, D. M.; Spellmeyer, D. C.; Fox, T.; Caldwell, J. W.; Kollman, P. A. *J. Am. Chem. Soc.* **1995**, *117*, 5179–5197.
(42) Bayly, C. I.; Cieplak, P.; Cornell, W. D.; Kollman, P. A. *J. Phys. Chem.* **1993**, *97*, 10269–10280.
(43) Lindahl, E.; Hess, B.; van der Spoel, D. *J. Mol. Model.* **2001**, *7*, 306–317.
(44) Skurski, P.; Simons, J.; Wang, X. B.; Wang, L. S. *J. Am. Chem. Soc.* **2000**, *122*, 4499–4507.
(45) Boldyrev, A. I.; Simons, J. *J. Phys. Chem.* **1994**, *98*, 2298–2300.
(46) Wang, X. B.; Nicholas, J. B.; Wang, L. S. *J. Chem. Phys.* **2000**, *113*, 10837–10840.

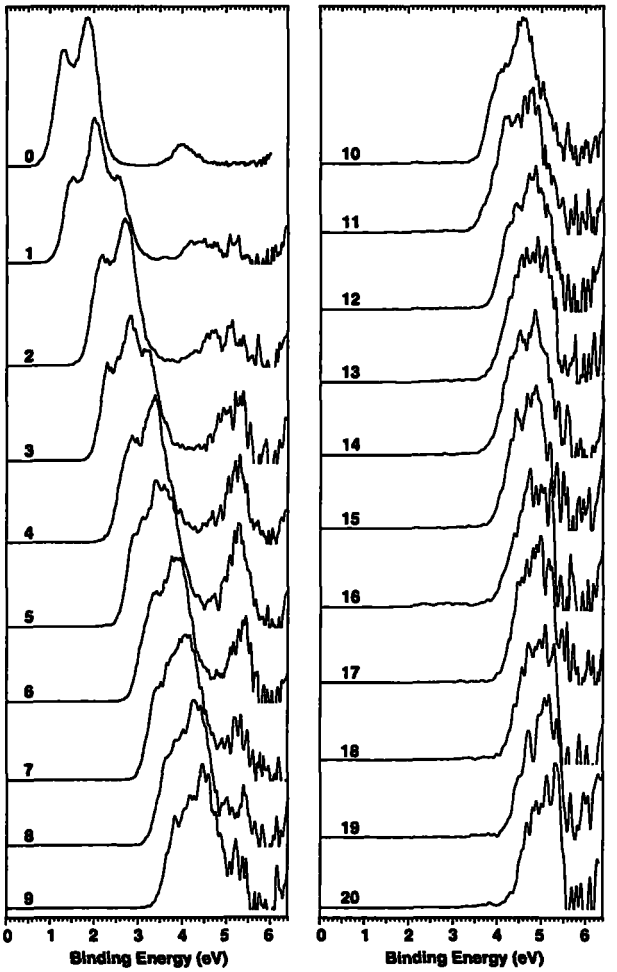

Figure 2. Photoelectron spectra of $^{-}O_2C-(CH_2)_4-CO_2^{-}(H_2O)_x$ ($x = 0-20$) at 193 nm.

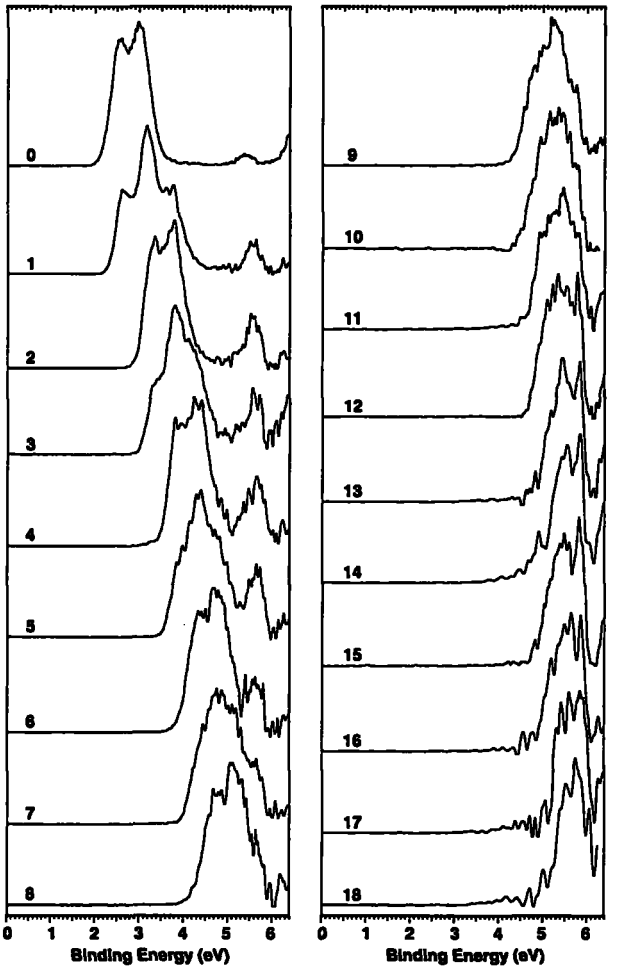

Figure 3. Photoelectron spectra of $^{-}O_2C-(CH_2)_{12}-CO_2^{-}(H_2O)_x$ ($x = 0-18$) at 193 nm.

only barely. The malonate dianion, which lies between oxalate and succinate in size, is expected to be unstable, and we have indeed failed to observe it in our electrospray source. In an unpublished work, we showed that we could readily observe malonate with three waters, $^{-}O_2CCH_2CO_2^{-}(H_2O)_3$, indicating that one to three water molecules are needed to stabilize the malonate dianion in the gas phase. We also showed previously that oxalate requires at least three waters to be stabilized.[30,31]

3.2. Hydrated Succinate, Adipate, and Tetradecandioic Dianions. The first solvent molecule caused the spectra of the dicarboxylate to split, as previously observed for the suberate system.[32] The first water can only solvate one of the $-CO_2^{-}$ groups, thus making the two carboxylate groups nonequivalent. The spectra of systems with two waters closely resemble those of the bare dianions, indicating that each water solvates one $-CO_2^{-}$ group separately. This even–odd pattern became difficult to recognize beyond four solvent waters for succinate and adipate, whereas for the hydrated suberate[32] and tetradecandioic dianions such even–odd changes were discernible for up to nine solvent molecules. The even–odd changes demonstrated that the water molecules tended to solvate the two $-CO_2^{-}$ groups independently and alternately. For large solvated dianions, the cluster intensity became relatively weak and the photoelectron spectral signal-to-noise ratios became poor. The high binding energy part of the spectra for the very large solvated clusters was cut off because of the repulsive Coulombic barrier universally present in multiply charged anions.[34] For $x = 1-7$, the weak feature at higher binding energies gained intensity and became broader. The binding energy of this feature seems to depend on the solvent number very weakly. We suspect that this weak band could also have contributions from ionization of the solvent, as was observed previously in the photoelectron spectra of hydrated sulfate and oxalate.[31]

3.3. Interior vs Exterior Solvation and Solvent-Induced Conformational Changes. The ADEs, estimated from the threshold of the photoelectron spectra shown in Figures 1–3, are plotted as a function of solvent number (x) in Figure 4a. The differential ADE (ΔADE), defined as [ADE($x + 1$) − ADE(x)], is the net stabilization of one water to the negative charge as water is sequentially added. It is plotted in Figure 4b as a function of x.

3.3.1. $^{-}O_2C(CH_2)_2CO_2^{-}(H_2O)_x$. The ADEs of the hydrated succinate exhibit a relatively smooth increase with the solvent number. The even–odd effect in the ADE is not very strong and seems to completely smooth out beyond five waters. These observations are consistent with the small size of succinate. Namely, after the first five or six waters, additional solvent can build around the dianion and effectively stabilize both negative

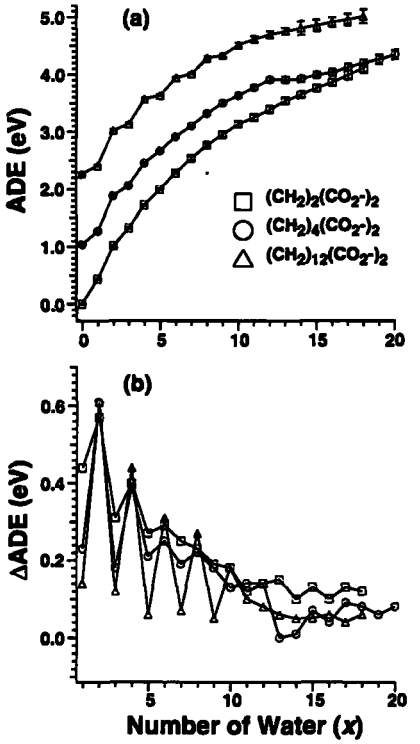

Figure 4. (a) Adiabatic electron binding energies (ADE) of hydrated succinate (□), adipate (○), and the tetradecandioic (△) dianions as a function of solvent numbers (x). (b) The differential ADE [$\Delta ADE = ADE(x + 1) - ADE(x)$] as a function of x.

charges more or less equally. This suggests an interior solvation state for succinate, analogous to sulfate and oxalate.[31] It is also expected that succinate prefers bulk solvation in extended aqueous systems.

3.3.2. $^{-}O_2C(CH_2)_4CO_2^{-}(H_2O)_x$. The ADE of the hydrated adipate as a function of the number of solvent molecules is more intriguing (Figure 4). First, the ΔADEs exhibited more pronounced even−odd changes than those of the succinate systems and tapered off beyond about eight waters. The ADEs then increased smoothly with x up to 12. But change in the slope was observed between $x = 12$ and 13: the ADEs of $x = 13$ and 14 showed no or little increase relative to that of $x = 12$. This is an indication of a conformation change. Previously, we observed that for the hydrated suberate systems folding takes place at $x = 16$, where the quasi-linear suberate dianion became bent and the two separately solvated $-CO_2^-$ centers merged.[32] The folding was caused by the strong cooperative H-bonding interactions between the solvent molecules and the hydrophobicity of the aliphatic chain. In the suberate systems, a dramatic ADE decrease was observed between the folded conformation at $x = 16$ relative to the unfolded conformation at $x = 15$. This is a result of the increased Coulombic repulsion upon folding, which brought the two negative charges closer to each other. Adipate has a shorter chain of four CH_2 spacer groups, which is not long enough to allow for such a dramatic folding structural change. But the ADE behavior between $x = 12$ and 13 signals a conformation change that brings the two carboxylates slightly closer to each other at $x = 13$. The fact that this happens at a smaller solvent number than in suberate is a manifestation of both the smaller size of adipate and the strong water−water interactions. At $x = 13$ and beyond, it is expected that the two separately solvated centers merge. Our current clusters were not large enough to extrapolate whether adipate assumes an interior or exterior solvation state in extended aqueous systems. Our computational study, described in detail below, suggests that adipate, as an intermediate size dicarboxylate dianion, prefers bulk solvation.

3.3.3. $^{-}O_2C(CH_2)_{12}CO_2^{-}(H_2O)_x$. The tetradecandioic dianion is the largest dicarboxylate systems that we have investigated. Its ADEs exhibit the most pronounced even−odd changes (Figure 4) since the two carboxylate groups are far apart and the solvation of each is almost independent of the other. However, the even−odd changes in the ADEs taper off beyond $x = 10$. This observation implies that five waters are needed to completely solvate the carboxylates on each end of the tetradecandioic dianion, presumably forming the first solvation shell. Additional waters exert a relatively small stabilization to the negative charges. Also, the even−odd effect was not measurable because of the large experimental uncertainty for large clusters, which were more difficult to produce because of the low solubility of this dianion. In analogy to the hydrated suberate systems, we expected that folding should happen for the tetradecandioic dianion at a certain solvation level. Because of the large distance between the two negative charge centers, a much more dramatic decrease in ADE was anticipated upon folding for the tetradecandioic dianion. It is apparent from the spectra that folding would require more solvent molecules than we were able to produce in our current experiment. The fact that the critical size is large (beyond those experimentally accessible) can be expected from the significant entropic contribution to the stability of the quasi-linear conformation at finite temperatures.[32] Twice as large as suberate, the tetradecandioic dianion is expected to prefer surface solvation with its hydrophobic aliphatic chains pointing into the vapor phase. This is exactly born out from the MD simulations presented below.

4. Computational Results and Discussion

4.1. Oxalate: $C_2O_4^{2-}$. The smallest dicarboxylate dianion, oxalate, does not contain any hydrophobic CH_2 groups. Experimentally, it was shown to sit in the center of water clusters, similarly to other small hydrophilic dianions (such as sulfate).[31] It was thus expected to solvate deeply in the aqueous bulk. This is indeed confirmed by the present MD simulations. Figure 5a shows the density profiles of the individual atomic species, i.e., histogrammed occurrences of the oxygen and carbon atoms of oxalate, the sodium counterions, and water oxygens across the water slab, averaged over the MD simulation. The water oxygen signal defines the extension of the slab, with an aqueous bulk region surrounded from both sides by a water/vapor interface. The signals from both oxalate oxygens and carbons clearly show that the smallest dicarboxylate dianion is strongly repelled from the aqueous surface and solvates deeply in the bulk region of the slab. As for aqueous sodium chloride, the sodium counterions are also, albeit somewhat less strongly, repelled from the water/vapor interface.

4.2. Adipate: $^{-}O_2C(CH_2)_4CO_2^{-}$. The next investigated aqueous dicarboxylate dianion − adipate, contains in addition to the two carboxylate groups a short aliphatic chain containing four CH_2 groups. The result of competition between the

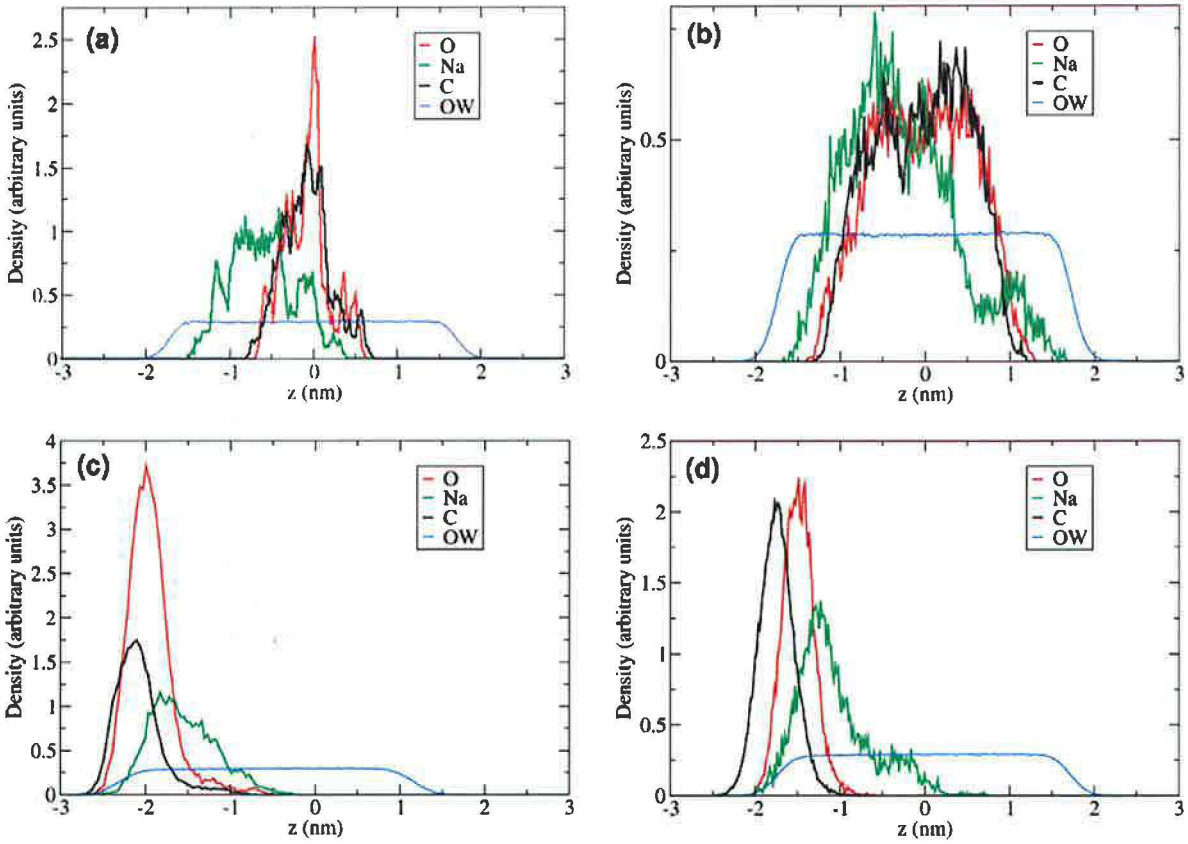

Figure 5. Density profiles of dicarboxylate dianions in an aqueous slab. Color coding: red, carboxylate oxygen; black, carbon; green, sodium counterions; and blue, water oxygen. (a) Oxalate (bulk salvation), (b) adipate (bulk salvation), (c) suberate (surface salvation), and (d) tetradecandioic dianion (surface salvation).

hydrophilic and hydrophobic forces is seen in density profiles shown in Figure 5b. Clearly, for this dianion the former forces won over the latter resulting in the interior solvation of adipate.

4.3. Suberate: $^{-}O_2C(CH_2)_6CO_2^{-}$. The aqueous clusters of suberate were the topic of our previous joint experimental and theoretical investigation.[32] In particular, experimentally inferred folding was born out nicely from the MD simulations. These cluster studies suggested that suberate would exhibit an interesting behavior in the interface with its hydrophobic aliphatic chain point out of the solution. This is clearly born out in the current MD simulation of an extended slab, as shown in the density profiles of aqueous suberate (Figure 5c). We see that upon moving from a dicarboxylate dianion with four to six CH_2 groups a transition from bulk to surface solvation occurred. This is demonstrated in Figure 5c by the signal from the aliphatic carbons, which peaks right at the water/vapor interface. Note that the signal of the carboxylate oxygens peaks closer to the bulk aqueous region than that of the carbon atoms. This reflects a generic pattern of longer, surface-solvated dicarboxylate dianions with the hydrophilic $-CO_2^{-}$ groups immersed in the surface solvent layer and the hydrophobic aliphatic chain repelled from water and, consequently, somewhat bent, analogous to the picture derived from our previous cluster study. Figure 6 shows a typical snapshot from the MD simulation, displaying the aqueous surface with the suberate dianion and demonstrating clearly this surface solvation behavior. Finally, note that the counterions also reside at the same side of the slab as suberate, albeit much deeper in the aqueous phase.

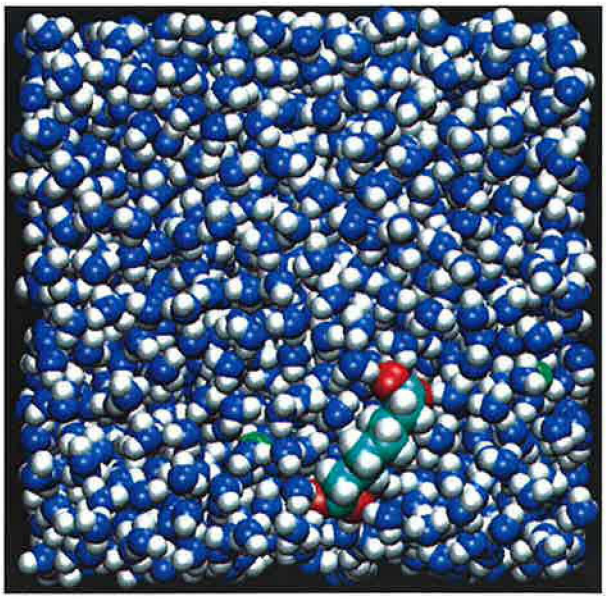

Figure 6. Typical snapshot from the simulation showing the surface-solvated suberate ion with the carboxylate groups solvated in the interfacial layer and the aliphatic carbon chain sticking into the vapor phase.

Sodium cations themselves have no propensity for the water/vapor interface, but rather they tend to neutralize the charges of the dicarboxylate dianion.

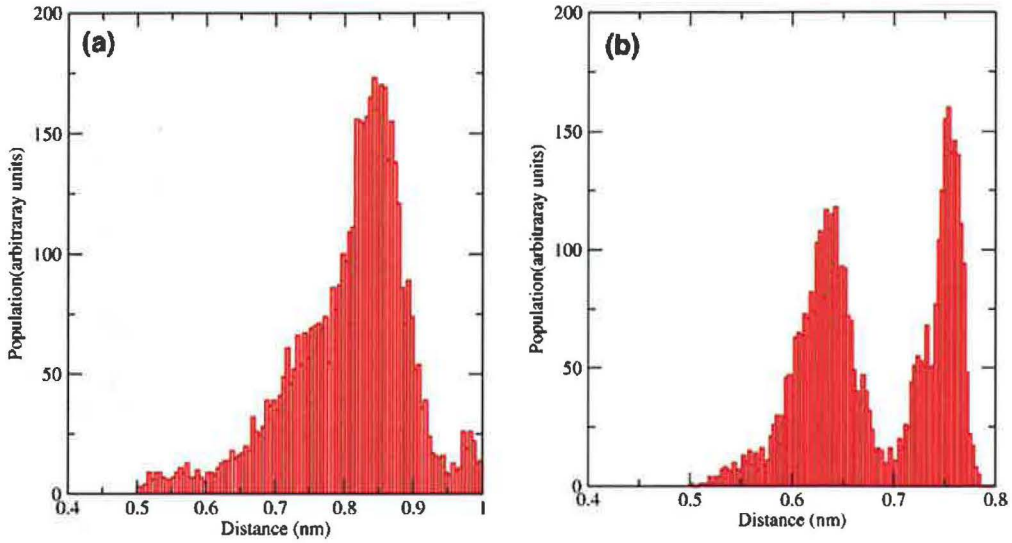

Figure 7. Distributions of carboxylate carbon−carbon distances for aqueous (a) adipate and (b) suberate. Unfolded structures dominate the bulk-solvated adipate, while suberate folds at the water/vapor interface.

4.4. The Tetradecandioic Dianion: $^{-}O_2C(CH_2)_{12}CO_2^{-}$. Upon prolonging the aliphatic chain of the dicarboxylate dianion the hydrophobic interactions can only become stronger and the aqueous surface solvation pertains. Figure 5d shows the density profiles for the largest investigated system, the tetradecandioic dianion. We see that the propensity of the dianion for the water/vapor interface is even stronger than in the case of suberate. Again, the aliphatic chain bends and sticks out into the vapor phase, while the carboxylate groups tend to solvate in the interfacial layer of the aqueous phase. The tendency of the sodium counterions to follow the dianion also pertains.

4.5. Folding of the Aliphatic Chains in the Water/Vapor Interface. A typical feature present in all but the shortest dicarboxylate dianions is the possible existence of a collinear and various folded structures due to the flexibility of the aliphatic chain. While in the gas phase all the dicarboxylate dianions tend to be collinear because of a strong Coulombic repulsion between the two carboxylate groups,[34] in an aqueous environment an efficient dielectric screening of the charged groups allows also for the occurrence of folded geometries. It is illuminating to compare the distribution in the aqueous slab of structures of a short, bulk-solvated adipate (see Figure 7a) with that of the longer, surface-solvated suberate (Figure 7b). In the case of adipate collinear geometries, corresponding to a distance between the carboxylate groups of 8−9 Å dominate. The situation is to some extent reversed for the surface-solvated suberate (Figure 7b). Because of the hydrophobic interactions of the aliphatic chain, which is pushed out of the aqueous phase, the suberate dianion tends to bend to solvate at the same time as the charged carboxylate groups. This corresponds to the peaks at 6.5 Å and 7.5 Å in Figure 7b, which reflect different degrees of folding of the aliphatic chain.

4.6. Solvation Structures of the Carboxylates. There is another interesting question pertaining to the bulk vs interfacial solvation of dicarboxylate dianions of varying aliphatic chain length. What is the structure of water molecules around the hydrophilic carboxylate groups, and are there differences between bulk- and surface-solvated dianions? A typical geometry of adipate with the surrounding 30 water molecules is depicted in Figure 8a, while a similar snapshot from a MD simulation of aqueous suberate is shown in Figure 8b. In both cases, the charged carboxylate groups are strongly hydrated. While the short aliphatic chain of the bulk-solvated adipate "squeezes" within the aqueous solvation shell, that of suberate is too long and is pushed out from the aqueous phase.

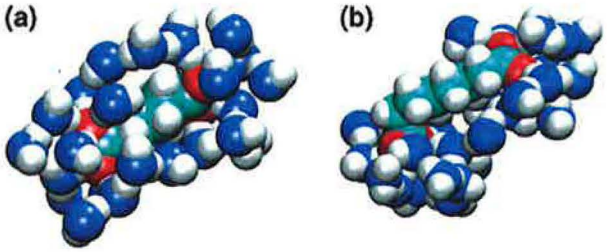

Figure 8. Structure of the solvation shell around (a) adipate and (b) suberate. While in the former case water molecules encompass the whole dianion, in the latter case the aliphatic chain remains unsolvated.

We have quantified the solvation structures in terms of radial distribution functions. Figure 9 shows the carboxylate oxygen−water oxygen radial distribution functions for adipate and suberate. On the first view the two curves look similar, with the first sharp (second broad and, in the case of suberate, somewhat structured) maximum corresponding to the first (second) solvation shell, despite the fact that the adipate solvates in the aqueous bulk while suberate sovates at the water/vapor interface. However, the integrals under the first peak, which give the numbers of the water molecules in the first solvation shell, are different for the two cases. Namely, while there are roughly seven water molecules around each of the carboxylate groups of the bulk-solvated adipate, this number drops to five for the surface-solvated suberate. We note that the first solvation shell of five waters in the surface-solvated suberate agrees remarkably well with the solvated cluster results. These show a negligible even−odd effect in the measured ADEs once each carboxylate is solvated by five waters since additional waters do not interact with the negative charges directly, i.e., they are added to the second solvation shell. Note that the first solvation shell derived from the solvated clusters of the tetradecandioic

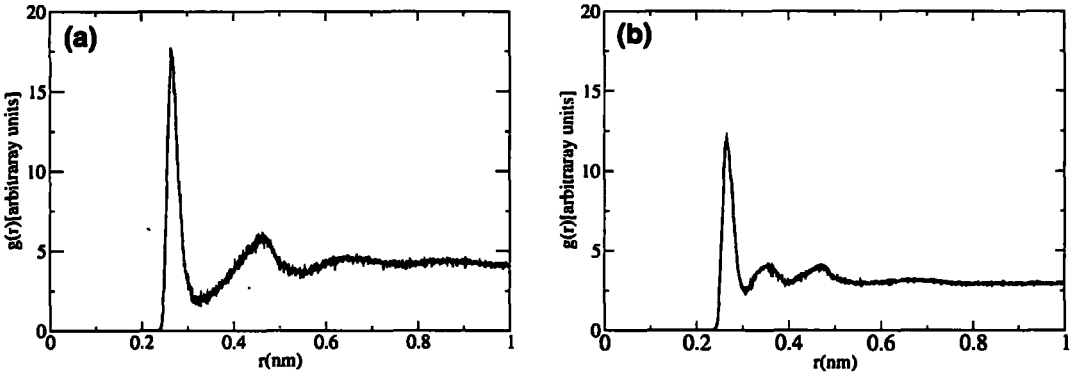

Figure 9. Carboxylate oxygen–water oxygen radial distribution functions for (a) adipate and (b) suberate.

dianion, which is surface-solvated as well, contains also five waters for each carboxylate group, as discussed above (see Section 3.3.3.).

5. Conclusions

We have investigated using molecular dynamics simulations and photoelectron spectroscopy aqueous solvation of a series of dicarboxylate dianions with 0, 2, 4, 6, and 12 CH_2 groups of the aliphatic chain connecting the two carboxylate groups. Photoelectron spectra of solvated clusters of succinate, adipate, and tetradecandioic dianions with up to 20 water molecules were obtained. Together with previous reports on solvated oxalate and suberate,[30-32] a relatively complete data set for solvated dicarboxylates with various chain lengths is available now. The isolated succinate dianion was observed for the first time and was shown to have an adiabatic electronic binding energy of ~0.0 eV, being the smallest stable dicarboxylate dianion. Photoelectron data of solvated succinate were consistent with an interior solvation state for this dianion. The electron binding energies as a function of solvation revealed for adipate that there was a small conformational change between 12 and 13 solvent molecules. The most pronounced even–odd effect was observed for the electron binding energies of the tetradecandioic dianion. The effect tapered off above 10 water molecules, suggesting that the first five water molecules form the first solvation shell for each of the carboxylate groups. A folding conformation change is expected for the tetradecandioic dianion as a function of solvation because of the hydrophobic interactions between water and the aliphatic chain and the strong water–water interactions; however, it was not observed within the currently accessible size range of up to 18 water molecules. This folding is likely to take place at larger sizes because of the entropic stabilization of the linear conformation at finite temperatures.

Molecular dynamics simulations revealed that the smallest of dicarboxylate dianions, oxalate, solvates deep in the aqueous bulk, similarly to other small dianions containing no hydrophobic group, such as sulfate. For all short dicarboxylate dianions up to adipate bulk aqueous solvation prevails, since hydrophilic interactions of the charged carboxylate groups win over the hydrophobic forces due to the aliphatic chain. However, upon further increasing the aliphatic chain length hydrophobic interactions overwhelm the hydrophilic ones. As a result, suberate and longer dicarboxylate dianion have a strong propensity for the water/vapor interface. This change of the aqueous solvation behavior of dicarboxylate dianions upon increasing the lengths of the aliphatic chain is in accord with the solubility data of the corresponding acids (obtainable, e.g., from the Beilstein database). Namely, the transition between soluble and insoluble acids correlates with that between the bulk vs surface located dianions, while oxalic, malonic, succinic, and glutaric acids are strongly soluble in water and adipic acid is moderately soluble, subaric acid is only slightly soluble, and acids with longer aliphatic chains are practically insoluble in water.

The bulk vs surface solvation of dicarboxylate dianions also has an effect on the structure of aqueous solvation shells and on the folding of the flexible aliphatic chain. Small bulk-solvated dicarboxylate dianions prefer more unfolded structures and a larger number of water molecules in the solvation shells around the carboxylate groups than large surface-solvated dianions.

Acknowledgment. The experimental work was supported by the U.S. Department of Energy (DOE), Office of Basic Energy Sciences, Chemical Science Division, and performed at EMSL, a national scientific user facility sponsored by DOE's Office of Biological and Environmental Research and located at Pacific Northwest National Laboratory, operated for DOE by Battelle. Support (to P.J.) from the Czech Ministry of Education (Grant LN00A032) and the National Science Foundation (Grant CHE-0209719) is gratefully acknowledged. Part of the work in Prague was completed within the framework of research project Z4 055 905.

JA0474931